

DOCTORAL THESIS

Influence of the Flow of Fresh Fiber Concrete on the Fiber Orientations

Oksana Goidyk

TALLINN UNIVERSITY OF TECHNOLOGY
DOCTORAL THESIS
12/2025

Influence of the Flow of Fresh Fiber Concrete on the Fiber Orientations

OKSANA GOIDYK



TALLINN UNIVERSITY OF TECHNOLOGY

School of Science

Department of Cybernetics

The dissertation was accepted for the defence of the degree of Doctor of Philosophy (Building and Civil Engineering and Architecture) on 10 February 2025

Supervisor: Dr. rer. nat. habil. Heiko Herrmann,
Department of Cybernetics, School of Science
Tallinn University of Technology
Tallinn, Estonia

Opponents: Professor Klaus Holschemacher,
Leipzig University of Applied Sciences (HTWK Leipzig),
Leipzig, Germany

Dr Valentin Antonovic,
Vilnius Gediminas Technical University,
Vilnius, Lithuania

Defence of the thesis: 17 March 2025, Tallinn

Declaration:

Hereby I declare that this doctoral thesis, my original investigation and achievement, submitted for the doctoral degree at Tallinn University of Technology, has not been submitted for any academic degree elsewhere.

Oksana Goidyk

Signature

The research was partially funded by the Estonian Research Council by the exploratory research grant PUT1146.

Copyright: Oksana Goidyk, 2025
ISSN 2585-6898 (publication)
ISBN 978-9916-80-269-4 (publication)
ISSN 2585-6901 (PDF)
ISBN 978-9916-80-270-0 (PDF)
DOI <https://doi.org/10.23658/taltech.12/2025>
Printed by Koopia Niini & Rauam

Goidyk, O. (2025). *Influence of the Flow of Fresh Fiber Concrete on the Fiber Orientations* [TalTech Press]. <https://doi.org/10.23658/taltech.12/2025>

TALLINNA TEHNIKAÜLIKOOL
DOKTORITÖÖ
12/2025

Vedela kiudbetooni voolamise mõju kiudude orientatsioonile

OKSANA GOIDYK

Contents

List of Publications	7
Author's Contributions to the Publications	8
Abbreviations.....	9
1 Introduction	10
1.1 Significance of research, problem statement	11
1.2 Objectives of the Research	14
1.3 State of the art	14
1.4 Novelty of the research and practical application	15
1.5 Factors influencing the fiber orientation and distribution	15
1.6 Overview of the Methods to Estimate the Fiber Orientation and Distribution	18
1.6.1 Manual fiber counting.....	18
1.6.2 Orientation factor	18
1.6.3 Image Analysis	18
1.6.4 Computed Tomography	19
1.6.5 Magnetic methods	20
1.6.6 Electrical resistivity methods	20
1.7 Research Methodology	20
2 Fiber Concrete Analysis.....	22
2.1 Simulation Experiments (Transparent Replacement Matrix).....	22
2.1.1 Mixing and Casting Process	22
2.1.2 Results: Simulation Experiments (Transparent Replacement Matrix)	23
2.2 Concrete Experiments: 3-beams plate and 40-beams slab	23
2.2.1 Materials and Casting Process	27
2.2.2 Results of the compression tests	31
2.2.3 Computed Tomography and Image Analysis	33
2.2.4 The bending test set-up	34
2.2.5 Results	39
2.3 Investigation of the Standard testing method according to EN14651	41
3 Numerical Modeling of SCC and FC	45
3.1 Sample preparation and testing according to EN 14651	46
3.2 Computational Fluid Dynamics simulations.....	47
3.3 Set-up of numerical simulations.....	48
3.4 Results of Numerical simulations.....	52
3.4.1 Dynamics of filling the form	52
3.4.2 Obtained final fiber orientation distributions	54
3.4.3 Self-leveling.....	56
3.4.4 High-viscous	57
3.4.5 Slump	57
3.4.6 Discussion.....	57
4 Main Conclusions and recommendations for future work	60
List of Figures	63

List of Tables	64
References	65
Acknowledgements	75
Abstract	76
Kokkuvõte	78
Appendix 1	81
Appendix 2	101
Appendix 3	117
Appendix 4	129
Appendix 5	145
Curriculum Vitae	164
Elulookirjeldus	166

List of Publications

The present thesis is based on the following publications that are referred to in the text by Roman numbers.

- I H. Herrmann, A. Braunbrück, T. Tuisk, O. Goidyk, and H. Naar. An initial report on the effect of the fiber orientation on the fracture behavior of steel fiber reinforced self-compacting concrete. In H. Herrmann and J. Schnell, editors, *Short fibre reinforced cementitious composites and ceramics*, pages 33–50. Springer, 2019
- II H. Herrmann, O. Goidyk, and A. Braunbrück. Influence of the flow of self-compacting steel fiber reinforced concrete on the fiber orientations, a report on work in progress. In H. Herrmann and J. Schnell, editors, *Short Fibre Reinforced Cementitious Composites and Ceramics*, pages 97–110. Springer, 2019
- III H. Herrmann, O. Goidyk, H. Naar, T. Tuisk, and A. Braunbrück. The influence of fibre orientation in self-compacting concrete on 4-point bending strength. *Proceedings of the Estonian Academy of Sciences*, 68(3):337–346, 2019
- IV D. Kartofelev, O. Goidyk, and H. Herrmann. A case study on the spatial variability of strength in a SFRSCC slab and its correlation with fibre orientation. *Proceedings of the Estonian Academy of Sciences*, 69(4):298–310, 2020
- V O. Goidyk, M. Heinštein, and H. Herrmann. CFD comparison of the influence of casting of samples on the fiber orientation distribution. *Fibers*, 11(1):6, 2023

Author's Contributions to the Publications

- I In this paper I conducted the experiments, carried out the analysis, and co-wrote the original draft of manuscript.
- II In this paper I was the second author, I conducted the experiments and simulation with transparent mixture, analyzed the results, prepared the figures, and co-wrote the original draft of manuscript.
- III In this paper I was the second author, I conducted the experiments, analyzed the results, prepared the figures, and co-wrote the original draft of manuscript.
- IV In this paper I was the second author, I conducted the experiments and data analysis, and co-wrote the original draft of manuscript.
- V In this paper I was the first author, I conducted the numerical simulations, the post-processing and analyzed the results, and co-wrote the original draft of the manuscript.

Abbreviations

FRC	Fiber Reinforced Concrete
SFRC	Steel Fiber Reinforced Concrete
SFRSCC	Steel Fiber Reinforced Self-Compacting Concrete
SCC	Self-Compacting Concrete
CO ₂	Carbon Dioxide
CT	Computed Tomography
CFD	Computational Fluid Dynamics
EN xxx	European Standard
AC-IS	Alternate Current Impedance Spectroscopy
PVM/MA	Polyvinyl methyl ether/maleic acid
NaOH	Sodium hydroxide
DAQ	Data Acquisition

1 Introduction

Concrete is the most common composite material that is widely used in the construction industry all over the world. The concrete mixture typically consists of cement, coarse and fine aggregate, water, and optionally admixtures. Concrete is highly popular construction material due to its fundamental advantages. Firstly, cementitious materials are sufficiently resistant to weathering, erosion and other environmental conditions without severe damage for decades making concrete the most appropriate material for building canal lines, bridges, roads, dams, pipes, floors, or exterior walls. Secondly, concrete is an ease-to-use material that can be poured freely in its fresh form into complex molds and forms of various sizes. Thirdly, concrete is a quite cost-effective building material with relatively available and inexpensive components [68].

However, conventional cement composites have some serious limitations, for example the tensile force transmission is far less pronounced than the ability to withstand compressive stresses. Additionally, composite materials have micro defects such as air voids and microcracks, also as it cures, it can experience significant volume changes due to plastic and drying shrinkage. These defects may occur due to various reasons both before and after hardening. Overloading, fire, alkali-silica reaction, erosion, freeze/thaw cycles and corrosion are just some of the processes to which concrete and reinforcing steel are exposed during their lifespan. The presence of the aforementioned defects has a direct influence on the strength and quality of cementitious materials, limiting their durability, service life, and long-term performance. However, to overcome some defects and to strengthen the mechanical properties of conventionally reinforced concrete different types of short fibers are embedded into the concrete matrix.

Several studies demonstrated that the use of steel fibers leads to higher resistance to shear failure of FRC beams resulting in the reduction of the need for stirrups [1, 52]. As was shown in [87, 58], different types of FRC have been successfully used as a repair material in various real-life projects including concrete dams, bridge decks, coupling beams in high-rise buildings, and tunnels in Japan, the USA, and Germany. Due to its better durability, FRC is also widely used for underground structures in seismically active areas and for strengthening structures sensitive to earthquakes [35, 18].

The addition of short fibers to the concrete mixture significantly reduces drying shrinkage, and microcracking and slows down the appearance of the first crack, as has been experimentally verified [72, 85, 129, 97]. However, the content of air voids in the fiber concrete mixture grows when the amount of the fibers increases [82, 48]. Moreover, too high content of air voids has a negative impact on the mechanical properties (strength, elastic modulus and durability) [51, 128]. Carbonation causes changes in permeability, strength, and pore size distribution, leading to the shrinkage and potential cracking of the concrete [8]. Several research groups demonstrated that the addition of the appropriate amount of fibers can delay of the carbonation process in FRC [69, 123]. The study described in [4] revealed that during the exposure of FRC to the high temperature, the presence of steel fibers has a positive effect on the restriction and formation of new cracks.

This research aims to develop practical guidelines for the optimal manufacturing process in precast factories to achieve reproducible and predictable results. In addition, to obtain the maximum benefits of adding fibers to the concrete matrix many factors should be considered and included in the concrete structural design.

1.1 Significance of research, problem statement

Nowadays, fiber reinforced composites in the construction industry have become a common modification of conventional concrete with traditional reinforcement and are widely used all over the world. The main benefit of using fiber concrete is that the fiber reinforced composite is less brittle and more durable, short fibers provide better ductility, arrest the cracks and prevent their growth and propagating, and thus, improve the flexural and shear strengths.

In several special applications these advantages allow the production of thinner constructions. In case of large areas of industry floors the reduction of the floor thickness might result in a significant saving of the raw natural resources (sand, cement, gravel) and less CO₂ will be produced. It will change the influence on the environment because natural resources are limited. Figures 1(a), 1(b), 1(c) demonstrate the impact of the raw material use on the environment, as an example the mining of the sand in Männiku quarry (Tallinn).

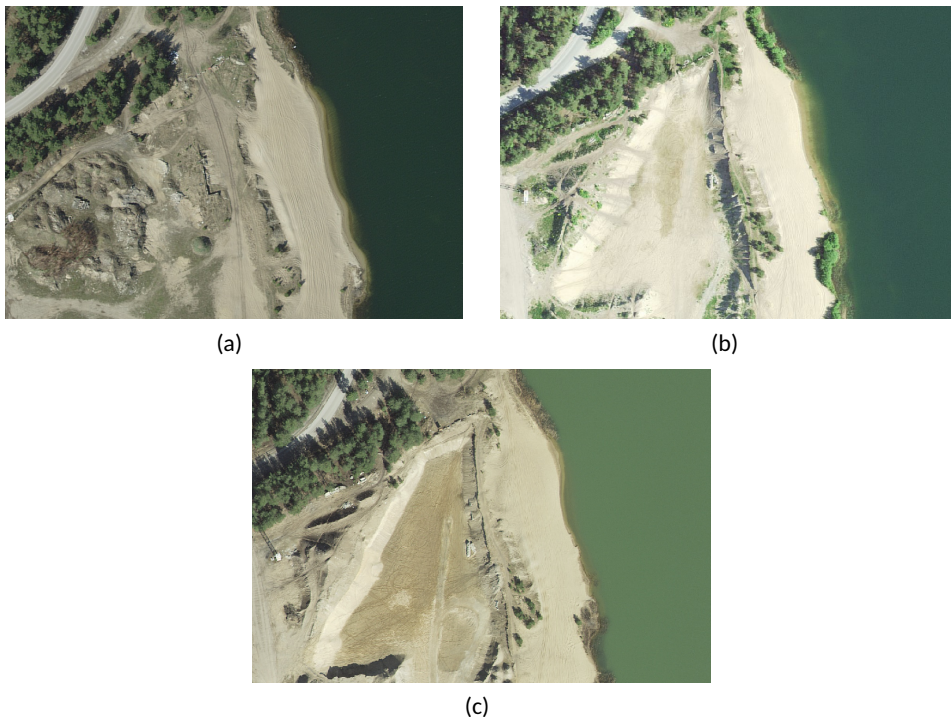


Figure 1: The changes of the sand amount in Männiku quarry (Tallinn) over the years; (a) in 2016, (b) in 2020, (c) in 2022, Map data: Estonian Land Board 2023

Due to the enhanced properties (e.g. better ductility (Figure 2), and improved resistance to cracking (Figure 3), drying shrinkage), fiber-reinforced concrete will prolong the lifetime of the building structures and by that reduce the costs of its maintenance overall.



Figure 2: Fiber concrete with visible fibers in the crack.



Figure 3: The restraining effect of the fibers in the crack.

In spite of the advantages of adding the short fibers into a composite matrix, some issues regarding this topic are still open. The main fundamental challenge is to define the optimal factors and conditions of the casting process that ensure obtaining the enhanced durable material. Optimization of the production method might positively effect the post-cracking behavior and also contribute to better performance of the material measured as the residual tensile strength.

In order to determine the most effective method of the estimation of the fiber spatial orientation, its distribution inside the concrete matrix and its influence on the durability and mechanical properties of cementitious materials more research needs to be done.

Assessing the fiber orientation and dispersion inside of concrete matrix immediately after the casting process is impossible due to the opacity of the concrete. Therefore, getting the full data about the inner constitution of the concrete element is an expensive, time- and resource-consuming process, or even impossible due to methodological restrictions on samples sizes.

For a reliable representation of the fiber distribution in a concrete specimen, a tomographic volume examination can be used. Nevertheless, the previously mentioned problem of size limitation occurs precisely here, since large samples cannot be scanned in one piece. Although the specimens can be cut, this is affected by the loss of material. By using the X-ray Computed Tomography scanning method, internal features in the hardened material can also be visualized (e.g. bridge effect of the fibers, pull-out of hook-end fibers, rupture of the fibers).

Since the internal state of the hardened concrete is analyzable and visualizable up to a certain level, the question remains as to the reliable design of the fiber flow, which is itself the starting point for the optimization of the casting. The application of numerical simulations of concrete flow is therefore necessary. It enables to reproduce the specific cases with varying constituents and performances of the mixture and different, simple or complicated, geometries of formwork.

Many researchers have implemented and improved the different algorithms for modeling fresh concrete flow [30, 34, 44, 57, 67, 78, 89, 100]. Generally, the simulation of concrete flow may include several applications: the mixing process and optimization of constituents, the standard tests that indicate the proper workability and rheology of the mixture (the slump, U-ring, or L-box tests), the filling process, the tests with hardened material (the compression or bending tests, the simulation of the crack formation and propagation). The use of numerical simulations allows to define the desired rheological parameters, uniformity of all constituents of the mixture, minimal mixing time, preferable casting method without blocking and segregation, or possible fiber orientation and distribution inside of the concrete structures. The proper composition of the concrete mixture and the mixing process of fresh concrete are extremely important procedures, as they have a significant impact on the mechanical properties of the hardened concrete.

In order to simulate casting by means of controlling the rheological behavior of concrete, it is essential that short fibers are modelled in the concrete flow. It is important to gain more accurate knowledge of the flow characteristics and factors affecting the flow casting process, as the high quality and durability of fiber-reinforced concrete is strongly dependent on the fiber orientation distribution.

1.2 Objectives of the Research

Current research is the continuation of the project 'Rheology of short fiber reinforced cementitious composites and influence on the fracture behavior' (PUT1146), funded by the Estonian Research Council. This project aimed to investigate the effect of rheology on the spatial and orientational distribution of short fibers in short fiber-reinforced cementitious composites, both numerically and experimentally. In addition, it includes the investigation of how these parameters may affect the fracture behavior and mechanical properties of the hardened concrete (compressive and flexural strength, toughness/energy absorption). Moreover, the PUT1146 research outcomes demonstrate how short steel fibers itself contribute to the residual flexural strength, ductility, and post-cracking behavior.

To achieve the primary aims of this research the following objectives of the thesis were established:

1. To analyze how the flow may affect on the uniformity, alignment and orientation of fibers in the preferred direction.
2. To analyze the correlation between the positions of the beams taken out from the slab and the orientation of short steel fibers and how it influences on the mechanical properties of the Fiber Reinforced Concrete by carrying out a series of three-point and four-point bending tests.
3. To assess the fiber orientation distribution inside of the testing specimens and its influence on the first crack appearance and post-cracking behavior by the application of X-ray Computed Tomography and image analysis method.
4. To investigate the rheology and material characteristics of short fiber reinforced cementitious composites and to define key factors (the casting method, the point of the filling, flowability of the mixture, etc.) influencing the final positioning of the short fibers inside of the cement matrix.
5. To understand how the different casting methods may affect the uniformity and orientation of the fibers over the full length, on the side and bottom of the specimen).
6. To apply the standard bending test method on a fiber-reinforced specimen with force application parallel and transverse to the formwork filling direction.

1.3 State of the art

Several countries, including Austria [135], Germany [19], Denmark [105], Sweden [93], USA [2, 14] and Russia [118, 119] have well-developed guidelines for using fiber-reinforced concrete (FRC) in construction. A key reference for national and international standards is the fib Model Code [95], which addresses various aspects of concrete design. These guidelines outline design rules and mainly cover calculations of the concrete contribution for the improved mechanical properties of steel fiber-reinforced concrete in structural applications.

However, only several of them mention the contribution of the added fibers to the improved mechanical properties [95]. In addition, only three national standards consider the fiber orientation and how it affects the material's ability to withstand tensile and shear stresses, resistance to cracking, and overall load-bearing capacity [95, 19, 119]. Moreover, even in these standards, the approaches to calculate the fiber orientation are quite different. This highlights the need for further research in this area.

Numerous research groups have proved the influence of fiber orientation distribution on mechanical properties [7, 9, 43, 46, 96, 130, 134]. Therefore, the presented research demonstrates the confirmation of the importance of fiber orientation in Chapter 2.

According to European standard EN 14651, bending tests on hardened specimens require a 90-degree rotation along the longitudinal axis to provide two smooth, parallel surfaces that will be in the contact with the experimental machine, leading to the improved test accuracy. However, this rotation is only feasible for lab samples or precast elements, not for in-situ cast structural elements that can not be adjusted post-casting, limiting the standard's applicability to real-world structural conditions.

In addition, during the testing with the rotation of the fiber concrete sample, it needs to be considered that the alignment and the orientation of the fibers on all sides of the sample are quite varied, leading to different mechanical properties of the concrete.

The ability to predict fiber orientation in fiber-reinforced concrete (FRC) has significant practical implications for the construction industry, especially in the production of precast elements and cast-in-place concrete structures. Fiber orientation is a key factor that determines the mechanical properties, durability, and performance of concrete materials. Accurate prediction and control of fiber orientation can directly influence the quality, cost-effectiveness, and reliability of concrete structures.

Therefore, the prediction of the fiber orientation distribution by numerical simulations is a promising alternative. Nowadays, several research groups present their findings on this topic.

Svec et al. [101, 102] have demonstrated the Lattice Boltzmann Method combined with the corrected Immersed boundary method and mass tracking algorithm for free surface representation for simulation of a non-Newtonian liquid with rigid round or elongated particle inclusions.

Herrmann and Lees [44] developed the rheology simulations of the casting of steel fiber-reinforced self-compacting concrete. The presented outcomes have shown the strong influence of the boundary properties (specific formwork surface conditions) on the fiber orientation.

The presented research has demonstrated the findings on the prediction of fiber orientation distribution by the numerical simulations of the different casting methods of the fresh concrete flow in Chapter 3.

1.4 Novelty of the research and practical application

This research proposes limitations of testing method and highlights the need for improvement, leading to a more accurate assessment of fiber orientation and post-cracking behavior in fiber-reinforced concrete. The casting simulations developed in this study provide valuable insights that can assist precast design companies optimise guidelines for casting processes across different element geometries and casting conditions. The outcomes of this research give a better understanding of the importance of the proper manufacturing process of fiber-reinforced concrete and can make a contribution to the development of standards within the European Construction Code, particularly by providing insights into fiber-reinforced concrete casting and performance criteria.

1.5 Factors influencing the fiber orientation and distribution

A study of the rheological properties of fiber reinforced concrete in the fresh state was performed by numerous research groups (see below), and revealed the importance of the proper casting conditions to achieve a desired fiber orientation.

Dupont and Vandewille [21] analyzed how boundary conditions affect the fiber orientation factor and described the simple method to calculate the average orientation coefficient of the fibers and the number of fibers crossing the crack. However, in this research, only the total number of fibers is defined, without distinguishing between effective and non-effective fibers.

The main idea of the research proposed by Martinie and Roussel [60] is that the main reasons/origins of the preferred fiber orientation are wall effect which highly depends on the geometry of specimens and shear-induced orientation that depends on both geometry of the element, rheological behavior of the material and the casting process.

Investigation of the fiber reinforced self-compacting concrete structural element was performed by Zerbino et al. [130] and the results demonstrate that fiber orientation varies due to wall effect and with the flow rate. In addition, different results in residual capacity and toughness are obtained during the analysis of the diverse directions and zones of the thin structural element. The fiber orientation differs regarding the direction of the flow: the beams cut perpendicular to the concrete flow direction always show a lower density of the fibers in comparison with the parallel direction.

The influence of the location of concrete casting points on the fiber spacing was analyzed by Ponikiewski et al. [81, 83] and revealed that at the concrete casting points the amount of fibers is mostly lower than at the rest volume. Moreover, the amount of fibers is different in the upper and lower parts of the tested slabs, and the maximum number of fibers is reached in the range of 25 mm to 45 mm from the bottom of formwork.

Zhou and Uchida have analysed the influence of flowability, formwork geometry, and casting time on the eventual fiber orientation [131, 132]. By testing the beams, slabs and walls that were cast with different degrees of flowability and casting time they demonstrated that the superior flowability dictates the final fiber orientation near the surfaces of the formwork and provokes more fibers being oriented parallel to the longitudinal direction of slabs in comparison with inferior flowability. Moreover, they performed the experiments using a transparent acrylic container and fibers with different colors and revealed that fibers were oriented in an oblique direction upward from the bottom vertically regardless of casting time and flowability. In the upper half of the specimen at horizontal surfaces, fibers were oriented in concentric circles longitudinally from the pouring point. Near the bottom of slabs due to shear force, the orientation of the fibers was mainly parallel to the longitudinal direction.

The pouring process is also a significant factor affecting fiber orientation and distribution. Barnett et al. [7] performed the experiments with the testing of round panel specimens that were cast in different ways: at a single point at the center of the panel, at several points around the perimeter of the panel and poured randomly. The fiber orientation and distribution were obtained by electric resistivity and confirmed by x-ray CT technique. It was revealed that the fibers had a tendency to be aligned perpendicularly to the flow direction. Particularly, the specimens that were cast from the centre showed significantly better results than the specimens that were cast by different methods. The alignment of fibers perpendicular to the radius of the panel and increased amount of fibers provided the bridging of the radial cracks that were formed during the mechanical tests producing an increased flexural strength and toughness of the specimens.

Torrijos et al. [115] evaluated the influence of three different casting methods on the fiber orientation and distribution in the steel fiber reinforced self-compacting concrete beams: standard filling method from the center of the mold in accordance with EN 14651, the filling of concrete with a tube from one end of the mold and the vertical filling of the mold. The authors demonstrated that the vertical casting of the beams provides more

homogeneous fiber orientation, however, the contribution of the fibers as reinforcement was notably less efficient than with other casting methods. Moreover, the results showed that the mechanical characteristics of the beams cast by longer steel fibers (50 mm length) were strongly influenced by the casting method.

Figure 4 demonstrates the main factors that have an influence on the fiber orientation distribution.

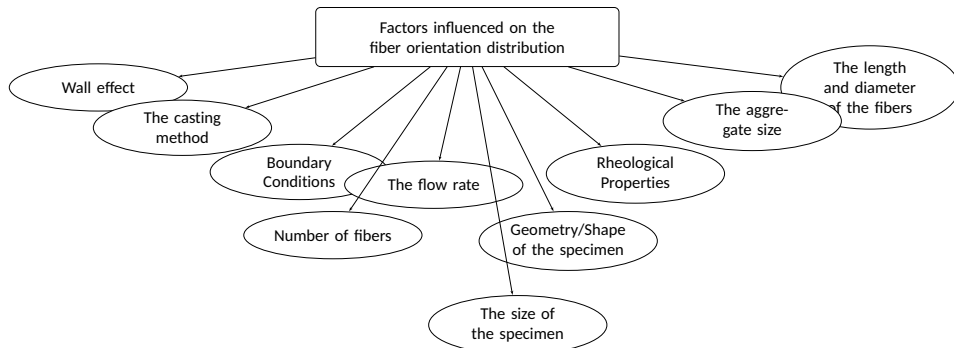


Figure 4: The main factors influenced on the fiber orientation

1.6 Overview of the Methods to Estimate the Fiber Orientation and Distribution

The existing methods to estimate the fiber orientation distribution can be divided into the destructive and non-destructive, and allowed its measurements directly or indirectly.

1.6.1 Manual fiber counting

Manual fibre counting is an easy and reliable technique which does not require any special skills or equipment but allows to determine fiber orientation and distribution [133]. Additionally, this method is suitable to measure the positions of fibers and quite useful for the detailed analysis of the specific zones, crack zone, for instance. However, manual counting method is destructive, based on indirect measurements and highly time-consuming. Moreover, this technique is mostly suitable for steel fiber reinforced concrete with normal volume of hooked-end fibers (up to 80 kg/m^3) [26].

In addition, according to [20], to estimate the fiber orientation is possible by counting the fibre number inside of the cut slice and then the orientation factor can be calculated and the results can be compared.

1.6.2 Orientation factor

Krenchel in 1975 [50] proposed to use the orientation factor that represents a coupled value of the fibre distribution and orientation. In his theory by using the amount of fibers crossing a unit area of cross-section the average fiber spacing can be calculated.

Martinie and Roussel [60] defined the orientation factor as 'fiber efficiency factor' and pointed out that specific values of the orientation factor reflect the direction of fibers relatively to the studied section.

Deeb et al. proposed a new orientation factor [17] that is defined in the vertical cut plane and the determination procedure consists of the calculation of the fibre number in the cutting section and their inclination angle to the cutting plane.

However, the determination of orientation number is rather approximative method and gives only an average orientation when the angle relatively to the projection direction is considered, while the in-plane angle in the cross-section is neglected. According to Herrmann and Eik [41], the orientation distribution function is a reasonable alternative which allows to describe the fiber orientation by spherical polar coordinates, because it is possible to calculate the fiber distribution accurately in three dimensions by using of high-order alignment tensors.

1.6.3 Image Analysis

This method is widely used by researchers due to its repeatability, high accuracy, in addition, it does not require expensive equipment [33, 53, 127]. As an enhancement with regard to the method presented by [33], Eik and Herrmann [22] used the cubes and several slices that increased an amount of the analysed fibers.

Kang and Kim in their research [46] compared the results of the impact of fiber orientation on the tensile behavior obtained analytically and by image analysis technique. Moreover, they considered two cases for the placing directions: placing of the concrete mass parallelly and transversely to the tensile direction. As a result, the authors concluded that the analytical approach to estimate the effect of fiber orientation on the tensile behavior demonstrated satisfactory agreement with the experimental outcomes. In addition, in the case of parallel placing and when fibers were uniformly dispersed, the post-cracking tensile strength is about 50% higher than in the case of the randomly distributed fibers.

Image analysis has similar principle as manual counting of fibers but enable to estimate the fiber distribution and orientation in the cross-section by post-processing of images with special computer software. It allows to analyse the higher amount of fibers and significantly short time [5]. However, image analysis method has several limitations that create opportunity for improvements of this method. Typically, for image analysis technique the concrete sample should be cut into slices or cubes, the surface of the samples should be an adequate quality to provide a reasonable contrast between fibers, concrete matrix and aggregate. For that purpose, special treatment - polishing of the tested surface can be applied. Moreover, during image analysis some issues could be encountered: deformed fibers due to the cutting process and merging of a neighboring fibers due to their close location [127].

1.6.4 Computed Tomography

X-ray Computed Tomography (CT) is an efficient radiographic method that is widely used in medical practice and research. The CT method is applied to obtain 3D visualization images of microstructural characteristics of objects in many scientific fields. Among other applications CT is successfully applied in the field of fiber reinforced cementitious composites due to the advantages of CT method: high accuracy, efficiency and in some cases the non-destructive nature [59, 103]. The CT, such as all radiographic methods, is based on the propagation of short wavelength x-rays or gamma-rays, that passes through solid materials but are partly absorbed by the material and partly reflected [66].

The application of X-ray CT also allows to assess the distribution of polymer fibers with small diameters without complicated sample preparation, because it is based on the difference in the linear X-ray attenuation coefficients of the concrete matrix and reinforcement and does not require other physical properties [70].

The major advantage of X-ray CT is that it allows to assess the individual objects and this method is based on a 3D voxel representation of each fiber located in the sample [98].

Several different areas of applications in the cementitious composites industry are commonly distinguished: the investigation of the internal microstructure, the analysis of fiber reinforced concrete and study of the cracking phenomenon. The investigation of the internal microstructure typically includes the analysis of the homogeneity and the presence of the microdefects, such as porosity, air voids and microcracks, their parameters: positions, size and volume, moreover, interfacial transition zone between the cement paste and aggregates and fibers [84]. Additionally, several research groups have investigated the correlation between the porosity and the durability of the composite materials, behaviour under cyclic fatigue loads [65, 117]. The analysis of fiber reinforced concrete contains a detailed description of the orientation, position, distribution and amount of the fibers made of different materials [6, 42]. The study of the cracking phenomenon examines the main stages of the cracking formation and development during deformation process, as well as, the crack pattern and width and its influence on the durability of concrete [86, 94].

For a long time a serious limitation of using X-ray method and CT scans has been related to the size of specimen, these methods were mostly restricted to the research purposes and laboratory specimens [54].

This method was chosen by us in the current research because it is the only method to get the information about 3D orientation of the individual fibers in the volume, and is described in Section 2.2.3.

1.6.5 Magnetic methods

Several methods based on the electrical properties of the cementitious materials with embedded short steel fibers has been applied by different research groups to analyse full-size structural elements. Non-destructive estimation of fiber orientation distribution can be performed by measuring specific properties of fibers: magnetic properties or inductivity, electrical resistivity and impedance (see below).

Magnetic methods have been represented as a feasible and non-destructive techniques that are able to quantify the presence of steel fibers and allow to estimate accurately both the fiber orientation and distribution [32, 114]. This method is characterized by a proper sensitivity, simplicity in use, since only the placing of the magnetic probe on the surface of the specimen is required, moreover, it guarantees a high degree of repeatability of the testing with a low measurement errors [23, 24].

The Inductive method, presented by Torrents et al. [114], is used to analyse a series of parameters (such as age of concrete, dosage, type and orientation of fibers) and its influence on the measurements and results to determine the amount of fibers.

1.6.6 Electrical resistivity methods

The Electrical resistivity method is a relevant tool for non-destructive estimation of the characteristics of fiber concrete that based on the measurements of electrical resistivity of material which is influenced by the distribution of metallic fibers was applied by Lataste et al. [56].

The Alternate Current Impedance Spectroscopy (AC-IS) is an electrical non-destructive method that allows to estimate the fiber dispersion, shows the sensitivity to fiber orientation, segregation or clustering in the cementitious materials [24]. AC-IS method was described by Ozyurt et al. [74, 75] and Ferrara et al. [24] as a method that is based on the frequency-dependent behavior of cement-based composites with embedded conductive short steel or carbon fibers.

Another research group [124, 125, 126] presented their work that is aimed to explore the use of AC-IS method for the characterization of the microstructure of the cement-based composites with discontinuous conductive (e.g. steel or carbon) fibers or microfibers. Moreover, AC-IS has been applied to evaluate fiber dispersion, including fiber orientation, local aggregation (clumping) and coarse-scale segregation.

The measurement and evaluation of density, distribution and orientation of ferromagnetic or non-ferromagnetic conductive fibers in composite materials by using electrical impedance has been done by Komarkova et al. [49].

However, most of the methods that are based on the electrical resistivity or inductivity are applicable for metallic or carbon fibers only.

1.7 Research Methodology

To achieve the objectives outlined in section 1.2, this research is divided into two main parts: experimental and modeling (numerical simulations).

The experimental part includes:

- Assessment of the fiber orientation by using the method of replacing the fiber-reinforced concrete with Sodium PVM/MA Stabilizer polymer solution.
- Producing several large slabs that were cast of the ordinary and fiber-reinforced self-compacting concrete with different casting methods and after hardening cut

into smaller test beams.

- Carrying out the three-point and four-point bending tests on the beams to analyze the flexural properties and post-cracking behavior, evaluate the peak loads, and the mid-span deflections, moreover, determine the contribution of fibers to the strength and ductility of the test specimens.
- Assessment of fiber orientation distribution by using X-ray Computed Tomography method and further image analysis procedure.

Numerical simulation part includes a series of different casting cases that represent the casting of fresh concrete flow using different filling methods:

- Filling of the formwork according to the standard EN 14651,
- Filling of the formwork from the end,
- Filling of the formwork from the center.

In addition, in this research, several concrete mixture flowabilities were compared: the self-leveling, high-viscous and slump cases.

Figure 5 demonstrates the main activities that were performed during the research. The diagram shows all the tasks and research questions that were planned to be solved.

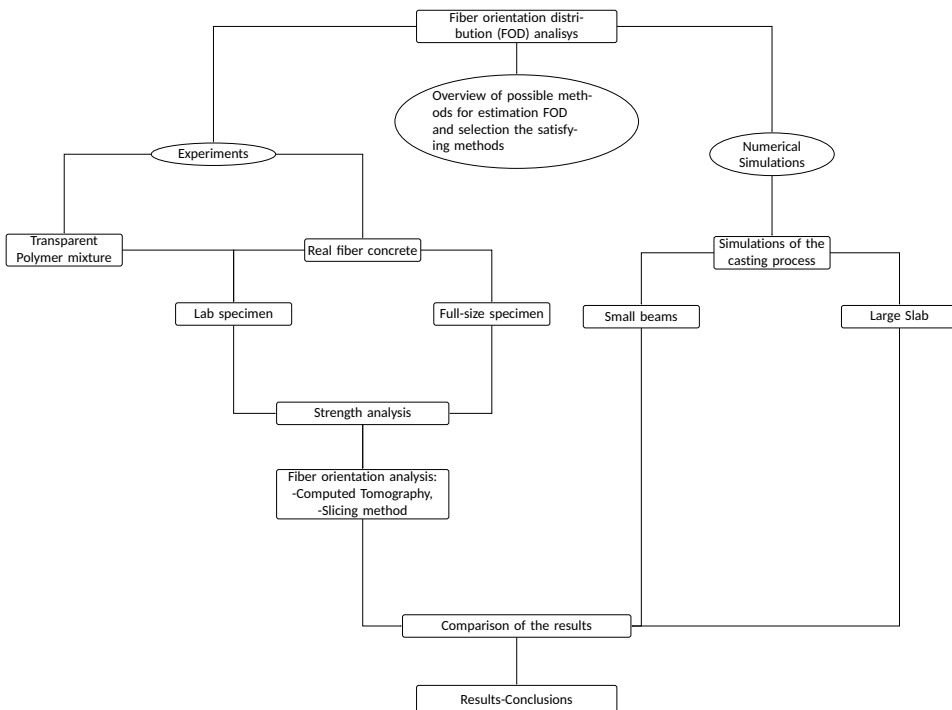


Figure 5: The main objectives and activities of the research.

2 Fiber Concrete Analysis

This chapter provides an overview of Papers I, II and III, and presents three experimental sets, beginning with simulations using concrete mass replacement and moving to the full preparation process for concrete mixtures for two types of construction elements: a plate and a slab. It details the concrete mix ingredients, casting methods, hardening process, and compressive strength testing of hardened concrete cubic specimens. Lastly, the chapter provides a thorough explanation of the bending test procedure for evaluating the flexural properties of the material produced. Key outlines of this chapter:

1. Simulation Experiments (Transparent Replacement Matrix) - Section 2.1
2. Concrete Experiments with the plate (Fiber concrete plate with the dimensions $90\text{ cm} \times 60\text{ cm} \times 20\text{ cm}$) - Section 2.2
3. Concrete Experiments with the large slabs (Ordinary concrete and fiber concrete slabs with the dimensions $400\text{ cm} \times 100\text{ cm} \times 10\text{ cm}$) - Section 2.3

2.1 Simulation Experiments (Transparent Replacement Matrix)

2.1.1 Mixing and Casting Process

Steel Fiber Reinforced Self-Compacting Concrete (SRFSCC) is an opaque composite material and obtaining its internal microstructure and properties is a challenging, time- and resource-consuming process. The existing numerous methods to evaluate the fiber orientation distribution involve a complex procedure that requires specialized equipment and custom software for data analysis.

For this research, we used the method with the replacement of Steel Fiber Reinforced Self-Compacting Concrete with the transparent polymer solution, enabling direct observation of fiber orientation and position during the casting process. This approach, similar to methods described in [9, 100, 131], allows immediate visual inspection of fiber distribution as the transparent mixture was placed into the formwork.

For this experiment, the solution of Sodium PVM/MA Stabilizer was prepared following the manufacturer's guidelines. The experimental solution was composed of three main ingredients: Stabilizer powder, distilled water, and the Sodium Hydroxide (NaOH).

The mixing procedure was performed in two stages. In the first stage, the stabilizer powder was dissolved in the distilled water at room temperature, further the obtained solution was neutralized with NaOH. The experimental solution was intensively stirred to achieve better consistency and homogeneity with the minimum bubbles and air voids. During the second stage, the mixture became noticeably transparent and turned into a viscous gel-like substance.

Finally, after the addition of the necessary amount of NaOH and intensive mixing, the obtained solution reached a pH of 7. Next, the prepared solution was left for several days to achieve the required rheological properties: transparency, uniformity, and viscosity.

Before casting experiments, we tested the flowability of the obtained polymer solution by using the slump flow test [10]. The slump flow test determines two properties: the filling ability which is measured as the diameter of the spread of the mixture; and the viscosity which is characterized by the time that is needed to achieve the diameter of mixture spread equals 500mm. The suitable polymer solution should look like a homogeneous and viscoplastic fluid and demonstrate Bingham-like behavior.

To simulate the fibers, we used wooden sticks because the metal fibers tend to sink too fast in the polymer mixture. After the mixture was prepared, we gradually added these wooden fibers in a proportion of 3 % per mixture volume. The length of the fibers was 50 mm \pm 2.0 mm, and the aspect ratio (fiber length/fiber diameter) was 25.

The main idea behind the polymer casting experiments is to investigate the correlation between the different casting conditions (e.g. formwork surface quality (smooth and rough), the velocity of casting (slow and fast), different pouring points (at the end and the middle of formwork), different casting methods (from the bucket and from the half-pipe)) and fiber orientation distribution experimentally.

Therefore, for this purpose, the following series of simulation experiments with different casting conditions and formwork surface quality was performed:

- Experiment with a rough formwork surface and use a fixed pipe located in the middle of the formwork edge;
- Experiment with a smooth formwork surface and use a fixed pipe located in the middle of the formwork edge;
- Experiment with a rough formwork surface and use a bucket located in the middle of the formwork edge;
- Experiment with a smooth formwork surface and use a bucket located in the middle of the formwork edge;
- Experiment with a smooth formwork surface and use a bucket moving back and forth along the formwork edge;
- Experiment with a rough formwork surface and use a bucket moving back and forth along the formwork edge.

2.1.2 Results: Simulation Experiments (Transparent Replacement Matrix)

Preliminary observations from each experiment, have shown that the fiber orientation is mainly perpendicular to the flow direction while spatial distribution is sufficiently different.

During each experiment, the images of the final fiber orientation distribution were taken and later were subjected to further image analysis. A typical image obtained during the experiment is presented in Table 1.

The main results of the orientational and spatial analysis for the different casting schemes are shown in Figs. 6–9. As can be seen, the fibers are mainly oriented perpendicular to the flow direction. The formwork's surface smoothness appears to have little impact on fiber orientation, whereas casting velocity plays a considerable role. At slower casting velocities, fibers tended to concentrate within a narrow channel.

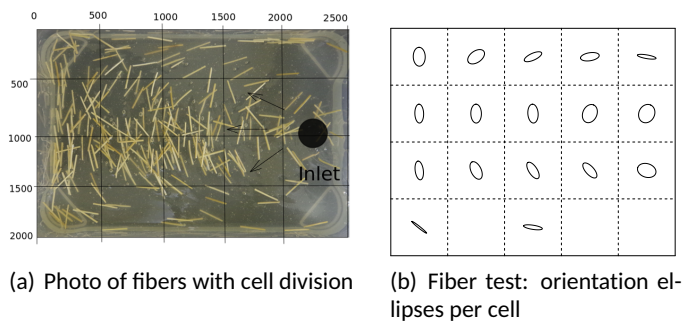
In summary, casting velocity significantly affect fiber spatial distribution but has minimal effect on the fiber orientation. While the roughness of the formwork surface introduces some variations in fiber orientation, it has only a minor effect on spatial placement.

2.2 Concrete Experiments: 3-beams plate and 40-beams slab

This section represents an overview of papers I, II and III that describe the full set of the experiments with concrete specimens. It includes the preparation (casting) of the specimens, Computed Tomography analysis, and the bending test.

Table 1: Matrix of Experiments. The table is adapted from Publication II.

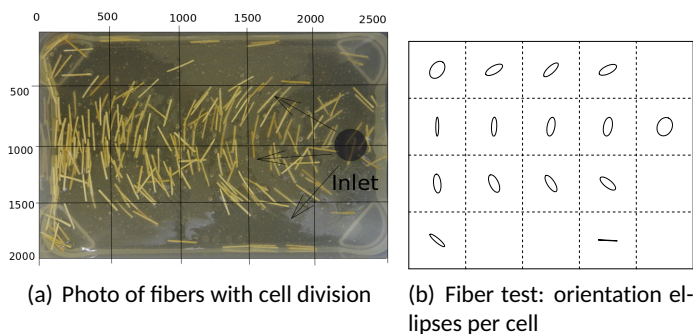
bottom	slow	fast
smooth dry		
smooth wet		
rough dry		



X, Y coordinates	0< x <500	500< x <1000	1000< x <1500	1500< x <2000	2000< x <2500	Number of Fibers in Each Region
0<y<500	18	17	8	8	4	55
500<y<1000	22	31	28	19	8	108
1000<y<1500	20	23	23	7	6	79
1500<y<2000	8	1	4	1	2	16
Number of Fibers	68	72	63	35	20	

(c) Fiber count per area

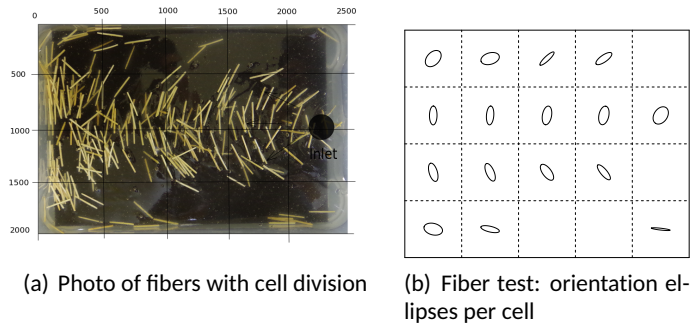
Figure 6: Fiber orientations, smooth bottom, fast casting. The figure is adapted from Publication II.



X, Y coordinates	0< x <500	500< x <1000	1000< x <1500	1500< x <2000	2000< x <2500	Number of Fibers in Each Region
0<y<500	13	6	4	6	2	31
500<y<1000	30	24	33	18	17	122
1000<y<1500	18	22	11	14	1	66
1500<y<2000	5	-	2	4	-	11
Number of Fibers	66	52	50	40	20	

(c) Fiber count per area

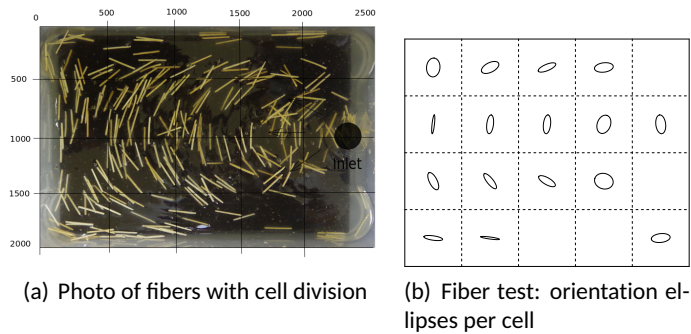
Figure 7: Fiber orientations, smooth bottom, slow casting. The figure is adapted from Publication II.



X, Y coordinates	0 < x < 500	500 < x < 1000	1000 < x < 1500	1500 < x < 2000	2000 < x < 2500	Number of Fibers in Each Region
0 < y < 500	13	8	4	4	1	30
500 < y < 1000	29	24	26	22	14	115
1000 < y < 1500	32	11	17	12	1	73
1500 < y < 2000	4	4	1	0	5	14
Number of Fibers	78	47	48	38	21	

(c) Fiber count per area

Figure 8: Fiber orientations, rough, slow. The figure is adapted from Publication II.



X, Y coordinates	0 < x < 500	500 < x < 1000	1000 < x < 1500	1500 < x < 2000	2000 < x < 2500	Number of Fibers in Each Region
0 < y < 500	17	17	14	12	4	64
500 < y < 1000	13	25	22	18	12	91
1000 < y < 1500	17	20	15	14	2	68
1500 < y < 2000	8	7	2	1	4	22
Number of Fibers	55	69	53	45	22	

(c) Fiber count per area

Figure 9: Fiber orientations, rough bottom, fast casting. The figure is adapted from Publication II.

For this study, several experimental specimens were prepared. One small plate was cast of SFRSCC by using the bucket and half-funnel as the casting method, and later the hardened plate was cut into three beams and two large slabs were cast of self-compacting ordinary concrete and SFRSCC concrete by using the moving bucket as a filling method that was moved in the longitudinal direction. The fiber orientation distribution of the beams was analysed by Computed Tomography analysis. To determine the strength and other mechanical properties, the beams were subjected to the bending test.

2.2.1 Materials and Casting Process

A mixture of self-compacting concrete was prepared according to a recipe from a manufacturer. An example of all the ingredients of the mixture is presented in Fig. 10.



Figure 10: The ingredients of the SFRSCC mixture.

Hooked-end steel fibers were gradually added to the self-compacting concrete mixture and thoroughly mixed. An example of the used steel fibers is presented in Fig. 11. The fiber volume ratio was 0.5%. The fiber length and the fiber diameter was 60 mm and 0.75 mm, respectively; the fiber properties are summarized in Table 2.

Table 2: Data of used fibers: Semtu WireFib 80/60; amount used 25 kg/m^3 , The table is adapted from Publication I.

length:	60 mm
diameter:	0.75 mm
aspect ratio:	80
number of fibers/kg n.	4600
tensile strength:	>1000 Mpa
coating:	uncoated
steel quality:	EN 10016-2 C9

The properties of the fiber concrete are given in Table 3. A slab of steel fiber reinforced self-compacting concrete (SFRSCC) of dimensions ($L \times W \times H$) $90 \text{ cm} \times 60 \text{ cm} \times 20 \text{ cm}$ was produced in this experiment. The slump-flow test, performed according to [10] had shown a diameter of 75 cm. The filling procedure was performed from a hopper positioned in the middle of the edge of the formwork. The point of the slump was located at one of



Figure 11: Hooked end steel fibers.

the 60 cm edges, with a 10 cm wide inlet, and the casting flow was performed along the length of the plate, see Fig. 12. The formwork was sprayed with a thin layer of oil before casting to simplify the further demolding process. The lifting anchors were added on one side of a slab to simplify the lifting of the specimen after hardening.



Figure 12: Casting of a small plate using a bucket and half-funnel. The figure is reproduced from Publication II.

After hardening the slab was cut into three beams of $90\text{ cm} \times 19.5\text{ cm} \times 19.5\text{ cm}$ using a diamond saw, as indicated in Fig. 13. The arrows represent the flow direction of concrete.

The process of the preparation of two large slabs was identical to the aforementioned described procedure. All materials were supplied by the manufacturer AS Betoonelement and used to produce the self-compacting concrete (SCC) specimens. The components of the mixture are presented in Table 4. The recipe of the testing mixtures was developed

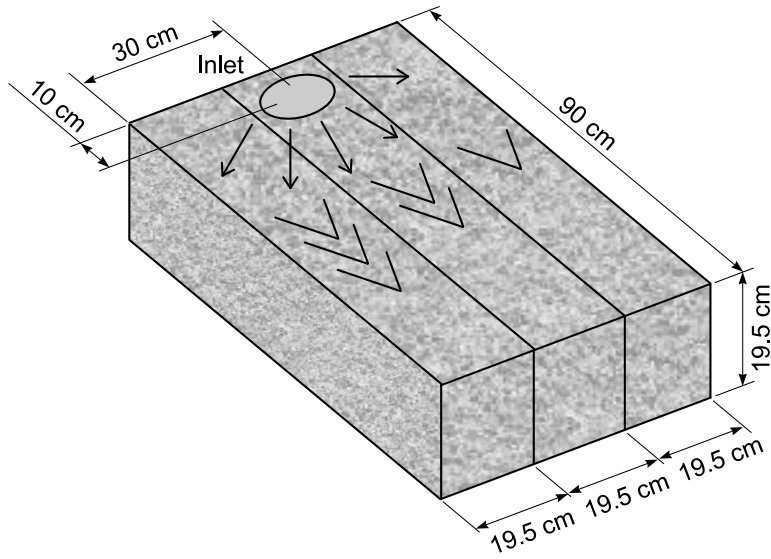


Figure 13: Layout of beam-cutting of small plate. The figure is reproduced from Publication I.

Table 3: Fiber concrete data. The table is adapted from Publication II.

Casting day		30.09.16
Slump (diameter) of concrete		75 cm
Temperature		20°C
Density and Compressive strength at 3 day	2470 kg/m ³	48.2 MPa
Density and Compressive strength at 7 day	2460 kg/m ³	61.1 MPa
Density and Compressive strength at 28 day	2470 kg/m ³	71.2 MPa
	2470 kg/m ³	67.5 MPa

by the manufacturer, according to their standard procedure of producing SCC. All constituent materials were mixed in a production-line mixer with a capacity of 1-2 t. To determine the required consistency and viscosity of SCC the obtained mixture was subjected to the slump-flow test, according to [10]. The spread of the slump was 70 cm. For these experiments, two different mixtures were produced: an ordinary (plain) self-compacting concrete (SCC) and short steel fiber reinforced self-compacting concrete (SFRSCC).

Table 4: Composition of SCC mix, amount mixed: 1 m³. The table is adapted from Publication III.

Cement (kg)	330
Sand (0-2mm) (kg)	398
Sand (0-4mm) (kg)	505
Crushed Stone (2-5) (kg)	336
Crushed Stone (8-11) (kg)	539
Filler (kg)	80
Admixture (kg)	5.1
Water (kg)	175
Fibers (SFSCC only)(kg)	50
extra water (SFSCC only)(kg)	~ 10

Two film-coated plywood molds were previously prepared by covering the bottom with the plastic foil. Further, the obtained mixture was poured into the molds by using the moving bucket as a filling method that was moved in the longitudinal direction.

The second mixture (SFRSCC) had the same mix proportions and was prepared similarly to the first one (SCC), with the exception that during the mixing process, the hooked-end steel fibers were added. The characteristics and physical properties of steel fibers are presented in Table 5. Steel fibers were gradually added and the mixture was mixed for a couple of minutes to ensure the proper uniformity and to avoid the clustering or balling of the fibers during the mixing and filling processes. The dosage of the fibers was 1 % per concrete volume. For the SFRSCC mixture, the water dosage was slightly increased to achieve the required rheological properties. The spread of the slump was 65 cm. The casting procedure was identical to the SCC mixture.

Table 5: Data of the steel fibers, according to [91]. The table is adapted from Publication III.

Manufacturer	Severstal Metiz
Model	Hendix prime 75/52
type	hooked end
length, mm	52 ± 2.0
diameter, mm	0.75 ± 0.04
hook length, mm	2.0 – 1.0 / + 2.0
hook height, mm	2.1 + 0.5 / – 0.0
bend angle, degrees	40 ± 5
tensile strength, MPa	1500
Elastic modulus, MPa	≥ 190000
number of fibers per kg, pcs.	~ 5545

To ensure a flat surface of the slabs the leveling procedure with a roller was performed immediately after the casting process in both cases. Finally, the lifting anchors were em-

bedded into the fresh concrete to provide the transportation of the slabs safely after hardening.

Full casting process was recorded by a camera for further analysis. Then both slabs were stored in the manufacturing hall at room temperature until hardening according to [11].

After hardening and demoulding the slabs had dimensions of $(L \times W \times H)$ 400 cm \times 100 cm \times 10 cm. The slab of SCC has been cut into 10 beams of size 100 cm \times 10 cm \times 10 cm. The slab of SFRSCC has been cut into 40 beams of size 100 cm \times 10 cm \times 10 cm. A principal layout of the specimens cut out of the cast slabs is presented in Fig. 14. The cutting of both slabs was done twenty days after the casting by a diamond saw.

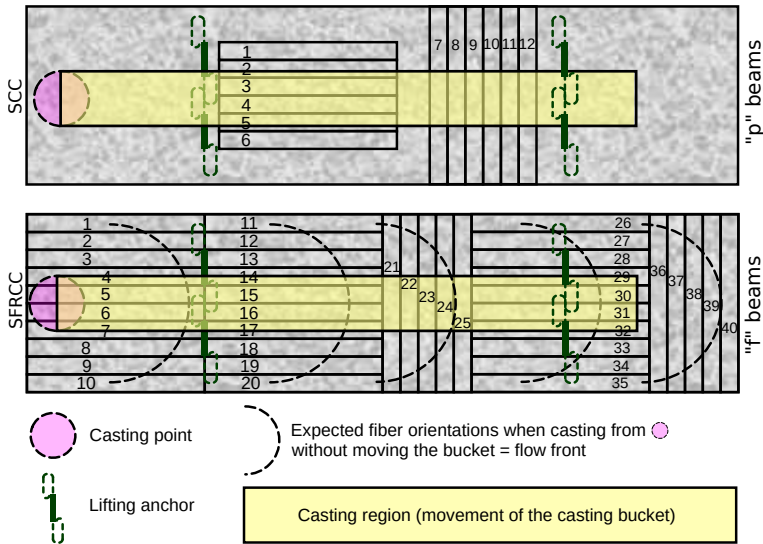


Figure 14: Beam layout of specimens cut out of the cast plates. The figure is reproduced from Publication III.

2.2.2 Results of the compression tests

Additionally, several cubic testing specimens with dimensions of 10 cm \times 10 cm \times 10 cm were taken out of each mixture and separately cast to perform the standard compression tests.

Compressive strength tests were carried out on the same cubic specimens according to [12].

The results of the compression tests are presented in Table 6. As can be seen from the table, ordinary concrete without fibers shows higher compressive strength at all ages compared to fiber-reinforced concrete. This difference can partly be explained by the higher water-cement ratio used in the fiber-reinforced mixture to achieve the proper workability.

Table 6: Results of compression tests for SCC and SFRSCC. The table is adapted from Publication III.

	age at test in days	4	4	4	7	7	7	28	28	28	28	28	28	28	28	28	28
SCC	ρ in kg/m ³	2330	2330	2330	2310	2340	2370	2380	2380	2370	2380	2360	2380	2390	2380	2380	2390
	$\bar{\rho}$ in kg/m ³		2330			2340						2379					
	stdev in kg/m ³		0			30						9					
	$\sigma_{u,c}$ in MPa	55.4	54.5	52.3	54.7	54.5	56.8	67.6	66.4	70.9	66.3	68.8	69	69.9	72.1	66	69
	$\bar{\sigma}_{u,c}$ in MPa		54.1			55.3						68.6					
	stdev in MPa		2			1						2					
SFRSCC	ρ in kg/m ³	2350	2350	2370	2380	2360	2370	2390	2370	2380	2380	2410	2390	2370	2390	2360	2380
	$\bar{\rho}$ in kg/m ³		2357			2370						2382					
	stdev in kg/m ³		12			10						14					
	$\sigma_{u,c}$ in MPa	45.1	45	44.5	46.1	45.3	45.1	55.7	55	57.2	58.1	57.3	57.4	56.9	55.9	58.1	54.9
	$\bar{\sigma}_{u,c}$ in MPa		44.9			45.5						56.6					
	stdev in MPa		0			1						1					

2.2.3 Computed Tomography and Image Analysis

For this research the CT method has been applied in order to obtain complete information about fiber orientation distribution in both, before and after the bending test, and by that, to verify the hypothesis that fibers are aligned longitudinally parallel to the main axis of the beam (due to the wall effect) and oriented more randomly in the disturbed zones (close to the pouring points and in the areas of the bucket movement). In addition, another purpose of this study is to analyse the microstructure of the specimens and its correlation with the failure process (i.e. to determine the weakest cross-section caused by the non-uniformity of the aggregate, the presence of air voids, or random fiber orientation).

The method to estimate the fiber orientation distribution by X-ray CT analysis is similar to the one, described by Pastorelli [76].

This chapter describes the non-destructive analysis procedure conducted using an X-ray CT scanner, with data acquisition, filtering, and analysis performed by using custom-developed software described by Pastorelli in the doctoral thesis [77].

The CT analysis includes the following steps:

- Vesselness filter: can be used in some cases to compensate cupping effect (it is concerning the radial grey level variation, when there is no distinct threshold between cement and fibers);
- Threshold filter is applied according to the gray level, and after that, the binary volume image was obtained where fibers are depicted with white color and the rest of the matrix - black;
- Label-map filter is applied to label each voxel of the object (fiber) by a different unique number;
- Removing of the small objects that do not represent any significant features;
- Gauss filter is applied to a binary volume to get a smooth transition from fiber to background;
- Hessian filter is applied to calculate the likeliness that a voxel belongs to a cylindrical object meaning that for each voxel we receive a vector that points along the local cylinder axis
- Analysis of each object:
 - a histogram is generated from the orientation data, if there is more than one high peak, it indicates the presense of multiple touching fibers
 - * Gauss filter is applied to orientation histogram for smoothing
 - * Label-map filter is applied to categorize the orientation histogram
 - * Voxels that belong to orientations of different peaks will be assigned to new volume objects
 - if histogram has a single peak, this peak gives the direction of main fiber axis (one vector per fiber object)
- Calculation of orientation tensor of all fibers based on the main direction vectors obtained from the analysis.

The hardened three beams have been scanned using a GE Medical Systems “Discovery STE” scanner, and the reconstruction of the volume was performed with 0.6 mm resolution. Unfortunately, the size of the beams (cross section is 19.5 cm × 19.5 cm) was slightly above the attenuation limit for this scanner, and it was only possible to identify clearly steel fibers that were close to the surfaces of the beam, not in the inner area. The bottom layer of the beams was thresholded and the 3D volume of fibers can be seen in Fig. 15.

The fiber orientations distributions were estimated using a measurement tool ImageJ with manual identification of the fibers. Automatic analysis of fibers was complicated due to the low resolution of the scanner, the large sample size compared to the fiber diameter had caused the noise and the low contrast of aggregates and fibers (and artifacts together with a strong cupping effect). Visually the fiber orientations correspond with the expectations from a casting into a slippery formwork [42, 44, 134]. The position and orientation analysis of the data obtained by CT was carried out using custom scripts developed in R that enabled to calculation of the orientation tensor and its eigenvalues and eigenvectors and, eventually, to plot [38] the orientation ellipses.

Figure 15 demonstrates the results of the spatial distribution and orientation analysis. As can be seen, the orientation distribution shows a resemblance to the one predicted for a slippery formwork [44]. Casting point was at the top of the middle beam. Particularly, the fibers are mostly oriented parallel to the flow front, meaning perpendicular to the flow velocity.

Post-processing of the CT scan images was performed by using an open-source software *3D Slicer* developed for visualization, segmentation and analysis of medical data [80]. *3D Slicer* allows us to visualize the 3D volumes and, by applying specific thresholds, to distinguish the fibers from the cement paste and aggregate. In case of analysis of the specimens with the fracture, *3D Slicer* enables to extraction of the crack zone and visual detection of the bridge or the rupture of the fibers.

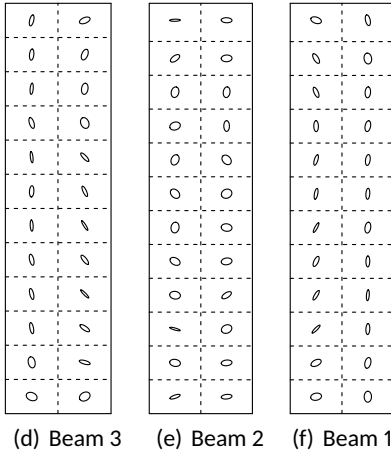
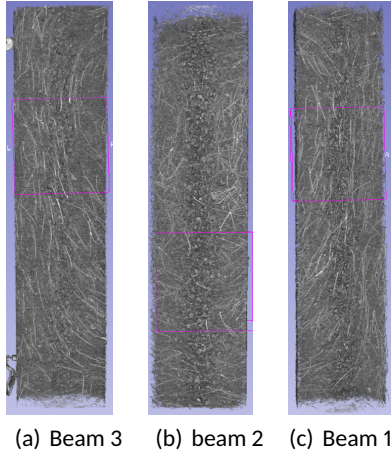
However, to obtain the exact positions and orientation of the fibers within each volume image, a specific image analysis software is needed. But the *3D Slicer* images with the extracted fibers can serve as a referencing image to compare with the extracted fibers after applying image analysis software, as shown in Fig. 16.

2.2.4 The bending test set-up

The bending test is the primary technique to determine the mechanical and post-cracking characteristics of concrete materials. This test allows to define the load of the first crack appeared, the peak load, the mid-span deflections, and to evaluate the contribution of the fibers in the post-cracking behavior of the material. Among the main mechanical properties that can be obtained during the bending test are flexural strength, toughness (or energy absorption), residual flexural strength, and post-cracking behavior (hardening or softening).

In different countries to obtain the aforementioned characteristics the concrete specimens are subjected either to a three-point bending test with the notch in the middle of the specimen or four-point bending test. Three-point bending test with the notch is described in [13]. In this case, the stress concentrates under the loading point and the crack will appear on the tip of the notch in the mid-span under the loading point. This testing method provides the determination of the crack mouth opening displacements, residual flexural tensile strength, and limit of the proportionality.

Three point bending test was carried out on three fiber-concrete beams with dimensions 90 × 19.5 × 19.5 cm using a *Zwick Roell z250* strength testing machine. The distance between two vertical supports *A* and *B* was $L = 0.78$ m, each support is positioned 6 cm



21	9
15	14
7	9
19	14
15	7
15	13
16	11
14	13
12	14
11	15
9	14
4	5

7	12
13	13
21	19
14	18
16	17
16	20
16	14
13	16
13	14
9	18
11	12
9	7

18	15
18	11
6	9
13	11
11	9
18	8
14	10
17	15
14	12
13	15
13	12
7	8

Figure 15: Bottom layer of the beams in x-ray CT. The figure is reproduced from Publication II.

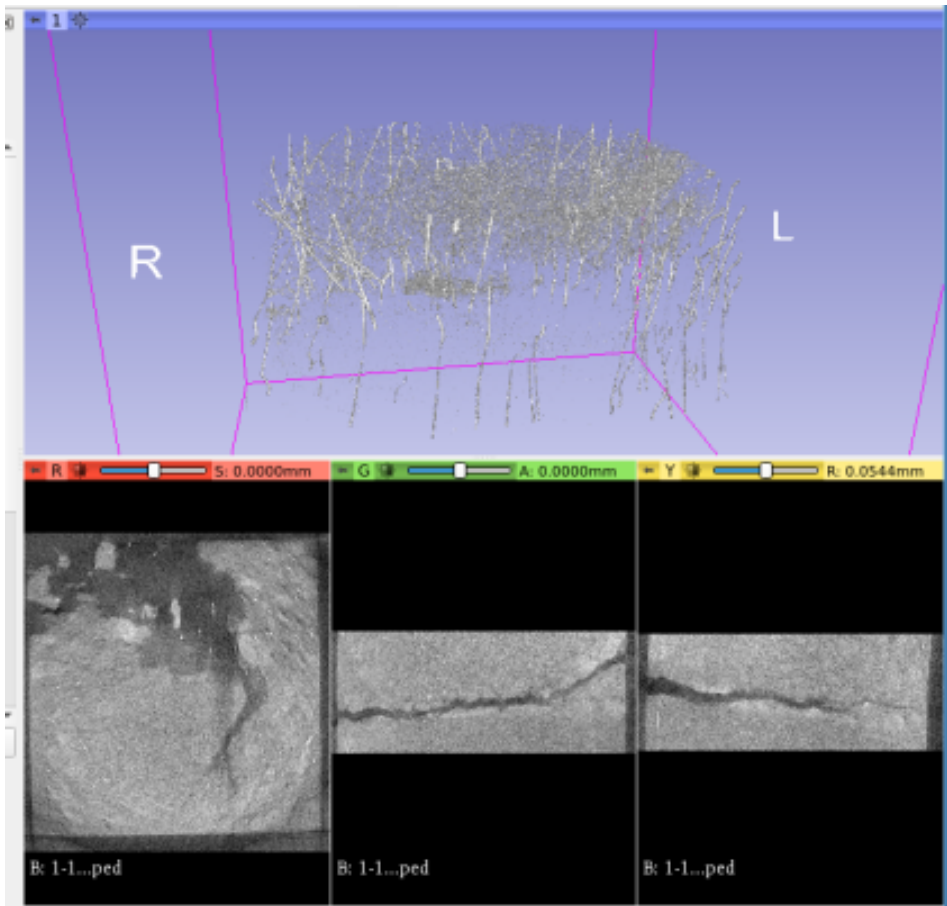


Figure 16: An example of the beam with extracted fibers in 3D Slicer.

inward from the end of the beam, Fig. 17. The point load F was applied at the middle of the cross-section C .

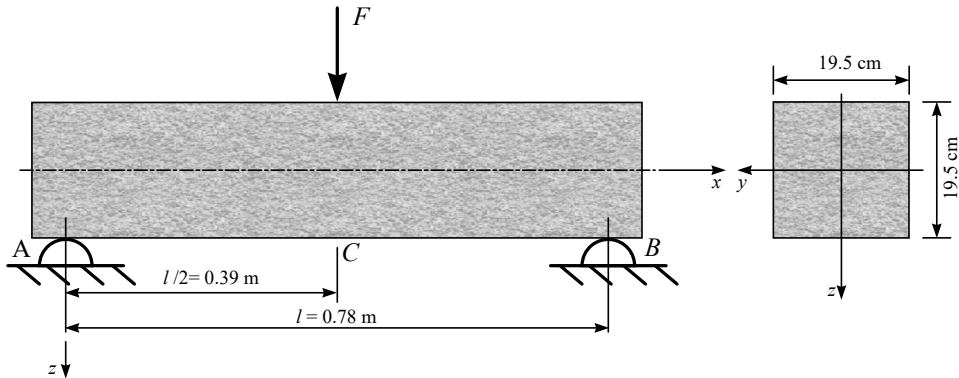


Figure 17: Bending test setup. The figure is reproduced from Publication I.



Figure 18: Photo of the bending test showing a beam sample in the testing machine with the frame for displacement measurements and displacement sensors. The figure is reproduced from Publication I.

However, one of the key objectives of this research is to analyse the influence of the fiber orientation distribution on the strength of the material and other mechanical properties. Therefore, using a three-point bending test with a notch would be less representative in this context, as the location of the crack would be predetermined by the notch. In contrast, the four-point bending test distributes stress over a larger area, allowing cracks to

form in the weakest cross-section, which is influenced by the anisotropic nature of the fiber orientation distribution.

Thus, for the testing of the beams that were cut out of the large slabs, it was reasonable to choose a four-point bending test without the notch. This test was carried out on a universal electro-mechanical/hydraulic testing machine *EU100*. To obtain the measurements of the load and displacements a *HBM Quantum MX840A* universal amplifier module that connected to the testing machine was used. Obtaining and visualization of the data were performed by the *CatmanEasy DAQ* software. The testing set-up, equipment for the four-point bending test, and the specimen mounted in the testing machine are depicted in Fig. 19.



Figure 19: Four-point bending test setup with a beam sample. The figure is reproduced from Publication III.

In this series of bending tests, the testing beams were maintained on two metal roller supports at the edges. Two thin metal plates were located on the top of the roller supports in order to avoid stress concentration. The distance between roller supports (i.e. the span length) was 90 cm, and 5 cm from each supports to the edges of the beams. All testing specimens were precisely centered with the support of the testing machine with accuracy ± 2.0 mm.

The load measuring device with the load cell *HBM U10M* has a capacity of 50 kN and an accuracy of 0.02 to 0.05 kN. The load was transferred through the steel bar connected with two metal cylinders of 1.5 cm diameter, positioned between two metal plates of size 2 cm \times 1 cm and a length of 15cm in order to ensure the stability and evenly distribute the loading force. The loading points were located at a distance 30 cm from each other (approximately 1/3 of the total range). The peak force for all specimens varied in the range of 6-8 kN.

To record the vertical displacements under the load, the displacement sensors *HBM WI/10mm-T* with accuracy ± 1.0 % were applied. The displacement sensors were located

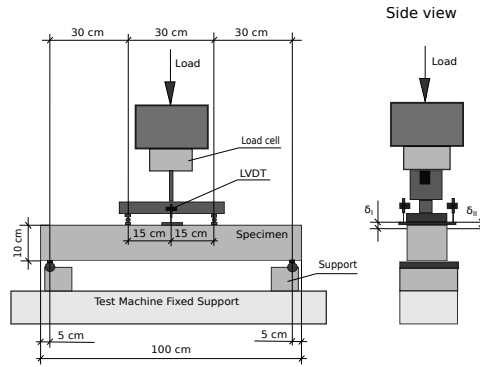


Figure 20: Sketch of the bending test showing a beam sample in the testing machine with the frame for displacement measurements and displacement sensors. The figure is reproduced from Publication III.

on a metal plate at half-length on the top surface of the specimen and fixed on two opposite sides of the specimen (δ_l, δ_r). The displacement transducers have to be accurately mounted in order to exclude any rotation. The schematic illustration of the displacement transducers is shown in Fig. 20.

The typical output file from the bending test results includes the data of time, load and displacements in .csv format.

2.2.5 Results

The obtained force-displacement diagrams are presented in Fig.21. The maximum force value before cracking is $F_1 = 45.36$ kN, $F_2 = 44.06$ kN and $F_3 = 43.18$ kN for beams 1, 2, and 3, respectively. To calculate the maximum bending stresses in a cross-section the formula $\sigma^{M_y} = \frac{M_y}{W_y}$ is used. The bending moment in the cross-section C is given by $M_y = FL/4$ and the section modulus is given by $W_y = (wh^2)/6$.

Flexural fracture strength (in MPa):

$$\sigma^{M_y} = \frac{M_y}{W_y} = \frac{FL}{4} \frac{6}{w * h^2} \quad (1)$$

$$\sigma_{fs} = \frac{1.5 * F * L}{w * h^2} \quad (2)$$

$$(3)$$

with F maximum force at cracking (in N) , L length between supports (in mm), w the width of the sample (in mm) and h the height of the sample (in mm).

For a cross-section of 19.5×19.5 cm the maximum stress is $\sigma_1^{M_y} = 7.16$ MPa, $\sigma_2^{M_y} = 6.95$ MPa, $\sigma_3^{M_y} = 6.81$ MPa for beams 1, 2, and 3, respectively, see Tab. 7. Over the three tests we obtain the averaged maximum stress $\bar{\sigma}^{M_y} = 6.97$ MPa.

Analyzing the results of the performed bending test with the number and fiber orientation in the bottom layer, the following can be observed:

- the peak strength shows no obvious correlation with the amount of fibers in/near the crack area,

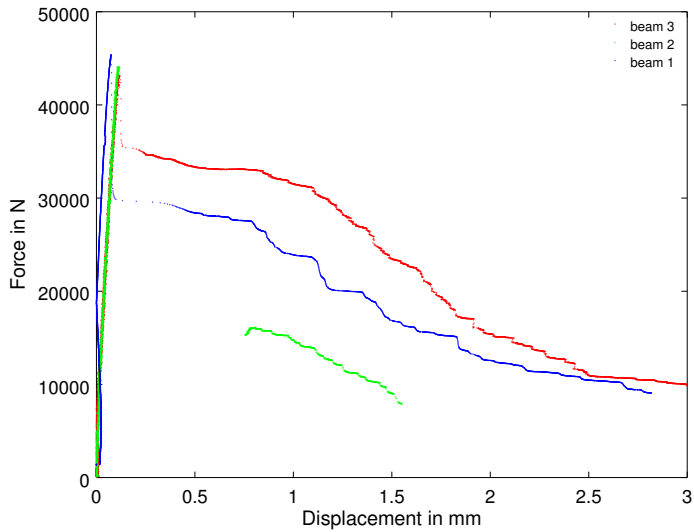


Figure 21: Force displacement curves for the three-point bending test of the three beams. The figure is reproduced from Publication I.

Table 7: Flexural fracture strength of the three beams; the average was $\bar{\sigma}^{M_y} = 6.97$ with a standard-deviation of 0.18. The table is adapted from Publication I.

Beam	max. force in N	FFS in MPa
1	45364.7	7.16
2	44058.4	6.95
3	43178.6	6.81

- although beam 2 has the highest amount of fibers in the cells next to the crack, it demonstrates the weakest post-cracking behavior,
- despite having the highest number of fibers, their orientations are the least beneficial in beam 2, this seems to point out the correlation with the post-cracking behavior.

Considering both fiber orientation distribution and fiber amount, one can conclude: beams 1 and 3 have both analogous fiber orientation distribution, and beam 3 has a higher fiber amount, beam 3 also demonstrates the best post-cracking behavior of the three beams.

The load-displacement diagrams obtained by four-point bending tests for 40 beams, taken out from a large slab, are presented in Fig. 22. As can be seen from the diagrams, the variation of post-cracking behavior between different beams is large. Moreover, all beams, that contain the fibers, demonstrated different levels of ductility and showed improved fracture behavior in comparison with self-compacting concrete beams without fibers.

In other words, all 40 beams demonstrated a range of post-cracking behavior that includes strain-hardening and strain-softening behavior. We can clearly distinguish three groups of post-cracking behavior, see in Fig. 22.

In case of strain-hardening behavior the max load is higher than the load at the first crack; and in case of strain-softening behavior the residual strength is only quarter of the load at the first crack. Fig. 23 demonstrates the load-displacement diagrams of the beams with different post-cracking behaviour.

The correlation between the position of the beam in the plate and the post-cracking behavior can be noticeable, namely the beams that were located at the edges of the plate have shown the strain-hardening post-cracking behavior, while the middle (central) beams have introduced the weak strain-softening post-cracking behavior, see in Fig. 24.

Figure 25 demonstrates the shape and position of the cracks associated with the main cracking of the beams. The cracks are replicated for all 40 beams. In some beams, we can observe the multiple cracking behavior. Centerline beams numbered 6, 16, 21–25, 31, 36–40 are highlighted using the colored backgrounds and bold arrows. A visual inspection of the obtained cracks, especially in beams 11–20, seems to have a tendency that the stronger beams, positioned at the edges of the slab, demonstrate the cracking near the upper loading points of the four-point bending machine shown in Fig. 20. This may be explained by the interaction of bending moments and shear stresses. The normal force introduced by the support of the bending machine simply *cuts* through/pushes itself into the material. This phenomenon is less observable in the other regions of the slab.

These results are in accordance with expectations due to fiber orientation: the edge beams should have mostly longitudinal in the direction of the tensile stresses (parallel to the walls) due to the wall-effect, while the middle (central) beams introduced more chaotic fiber orientation due to the reason that the middle beams were mostly located on the way of the casting bucket. Thus, the mechanical properties of fibered concrete are highly sensitive to the casting procedure. Therefore, it is important to provide special care to design the casting methods to ensure uniform and favorable fiber orientation distribution.

2.3 Investigation of the Standard testing method according to EN14651

The main purpose of carrying out these experiments is to investigate the influence of the position of the beam during the bending test according to the Standard EN14651 [109].

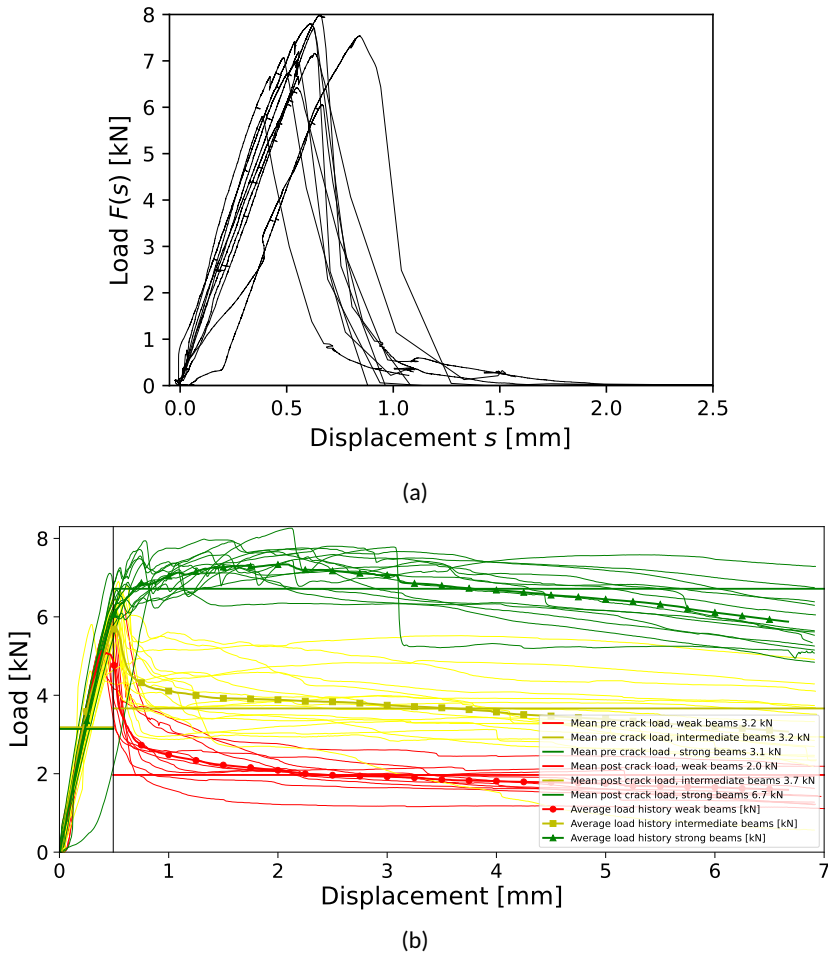


Figure 22: Load-displacement diagrams for the tested beams; (a) SCC, (b) SFRSCC. The figure is reproduced from Publication IV.

Namely, the standard requires the rotation of the samples 90 degrees along the longitudinal axes of the samples.

For this purpose, we carried out the set of experiments on the bending test of four beams. The concrete mixture was identical for all four beams. However, due to the limited amount of the prepared concrete mixture in the mixer, the mixture was prepared twice. Therefore the obtained beams were named according to the prepared mixtures: namely, Beam1-1 and Beam1-2 were poured from the first mixture, and Beam2-1 and Beam2-2 from the second prepared mixture. The casting method of all the beams was also identical, and the filling of the formwork was done from the center of the formwork. The dimensions of the testing beams were ($L \times W \times H$) 620 cm \times 15 cm \times 15 cm.

The three-point bending test was carried out according to the standard [13]. However, before the bending test two beams were rotated 90 degrees, as the standard requires, and thereby the load was applied transversely to the formwork filling direction, while two other beams were tested without the rotation, namely, on the casting side. To exclude the dependence on the prepared mixtures, we chose the different testing methods pairwise,

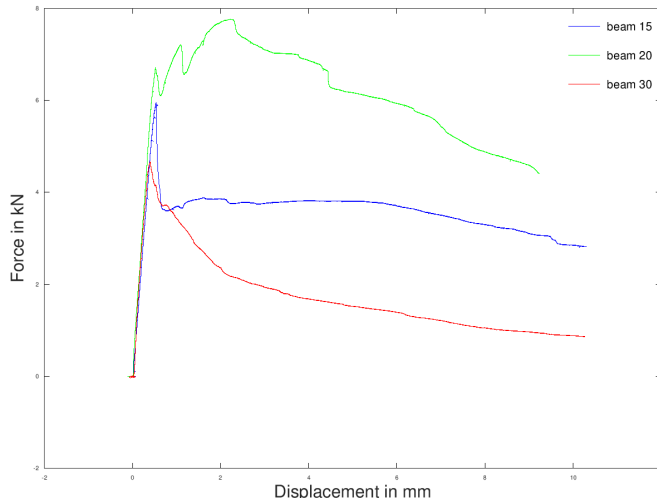


Figure 23: The diagrams of three beams with different post-cracking behavior: strain-hardening, intermediate and strain-softening.

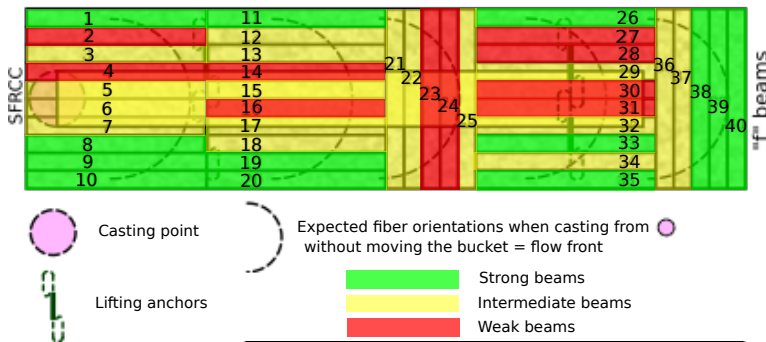


Figure 24: The correlation between the beam position in the plate and the post-cracking behavior.

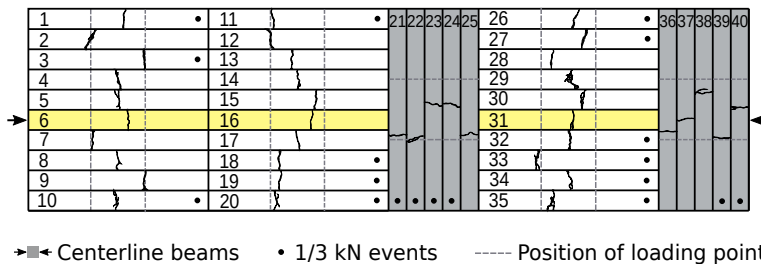


Figure 25: Positions and shapes (bottom view) of the cracks sustained at the main cracking are shown using the realistic crack patterns. The figure is reproduced from Publication IV.

which means Beam1-1 and Beam2-1 were rotated during the bending test, but Beam1-2 and Beam2-2 were tested on the casting side.

The results of the bending test for all four beams are presented in Fig. 26.

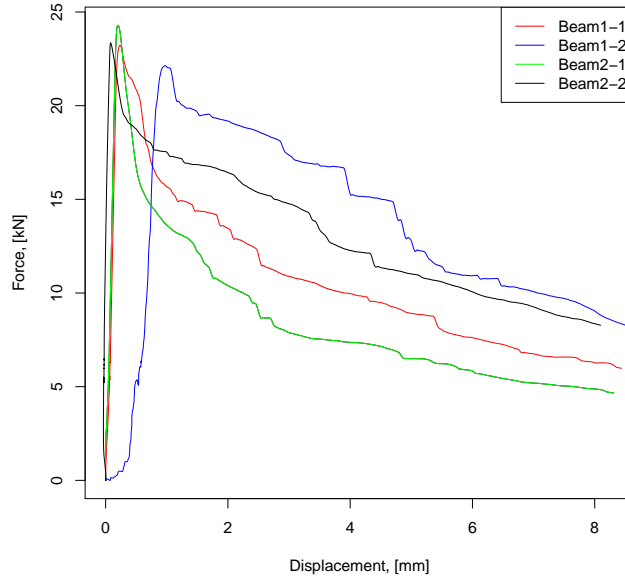


Figure 26: Force-Displacement Diagram of four beams that were tested according to EN14651 with and without rotation of the testing beams.

The results show some similarity between two beams that were tested by identical method, see Figs. 26. At first glance, it can be seen that the blue curve is shifted to the right. This curve corresponds to Beam1-2, which was not rotated before the bending test. This may be due to the unevenness of the test surface, indicating that it makes sense to rotate the specimen to provide two smooth parallel surfaces and better contact with the testing machine, leading to more accurate results.

The obtained bending test results revealed the similarity of the force-displacement diagrams according to the test method. In particular, beams in which the force was applied parallel to the formwork filling direction demonstrated slightly better post-cracking behavior compared to beams that were tested with a force applied transverse to the formwork filling direction. This leads to the conclusion that the rotation of the beam before bending test has a great influence on the measured value of the mechanical properties of cementitious composites.

3 Numerical Modeling of SCC and FC

Recently, numerical simulations have become one of the most popular topics across varying engineering fields, including medicine, building technologies, automotive, and aerospace industries.

Numerical simulations in building materials technology are a quite powerful tool that helps to analyze the rheological properties and optimize the production process of high-quality cementitious materials. The main advantages of implementation of numerical simulations in the production of advanced building materials are cost-savings and significant simplification and in some cases even replacing the planning and experimental part of the research and development stages.

The most widely used applications for numerical simulations are (see below): simulations of the standard tests, the simulation and optimization of the mixing process, the casting and placement optimization, the simulation of the tests in a hardened state (such as bending tests).

The first attempts to simulate the slump test and other concrete flow problems using the Finite Element Method were performed by Tanigawa and colleagues in Japan in 1986 [107]. Viscoplastic Suspension Element Method (VFEM) to model a homogeneous continuum by Tanigawa et al. [106, 108] and Viscoplastic Suspension Element Method (VSEM) to model a non-continuum by Odaka et al. [73] were presented. The set of laboratory experiments and numerical simulations of the slump test, JRing, and L-box was carried out using a Distinct Element approach by Petersson and Hakami [78, 79] where the concrete flow was treated as two phases: mortar and the particles of aggregate with different sizes and shapes. Moreover, the Distinct Element Method for modeling of fresh concrete that transforms to a hardened state was applied by [67, 92]. Another numerical study of self-compacting concrete flow in L-box test with different implemented rheological models that provided the contribution to the consistent modeling approach was carried out by Modigell et al. [71].

The simulations of the formwork filling process with the self-compacting concrete flow in the slump flow test and the L-box test based on Bingham rheological parameters were carried out by Thrane and co-authors [111, 112, 113]. Results have shown that the rheological properties of the mixture and flow pattern strongly increase the risk of blocking and dynamic segregation.

Two types of approaches to simulate the self-compacting flow were presented by Gram and coworkers [29, 30, 31]. The first approach describes the development of the Distinct Element Method based on the modeling of the movement and interaction of spherical particles including particle contact forces and conglomerated superparticles. The second approach represents a homogeneous fluid model using Computational Fluid Dynamics. Vasilic et al. [116] presented a detailed review of the existing numerical simulation methods and main challenges during the modeling of fresh concrete flow, in addition, application fields and future perspectives for using numerical tools are discussed.

Roussel et al. [89] defined two benchmark flows for concrete flow prediction and compared the results of concrete flow predictions with the results obtained by other research teams around the world. Moreover, Roussel et al. [90] presented a detailed review of the available numerical modeling tools to optimize the material properties and manufacturing process.

The method presented by Martys and Ferraris [61] is based on the visualization of the rigid body motion (concrete particles) in the fluid using Dissipative Particle Dynamics (DPD). Martys et al. has presented several computational approaches based on DPD [63], Lattice Boltzmann simulations [62] and Smoothed Particle Hydrodynamics (SPH) [64].

Wallevik has used numerical simulations to investigate the rheological relationships between concrete and mortar, the thixotropic behavior of cement paste, and migration of suspended particles [120]. In addition, the simulations of the mixing process of the fresh concrete in the concrete truck mixer during transportation using CFD (OpenFOAM software) were carried out by Wallevik [121, 122]. The simulations have shown that a higher shear rate leads to more flowable concrete at arrival.

Several research groups are studying fiber orientation estimation by numerical simulation tools (see below). Laure et al. [57] proposed a multi-domain approach that focused on the modeling of the free-surface flow motion, material interfaces, and fiber orientation described by Folgar and Tucker equations.

Svec et al. [99, 100, 102, 104] carried out a series of experiments coupled with numerical simulations of the casting process of the fiber reinforced self-compacting concrete with different factors including the formwork geometry and the surface roughness.

Gudžulić et al. [34] have presented the results of the casting simulations using Smoothed Particle Hydrodynamics needed to predict the spatial-temporal evolution of the probability density function of fiber orientation.

Herrmann and Lees [44] have performed the simulations of the casting process of steel fiber reinforced concrete and studied the influence of the boundary conditions on the fiber orientation distribution using OpenFOAM 2.3.0.

This chapter presents an overview of the paper IV and describes the comparison of the different casting methods with several viscosities.

The performed numerical simulations have demonstrated the casting process of fresh concrete with embedded short fibers, poured into the formwork by three different casting methods: the normative casting according to the standard EN 14651, the filling of the formwork from the center, and the filling from one edge of the formwork.

3.1 Sample preparation and testing according to EN 14651

According to the Standard EN 14651 [109] the testing specimens are beams with dimensions of 15 cm * 15 cm and with a length of 550 to 700 mm. Steel fibers length is equal to 60 mm. The casting process of the specimen is done in two steps. Firstly, 2/3 of the volume of concrete mass is poured into the center of the formwork. The remaining amount of 1/3 of the concrete volume is divided in half and poured into a formwork from its two opposite ends. The filling process according to Standard EN 14651 is shown in Figure 27. The filling process lasts till the formwork is filled up to the top edge. Typically, after the filling the top side of the specimen may show unevenness after hardening of the concrete. Hence, the standard EN 14651 requires that the specimen is rotated by 90 degrees to ensure two plane-parallel surfaces during the loading of the specimens and measuring the tensile strength.

Further, our numerical simulations, performed in this research, have demonstrated how the testing specimens were filled with different filling methods. The filling process of formwork from one end is performed by simply pouring a whole amount of the concrete volume from one edge of the formwork. Analogously, the filling of the formwork from the center is done by pouring a whole amount of the concrete volume from the center of the formwork.

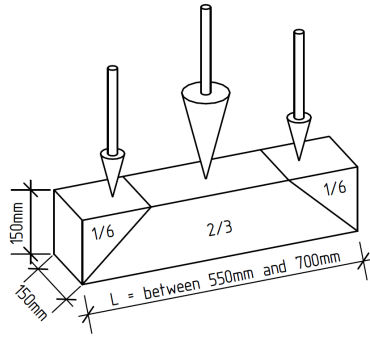


Figure 27: Casting of samples according to EN 14651, arrows denote filling areas. The figure is reproduced from Publication V.

3.2 Computational Fluid Dynamics simulations

Studies have shown that the flow of a slurry, like self-compacting concrete, can be simulated by using a homogeneous replacement material with a Bingham-plastic behaviour [88, 29], see in Figure 28.

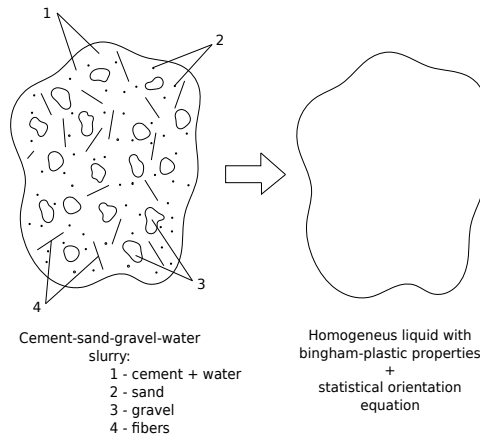


Figure 28: The replacement of self-compacting concrete by using a homogeneous material with a Bingham-plastic behaviour.

To model a Bingham fluid behavior for the concrete phase the Herschel-Bulkley viscosity model was used [16]. The orientation of fibers can be described by a probability distribution function that can be expanded in a series of tensors of increasing order [25, 3, 41]. For this, the OpenFOAM interFoam solver is used, which allows the simulation of free-surface flow, for which the liquid (concrete slurry) and surrounding air need to be simulated. The solver had been modified by Lees and Herrmann [44] and a statistical equation for the fiber orientation distribution, in form of an evolution equation for the second order orientation tensor, was added.

3.3 Set-up of numerical simulations

Generally, numerical simulations in OpenFOAM include three main stages: pre-processing, processing (running of the solver), and post-processing.

As was mentioned before, the simulation case represents the casting process of fresh concrete carried out by different methods of formwork filling.

The full description of the setting up of the numerical simulation study case is presented in Figure 29.

The pre-processing stage includes:

- the determination of the geometry of the area of interest (the computational domain). The simulated geometry of this study case is the beam geometry with dimensions of $L \times W \times H$: 62 cm \times 15 cm \times 15 cm, filled with the fresh concrete according to EN 14651, using three casting containers, see Figure 30. The mesh has 7023 nodes and 37020 cells. The inlet \varnothing 10 cm, located in the center on the beam axis and 8 cm from the end-walls.

The geometry of the beam has been modeled and meshed in Gmsh [27]. The study case consists of three casting containers coupled with the rectangular formwork with the air above.

- the setting up the initial conditions, mesh boundaries and the mesh generation:
All simulations are carried out on the same mesh, however, the initial pouring container can be changed. For the simulation a different casting method any number of containers can be active simultaneously or one after the other.

- the selection of an appropriate model of simulated physical phenomena:
In the described numerical simulations interFiberFoam [44], a modified interFoam solver from the OpenFOAM 2.3.0 library, was applied [110]. The implementation was adapted from the icoFiberFoam introduced in [36]. The solver is based on the so-called Weller-VOF (volume of fluid) method [15] to simulate the multiphase free-surface flow. The modified solver includes the calculations of the equation of change for the second-order fiber orientation tensor field in the concrete phase [44]. The fiber orientations are described by an evolution equations for the second order orientation tensor, which are solved at every time-step. The presented simulations are one-way coupled, meaning the flow-field affects the fiber orientation distribution whereas the fiber orientation has no effect on the flow-field. The implemented solver had been verified in [44] by comparison with results of numerical simulations published by other research groups.

- the definition of fluid properties:
The material parameters used in the simulation are given in Table 8. The notation of the parameters follows the naming in OpenFOAM, i.e. ρ is the density, τ_0 is the yield stress, k controls the viscosity of the flowing mass and ν_0 is the viscosity used if stress is below yield stress. The parameters are in the range published by [16, 55]. Obtained rheological properties of the simulated SFRC mass using simulated funnel flow test and flow table test (with Abram's cone, dropping of plate was not simulated) are given in Table 9.

- the characterization of suitable physical boundary conditions:
In these simulations, for the velocity: a zero gradient boundary condition was used. This indicates that the velocity does not change normal to the boundary, implying

no flow across this surface. For the atmosphere above the formwork: a fixed total pressure was applied.

At the walls of the formwork, for the pressure field: a zero gradient condition was applied. This ensures that the pressure does not change at the walls, implying that there is no flow or pressure gradient at the boundaries. For the fibers, a planar state of orientation in the plane of the walls was assumed, meaning the fiber orientations are restricted to align within the surface of the formwork walls.

Table 8: Transport properties used in the OpenFOAM simulation. The table is adapted from Publication V.

	case	OpenFOAM value	physical value
ρ	self-leveling	2300	2300 $\frac{\text{kg}}{\text{m}^3}$
	high-viscous	2300	2300 $\frac{\text{kg}}{\text{m}^3}$
	slump	2300	2300 $\frac{\text{kg}}{\text{m}^3}$
τ_0	self-leveling	3.47e-02	79.810 Pa
	high-viscous	5.47e-02	125.81 Pa
	slump	9.47e-02	217.81 Pa
κ	self-leveling	2.17e-02	49.910 Pa · s ⁿ
	high-viscous	4.17e-02	95.910 Pa · s ⁿ
	slump	9.17e-02	210.91 Pa · s ⁿ
ν_0	all cases	1000	1000 $\frac{\text{m}^2}{\text{s}}$
n	all cases	1	1

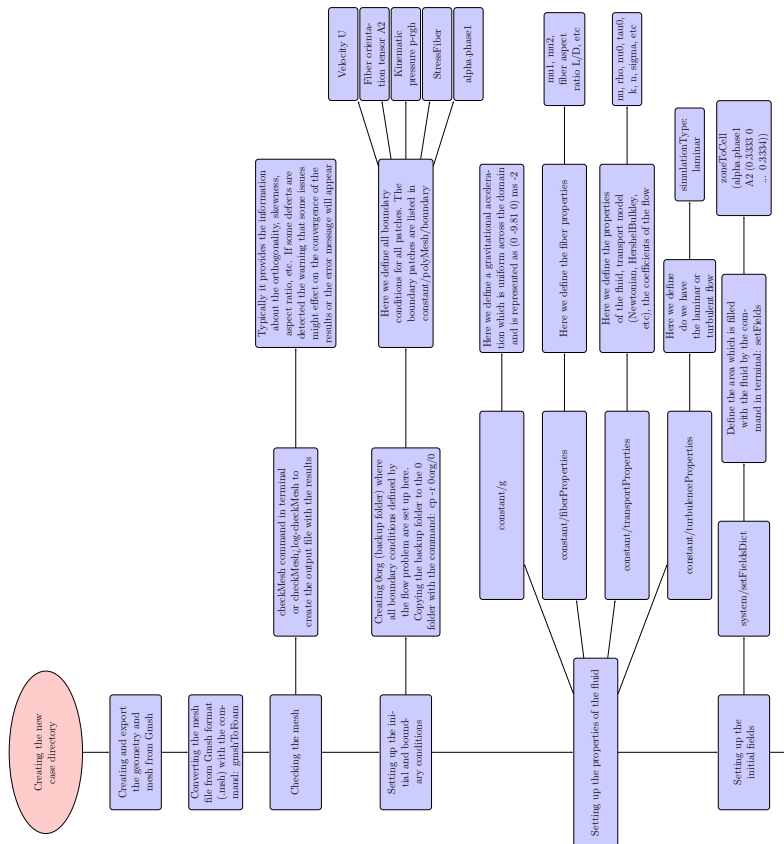
Table 9: The results of simulated flowability tests. The table is adapted from Publication V.

case	funnel outflow time	flow table diameter
self-leveling	2.5-3.2 s	108 cm
high-viscous	5-7 s	78 cm
slump	16 s	62 cm

Post-processing has been done in ParaView [37]. The OpenFOAM solver provides the following output fields: velocity U , phase volume fraction α , hydrostatic perturbation pressure p_{rgh} and fiber orientation tensor A_2 .

To visualize the simulation results in Paraview the following filters are used:

- The Tensor Glyph filter is used to generate an ellipsoid glyph at every point in the input dataset. The glyphs are oriented according to eigenvalues and eigenvectors of tensor point data of the input data set, representing the fiber orientation at each point.
- The Threshold filter is used to extract cells of the input dataset with scalar values in the specified range, depending on the selected threshold method.
- The Clip filter is used to cut any dataset using a plane, sphere, box or values of a scalar data array in the input dataset. Clipping includes iterating over all cells in the input dataset and after that removing cells that are considered outside of the space. It helps to focus on specific parts of the simulation domain.



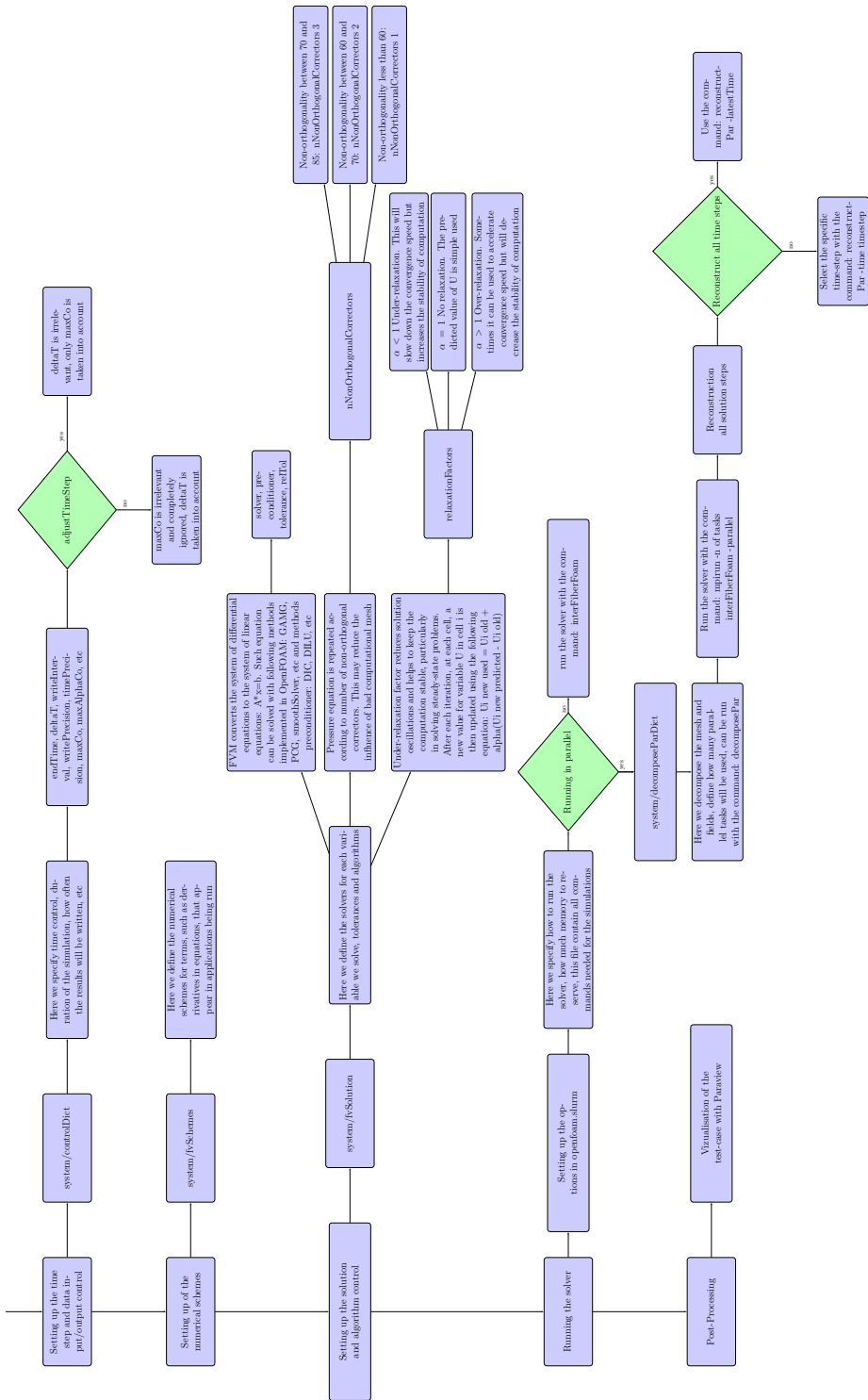


Figure 29: Flowchart of the study case set up.

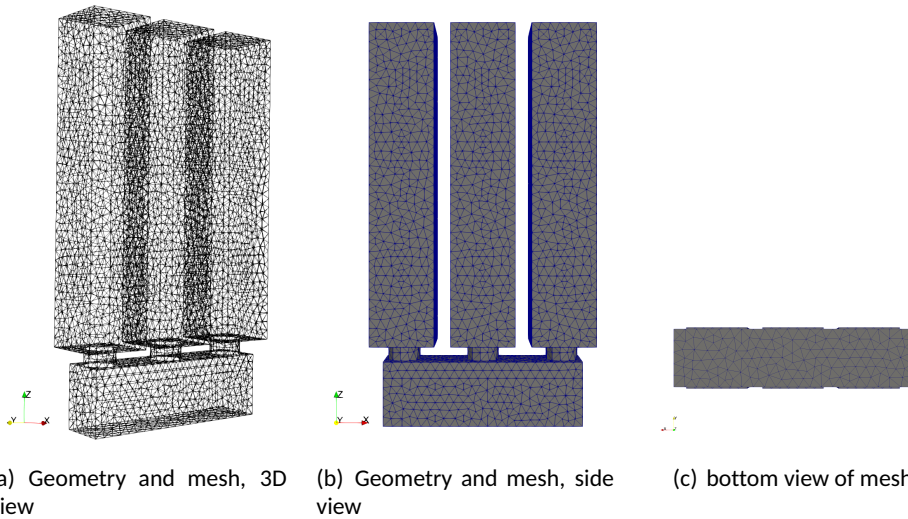


Figure 30: Geometry and mesh of the simulation. The figure is reproduced from Publication V.

- The Contour filter is used to compute isosurfaces (surfaces of constant value) or iso-lines (lines of constant value) using a selected point-centered scalar array. It helps in visualizing regions with specific scalar values, such as the boundary between different phases in the flow.

3.4 Results of Numerical simulations

3.4.1 Dynamics of filling the form

An intermediate state of the filling of the formwork can be seen in Fig. 31. To demonstrate the difference in flow behavior the screenshots are taken at different time-steps for different flowabilities.

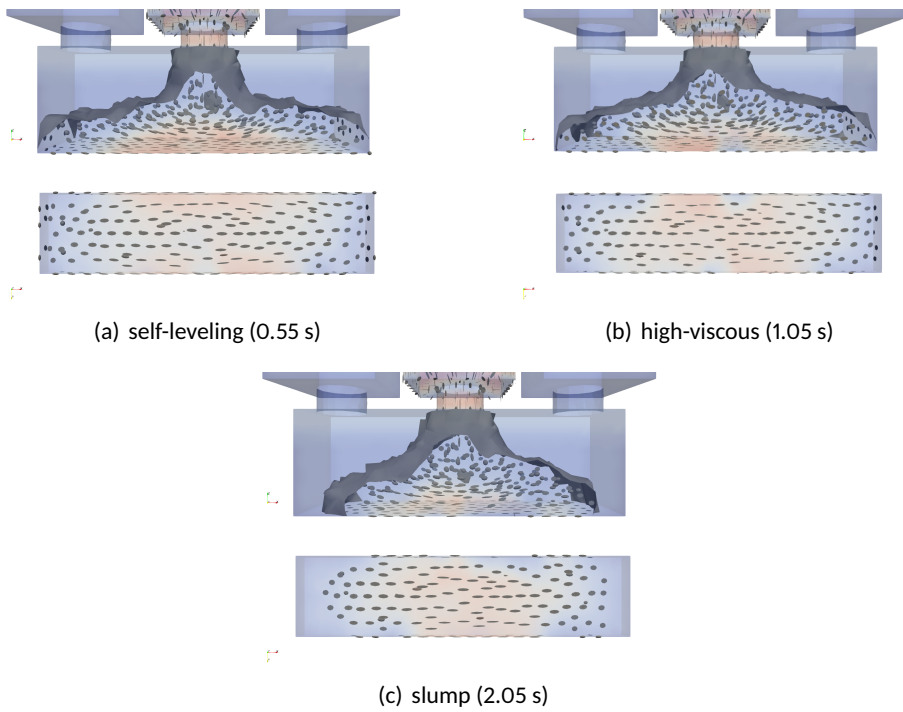


Figure 31: Comparison of the flow behaviour, shown are intermediate time-steps. The figure is adapted from Publication V.

3.4.2 Obtained final fiber orientation distributions

A visual representation of the orientation tensor obtained by solving the evolution equation is represented in Fig. 32. The second order orientation tensor is symmetric, so it owns three orthogonal eigenvectors and three accompanying eigenvalues. These eigenvectors characterize the principal axes of the tensor which represent an orientation, while the eigenvalues are its principal values and represent the length of the glyph.

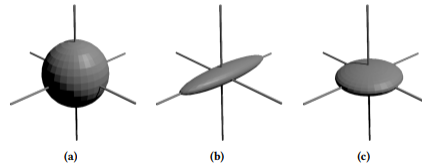


Figure 32: A visual representation of the orientation tensor. The figure is reproduced from E. Pastorelli thesis, 2015.

When all three eigenvalues are equal, the tensor represents isotropy, which is depicted by spherical-shaped glyphs, as shown in Fig. 32 (a). When one eigenvalue is much bigger than the other two, we have a linear anisotropy depicted by the elongated (cigar) shape glyphs. It represents the zones where the fibers are well-aligned with each other in one direction, Fig. 32 (b). When one eigenvalue is smaller than the another two, we have a planar anisotropy, depicted as the penny-shaped glyphs. It represents a fiber distribution with orientations mostly within a plane, Fig. 32 (c).

An additional hint is given by the colors from blue to red, where well-aligned in one direction fibers are highlighted by red color.

The comparison of the numerical simulation results of the fresh fiber concrete flow with different rheological parameters and the filling of the formwork by several casting methods are shown in Table 10. The results of numerical simulations are presented in two views: a front view and a bottom view of the specimen. The front view includes the glyphs of the whole specimen volume, while the bottom view only presents the bottom layer of the specimen.

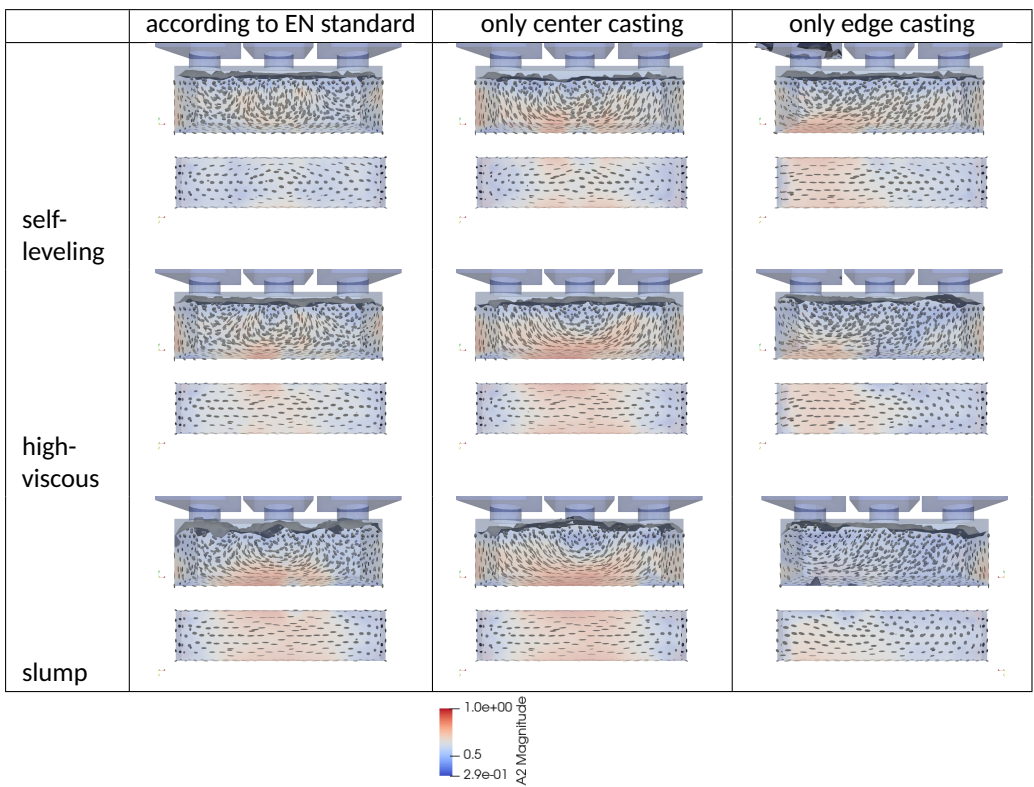
Main results of the normative filling process according to EN 14651 are presented in the first column of Table 10 and in Fig. 34. The second column shows the results of only center casting. The third column depicts casting from one end (in this case left side). Each method is compared for three flowabilities ranging from self-leveling, over high-viscous to slump.

In the following, first main observations valid for all cases are described, and then for each flowability, the different casting methods are compared.

A general observation of the numerical simulation results allows us to conclude, that under the (final) casting points the fibers tend to be aligned along the beam axis close to the bottom layer of the specimen. However, fibers tend to align vertically at a large distance from the final casting point, which can be the center of the formwork in the normative filling simulation.

During the Standard casting, the main concrete mass is placed in the center of the formwork, with the remaining mass distributed towards the end. As can be seen from results, casting of the concrete in several steps makes the fiber orientation more random, and U-shaped glyph patterns forms under each casting points, where fibers were vertically aligned (perpendicular to the flow direction) along the boundary between different pouring portions. During the center or edge castings we can see that the U-shape glyph

Table 10: Comparison of fiber orientations for different flowabilities and casting points. The figure is adapted from Publication V.



patterns appeared mostly under the casting points, while glyphs reoriented to be perpendicular to the flow direction at the greater distances from the casting points.

Another important observation is that the higher the viscosity and yield stress, the better fibers are aligned with each other in one direction, and this correlation lasts for a longer range.

Regarding different viscosities of a mixture, generally, one can conclude that with increasing viscosity, the fibers are better aligned in one direction. However, the most viscous case — the slump case — has demonstrated that during casting of a highly viscous material air bubbles can appear and remain in the concrete mass.

The orientation of fibers is quantified, according to three parameters: the scalar order parameter S , the biaxiality b , and the director d , which is the eigenvector that corresponds to the largest eigenvalue of the second order alignment tensor, are presented in Table 11.

The scalar order parameter S is $S = \frac{3}{2}\lambda_1$ ($|\lambda_1| \geq |\lambda_2| \geq |\lambda_3|$), $b_S = \frac{1}{2}(\lambda_3 - \lambda_2)$, $b_S = \text{sign}(S)b$, with the biaxiality $b \in [0, \frac{1}{3}|S|]$ and $S \in [-\frac{1}{2}, 1]$, see [41, 39].

A value $S = 1$ corresponds to a well-aligned in one direction fibers, $S = 0$ corresponds to isotropically oriented fibers and $S = -\frac{1}{2}$ shows the case when all fibers are aligned in a plane, see [41, 45].

Figure 33 demonstrates a sketch showing the location of the fiber orientation probe. The two probes are located 2.5 cm above the bottom and centered in the other directions for probe 1, and 2.5 cm from the side wall and centered in the other directions for probe 2. Thus they would be located at the tip of a notch cut into the bottom or side, respectively.

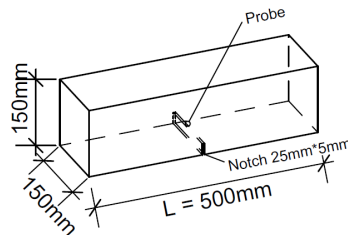


Figure 33: A sketch showing the location of the fiber orientation probe. The figure is reproduced from Publication V.

3.4.3 Self-leveling

Analysing the results of the numerical simulations for the self-leveling case, depicted in the Table 10, one can observe – certain pattern in the glyphs distribution emerging. The ellipsoidal glyphs in the side view follows a circle around the inflow point. For the filling of the formwork from the center, the fibers are starting to tend to be aligned along the beam axis in the bottom layer, but with increasing distance from the center the director turns upwards. For the side casting the same tendency of the director turning upwards can be observed, though it is less expressed here. Looking at the results of normative casting, one can notice that there are regions between the three casting points where the director is pointed upwards.

Numerically one can observe from Table 11, that the probe 1 demonstrates the director is aligned along the x -axis for the side and center casting with a moderate fiber alignment of $S = 0.38$, while the normative casting demonstrates a tendency of flat-isotropic distribution in the x - y -plane. For probe 2, we can see, that the situation is reversed with

moderately aligned fibers in z direction for the normative casting, and plane-isotropy in the x - z -plane for the side and center castings.

3.4.4 High-viscous

Results of the casting of the high-viscous case demonstrates the highest degree of alignment in the center casting at probe 1, but all casting positions show at least moderate alignment in x -direction, see Table 11. For all casting positions and on both probe locations the scalar order parameter is positive. In the normative casting, the director at probe 2 is almost along z -axis, while in the center and edge casting it is oriented in x -direction.

The visual trend observed in the case of self-leveling mixture is more expressed here, the glyphs presented in Table 10 follow the same trend.

3.4.5 Slump

For the slump case visually, the same trends as in the high-viscous and self-leveling cases can be seen in Table 10. Quantitatively one can notice from the Table 11, that the degree of orientation at probe 1 is lower for the edge casting, but higher for the normative and center casting. In the normative casting at probe 2, there is a planar-isotropic orientation in the x - z -plane, while in the center casting the orientation is in x -direction and for the edge casting somewhat tilted from the x in negative z -direction.

Table 11: Orientation parameters at two probe positions. The table is adapted from Publication V.

cast position	flowability	position	S	b	$EV(\lambda_1)$
Norm	self-leveling	bottom 1	-0.25	0.08	(0.045, 0.042, -0.99)
Norm	self-leveling	side 2	0.38	0.09	(-0.26, -0.101, -0.96)
Center	self-leveling	bottom 1	0.37	0.10	(0.99, 0.15, 0.034)
Center	self-leveling	side 2	-0.33	0.10	(0.078, -0.99, 0.15)
Side	self-leveling	bottom 1	0.38	0.08	(0.98, 0.031, 0.18)
Side	self-leveling	side 2	-0.37	0.12	(0.19, 0.96, -0.22)
Norm	high-viscous	bottom 1	0.35	0.07	(0.99, -0.002, 0.007)
Norm	high-viscous	side 2	0.37	0.10	(-0.17, -0.14, -0.97)
Center	high-viscous	bottom 1	0.63	0.05	(0.99, 0.05, -0.008)
Center	high-viscous	side 2	0.42	0.10	(0.99, 0.05, 0.073)
Side	high-viscous	bottom 1	0.51	0.05	(0.99, 0.074, 0.11)
Side	high-viscous	side 2	0.41	0.09	(0.84, -0.045, 0.54)
Norm	slump	bottom 1	0.59	0.05	(0.99, 0.007, -0.009)
Norm	slump	side 2	-0.28	0.09	(0.024, -0.96, 0.27)
Center	slump	bottom 1	0.65	0.04	(1.0, 0.01, -0.01)
Center	slump	side 2	0.40	0.07	(0.99, -0.04, -0.12)
Side	slump	bottom 1	0.38	0.08	(0.98, 0.007, -0.19)
Side	slump	side 2	0.29	0.09	(0.83, 0.054, -0.56)

3.4.6 Discussion

The standard EN 14651 has been prepared by the Technical Committee CEN/TS 229 Pre-cast concrete products. In this context, it is worth mentioning that the development of technologies for predictable fiber distribution has good chances, especially in the field of precast concrete products. In precast plants controllable manufacturing conditions prevail, which allow high reproducibility of components and precast elements with lower

tolerance deviations. In addition, it is possible —especially in precast construction— to arrange the filling side of the precast elements at the correct angles to the subsequent loading direction. This possibility is often not available for in situ casting.

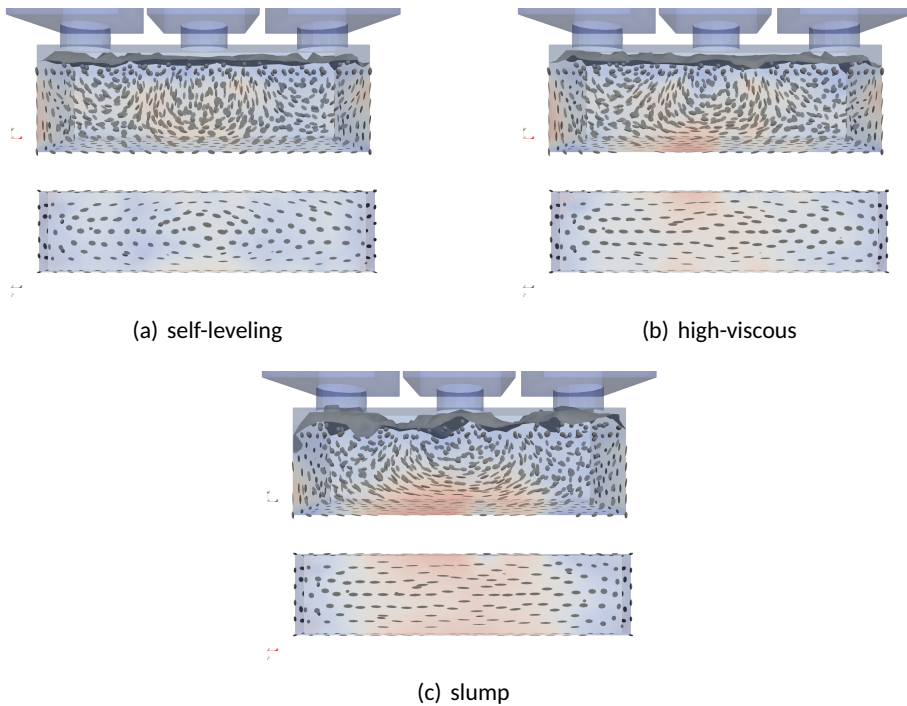


Figure 34: Comparison of the castings according to EN 14651 (first center, then edges). The figure is adapted from Publication V.

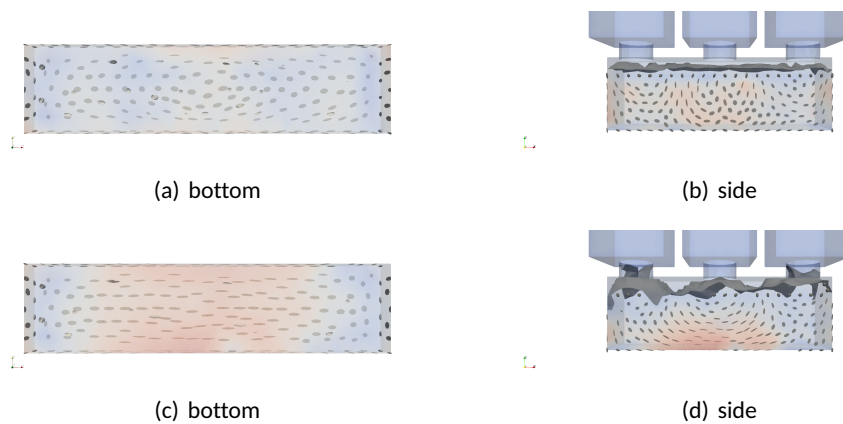


Figure 35: Side-by-side comparison of the fiber orientations in the bottom layer and in the side layer. The figure is reproduced from Publication V.

As can be seen from the Tables 10 and 11, the most beneficial fiber orientation in the

bottom layer was present in the case of the high-viscous and slump flow that had been cast by the normative filling method and from the center of the formwork. These methods produce a better alignment of fibers in the bottom layer, which is crucial for structural performance, especially in bending tests.

However, as specified in standard EN14651, that the concrete sample needs to be rotated about 90 degrees around the longitudinal axis, which means the fiber orientation distribution on the side becomes the bottom in the bending test and has to cope with the strongest tension. As can be seen from Fig. 35, the difference in the bottom layer orientation distributions differs from the side distributions, since in a bending test, the part that is on the under or top side takes the largest stress, turning a sample side-ways changes the tested distribution.

Simulations of different casting scenarios show, that extreme care must be taken when trying to reproduce reality in the simulation, it also shows that for simulations to be used in predicting fiber distributions in structural elements, care must be taken to ensure the construction crew follows precisely the prescribed casting procedure.

4 Main Conclusions and recommendations for future work

This thesis presents experimental research on the influence of the casting methods on the fiber orientation distribution and how it affects the mechanical properties of the concrete.

According to the aims, defined in section 1.2, the following new findings were obtained while investigating the rheology of short fiber reinforced cementitious composites:

1. Based on our experiments described in (Publication II), it can be concluded that different scenarios of the casting of the viscous mixture with the embedded fibers have an essential influence on the fiber orientation distribution and its uniformity.

The casting velocity has a significant effect on the spatial distribution of fibers in the formwork. For instance, during an extremely slow filling process, fibers gather in a narrow channel, while during fast casting we observed more uniformly spread fibers.

Concerning fiber orientation, one can notice that the comparison of different scenarios (casting velocity, surface roughness of the formwork) does not demonstrate a big difference and fibers were mostly oriented perpendicular to the flow direction.

2. Analysis of the correlation between the position of the beams in the plate revealed several important findings. The plate with dimensions of ($L \times W \times H$) 90 cm \times 60 cm \times 20 cm (Publication I) was cut into 3 beams and 3-point bending test was carried out. The edge beams demonstrated a better post-cracking behavior in comparison with the center beam. The plate with dimensions of 400 cm \times 100 cm \times 10 cm (Publications III, IV) was cut into 40 beams and 4-point bending test for all beams was carried out. The obtained mechanical properties and post-cracking behavior demonstrated a large variability and highly depend on the position within a slab where the specimens were taken from. Specifically, the specimens taken from the edges of the slab showed strain-hardening post-cracking behavior, where the maximum load is higher than the load at the first crack. However, the specimens positioned in the center of the slab demonstrated strain-softening or near-to-brittle post-cracking behavior, where the residual strength was only a quarter or even lower than the load at the first crack.
3. The assessment of the fiber orientation distribution inside of the concrete specimen by x-ray Computed Tomography and image analysis methods was performed (Publication II). The fiber amount and fiber orientation inside of the testing beams were analyzed. The middle beam with the highest amount of fibers in the bottom layer where the highest tensile stresses occurred has introduced the least efficient fiber orientation distribution and demonstrated the weakest post-cracking behavior. Nevertheless, two edge beams with similar beneficial fiber orientation distribution demonstrated a better post-cracking behavior, particularly, the one beam with a slightly higher fiber amount had a stronger post-cracking behavior than the other one.
4. The visual analysis of the numerical simulations showed differences of the fiber orientation in dependency of the position of the filling point. This should be verified by a Computed Tomography analysis to avoid misconclusions and give more precise evaluation of the differences in the fiber orientation distribution. Another key factor is the viscosity of the fiber reinforced cementitious composite (Publication V). The numerical simulations of mixtures with different viscosities showed more preferable fiber orientation distribution in higher viscous mixtures, where fibers were aligned parallel to the casting direction.

5. As our numerical simulations demonstrated (Publication V), fiber orientation distribution significantly varies depending on the different casting methods. In addition, it is worth to mention that the fiber orientation distribution is quite different on the side and the bottom of the specimen. Namely, on the bottom layer of the specimens fibers are mostly represented by cigar-shaped ellipsoidal glyphs that corresponds to the most favorable fiber orientation improving the post-cracking behavior.
6. The comparison of the standard bending test methods on a fiber reinforced specimens with force application parallel and transverse to the formwork filling direction was performed and described in section 2.3. The results demonstrated the similarity of the force-displacement diagrams, according to the testing method. Particularly, beams in which the force was applied parallel to the formwork filling direction demonstrated a slightly better post-cracking behavior compared to beams that were tested with a force applied transverse to the formwork filling direction. This result coincides with the results of the numerical simulations described in (Publication V), which leads to the conclusion that the fiber orientation distribution is different on the side and bottom of the specimen and rotation before the bending test has a significant effect on the measured mechanical properties of cementitious composites.

The numerical simulations of the flow of the cementitious composites, that was used in this research, can be applied for the approximate prediction of the fiber distribution in fiber-reinforced structural elements.

The future perspective of the implementation of numerical simulations can be used by precast design companies and precast element manufacturers in developing guidelines for casting procedures of different element geometries.

At the highest level, the results obtained in this research can be used as a contribution to further development of the European Construction Code.

List of Figures

1	The changes of the sand amount in Männiku quarry (Tallinn) over the years; (a) in 2016, (b) in 2020, (c) in 2022, Map data: Estonian Land Board 2023	11
2	Fiber concrete with visible fibers in the crack.....	12
3	The restraining effect of the fibers in the crack.	12
4	The main factors influenced on the fiber orientation	17
5	The main objectives and activities of the research.	21
6	Fiber orientations, smooth bottom, fast casting. The figure is adapted from Publication II.	25
7	Fiber orientations, smooth bottom, slow casting. The figure is adapted from Publication II.	25
8	Fiber orientations, rough, slow. The figure is adapted from Publication II. ..	26
9	Fiber orientations, rough bottom, fast casting. The figure is adapted from Publication II.	26
10	The ingredients of the SFRSCC mixture.....	27
11	Hooked end steel fibers.	28
12	Casting of a small plate using a bucket and half-funnel. The figure is reproduced from Publication II.	28
13	Layout of beam-cutting of small plate. The figure is reproduced from Publication I.	29
14	Beam layout of specimens cut out of the cast plates. The figure is reproduced from Publication III.....	31
15	Bottom layer of the beams in x-ray CT. The figure is reproduced from Publication II.	35
16	An example of the beam with extracted fibers in 3D Slicer.....	36
17	Bending test setup. The figure is reproduced from Publication I.	37
18	Photo of the bending test showing a beam sample in the testing machine with the frame for displacement measurements and displacement sensors. The figure is reproduced from Publication I.....	37
19	Four-point bending test setup with a beam sample. The figure is reproduced from Publication III.....	38
20	Sketch of the bending test showing a beam sample in the testing machine with the frame for displacement measurements and displacement sensors. The figure is reproduced from Publication III.	39
21	Force displacement curves for the three-point bending test of the three beams. The figure is reproduced from Publication I.	40
22	Load-displacement diagrams for the tested beams; (a) SCC, (b) SFRSCC. The figure is reproduced from Publication IV.	42
23	The diagrams of three beams with different post-cracking behavior: strain-hardening, intermediate and strain-softening.	43
24	The correlation between the beam position in the plate and the post-cracking behavior.	43
25	Positions and shapes (bottom view) of the cracks sustained at the main cracking are shown using the realistic crack patterns. The figure is reproduced from Publication IV.....	43
26	Force-Displacement Diagram of four beams that were tested according to EN14651 with and without rotation of the testing beams.	44

27	Casting of samples according to EN 14651, arrows denote filling areas. The figure is reproduced from Publication V.	47
28	The replacement of self-compacting concrete by using a homogeneous material with a Bingham-plastic behaviour.	47
29	Flowchart of the study case set up.	51
30	Geometry and mesh of the simulation. The figure is reproduced from Publication V.	52
31	Comparison of the flow behaviour, shown are intermediate time-steps. The figure is adapted from Publication V.	53
32	A visual representation of the orientation tensor. The figure is reproduced from E. Pastorelli thesis, 2015.	54
33	A sketch showing the location of the fiber orientation probe. The figure is reproduced from Publication V.	56
34	Comparison of the castings according to EN 14651 (first center, then edges). The figure is adapted from Publication V.	58
35	Side-by-side comparison of the fiber orientations in the bottom layer and in the side layer. The figure is reproduced from Publication V.	58

List of Tables

1	Matrix of Experiments. The table is adapted from Publication II.	24
2	Data of used fibers: Semtu WireFib 80/60; amount used 25 kg/m^3 , The table is adapted from Publication I.	27
3	Fiber concrete data. The table is adapted from Publication II.....	29
4	Composition of SCC mix, amount mixed: 1 m^3 . The table is adapted from Publication III.	30
5	Data of the steel fibers, according to [91]. The table is adapted from Publication III.....	30
6	Results of compression tests for SCC and SFRSCC. The table is adapted from Publication III.	32
7	Flexural fracture strength of the three beams; the average was $\bar{\sigma}^{M_y} = 6.97$ with a standard-deviation of 0.18. The table is adapted from Publication I. .	40
8	Transport properties used in the OpenFOAM simulation. The table is adapted from Publication V.	49
9	The results of simulated flowability tests. The table is adapted from Publication V.	49
10	Comparison of fiber orientations for different flowabilities and casting points. The figure is adapted from Publication V.	55
11	Orientation parameters at two probe positions. The table is adapted from Publication V.	57

References

- [1] M. Abambres and E. O. Lantsoght. Ann-based shear capacity of steel fiber-reinforced concrete beams without stirrups. *Fibers*, 7(10):88, 2019.
- [2] ACI Committee 544. 544.4r-88: Design considerations for steel fiber reinforced concrete. Technical report, American Concrete Institute, 1999.
- [3] S. G. Advani and C. L. Tucker III. The use of tensors to describe and predict fiber orientation in short fiber composites. *Journal of rheology*, 31(8):751–784, 1987.
- [4] A. H. Akca and N. Özyurt. Deterioration and recovery of frc after high temperature exposure. *Cement and Concrete Composites*, 93:260–273, 2018.
- [5] J. Andries, P. Van Itterbeeck, L. Vandewalle, and A. Van Geysel. Influence of concrete flow on spatial distribution and orientation of fibres in steel fibre reinforced self-compacting concrete. In *fib symposium, Copenhagen, Denmark*, 2015.
- [6] G. L. Balázs, O. Czoboly, É. Lublós, K. Kapitány, and Á. Barsi. Observation of steel fibres in concrete with Computed Tomography. *Construction and Building Materials*, 140:534–541, 2017.
- [7] S. J. Barnett, J.-F. Lataste, T. Parry, S. G. Millard, and M. N. Soutsos. Assessment of fibre orientation in ultra high performance fibre reinforced concrete and its effect on flexural strength. *Materials and Structures*, 43(7):1009–1023, 2010.
- [8] L. Bertolini, B. Elsener, P. Pedferri, E. Redaelli, and R. Polder. *Corrosion of Steel in Concrete: Prevention, Diagnosis, Repair*. John Wiley & Sons, 04 2013.
- [9] B. Boulekbatche, M. Hamrat, M. Chemrouk, and S. Amziane. Flowability of fibre-reinforced concrete and its effect on the mechanical properties of the material. *Construction and Building Materials*, 24(9):1664–1671, 2010.
- [10] BSI. BS EN 12350-2: 2019: Testing fresh concrete. *Slump test*, 2019.
- [11] BSI. BS EN 12390-2: 2009: Testing hardened concrete. part 2: Making and curing specimens for strength tests. *BSI British standard Institution*, pages 1–12, 2019.
- [12] BSI. *BS EN 12390-3: Testing Hardened Concrete. Part 3: Compressive Strength of Test Specimens*. BSI British Standards Institution, 2019.
- [13] BSI. *BS EN 12390-5: Testing Hardened Concrete. Part 5: Flexural Strength of Test Specimens*. BSI British Standards Institution, 2019.
- [14] A. Committee 544. 544.5r-10: Report on the physical properties and durability of fiber reinforced concrete. Technical report, American Concrete Institute, 2010.
- [15] S. M. Damian. *An Extended Mixture Model for the Simultaneous Treatment of Short and Long Scale Interfaces*. PhD thesis, National University of the Littoral, 2013.
- [16] F. de Larrard, C. F. Ferraris, and T. Sedran. Fresh concrete: A Herschel-Bulkley material. *Materials and Structures*, 31(7):494–498, Aug 1998.
- [17] R. Deeb, B. L. Karihaloo, and S. Kulasegaram. Reorientation of short steel fibres during the flow of self-compacting concrete mix and determination of the fibre orientation factor. *Cement and Concrete Research*, 56:112–120, 2014.

- [18] C. Del Vecchio, M. Di Ludovico, A. Balsamo, and A. Prota. Seismic retrofit of real beam-column joints using fiber-reinforced cement composites. *Journal of Structural Engineering*, 144(5):04018026, 2018.
- [19] Deutscher Ausschuss für Stahlbeton. DAFStb-Richtlinie. Technical report, Beuth Verlag GmbH, Berlin, 2010.
- [20] Å. L. Døssland. *Fibre reinforcement in load carrying concrete structures: laboratory and field investigations compared with theory and finite element analysis*. PhD thesis, Fakultet for naturvitenskap og teknologi, 2008.
- [21] D. Dupont and L. Vandewalle. Distribution of steel fibres in rectangular sections. *Cement and Concrete Composites*, 27(3):391–398, 2005.
- [22] M. Eik and H. Herrmann. Raytraced images for testing the reconstruction of fibre orientation distributions. *Proceedings of the Estonian Academy of Sciences*, 61(2):128–136, 2012.
- [23] L. Ferrara, M. Faifer, M. Muhaxheri, and S. Toscani. A magnetic method for non destructive monitoring of fiber dispersion and orientation in steel fiber reinforced cementitious composites. part 2: Correlation to tensile fracture toughness. *Materials and Structures*, 45(4):591–598, 2012.
- [24] L. Ferrara, M. Faifer, and S. Toscani. A magnetic method for non destructive monitoring of fiber dispersion and orientation in steel fiber reinforced cementitious composites. part 1: method calibration. *Materials and Structures*, 45(4):575–589, 2012.
- [25] F. Folgar and C. L. Tucker III. Orientation behavior of fibers in concentrated suspensions. *Journal of reinforced plastics and composites*, 3(2):98–119, 1984.
- [26] R. Gettu, D. R. Gardner, H. Saldivar, and B. Barragán. Study of the distribution and orientation of fibers in SFRC specimens. *Materials and Structures*, 38(1):31–37, 2005.
- [27] C. Geuzaine and J.-F. Remacle. Gmsh: A 3-D finite element mesh generator with built-in pre- and post-processing facilities. *International Journal for Numerical Methods in Engineering*, 79(11):1309–1331, 2009.
- [28] O. Goidyk, M. Heinštein, and H. Herrmann. CFD comparison of the influence of casting of samples on the fiber orientation distribution. *Fibers*, 11(1):6, 2023.
- [29] A. Gram. *Numerical modelling of self-compacting concrete flow: Discrete and continuous approach*. Licentiate thesis, KTH Royal Institute of Technology, Stockholm, 2009.
- [30] A. Gram, A. Farhang, and J. Silfwerbrand. Computer-aided modelling and simulation of self-compacting concrete flow. In G. D. Schutter and V. Boel, editors, *5th International RILEM Symposium on Self-Compacting Concrete, SCC 2007, Ghent, Belgium, 3-5 September 2007*, pages 455–460. RILEM Publications SARL, 2007.
- [31] A. Gram and J. Silfwerbrand. Numerical simulation of fresh SCC flow: applications. *Materials and Structures*, 44:805–813, 2011.

- [32] P. Grigaliunas, T. Kringelis, and Ž. Rudžionis. SCC flow induced steel fiber distribution and orientation. non-destructive inductive method. In *11th European Conference on Non-Destructive Testing, Prague, Czech Republic*, pages 408–413, 2014.
- [33] S. Grünewald. *Performance-based design of self-compacting fibre reinforced concrete*. PhD thesis, Delft University Press, 2004.
- [34] V. Gudžulić, T. S. Dang, and G. Meschke. Computational modeling of fiber flow during casting of fresh concrete. *Computational Mechanics*, 63:1111–1129, 2019.
- [35] Y. M. Hashash, J. J. Hook, B. Schmidt, I. John, and C. Yao. Seismic design and analysis of underground structures. *Tunnelling and underground space technology*, 16(4):247–293, 2001.
- [36] K. Heinen. *Mikrostrukturelle Orientierungszustände strömender Polymerlösungen und Fasersuspensionen*. PhD thesis, Universität Dortmund, 2007.
- [37] A. Henderson, J. Ahrens, and C. Law. *The ParaView Guide*. Kitware Inc., Clifton Park, NY., 2004.
- [38] H. Herrmann. <https://bitbucket.org/VisParGroup/workspace/repositories/>.
- [39] H. Herrmann and M. Beddig. Tensor series expansion of a spherical function for use in constitutive theory of materials containing orientable particles. *Proceedings of the Estonian Academy of Sciences*, 67(1):73–92, Mar. 2018. Open-Access CC-BY-NC 4.0.
- [40] H. Herrmann, A. Braunbrück, T. Tuisk, O. Goidyk, and H. Naar. An initial report on the effect of the fiber orientation on the fracture behavior of steel fiber reinforced self-compacting concrete. In H. Herrmann and J. Schnell, editors, *Short fibre reinforced cementitious composites and ceramics*, pages 33–50. Springer, 2019.
- [41] H. Herrmann and M. Eik. Some comments on the theory of short fibre reinforced materials. *Proceedings of the Estonian Academy of Sciences*, 60(3):179–183, 2011.
- [42] H. Herrmann, O. Goidyk, and A. Braunbrück. Influence of the flow of self-compacting steel fiber reinforced concrete on the fiber orientations, a report on work in progress. In H. Herrmann and J. Schnell, editors, *Short Fibre Reinforced Cementitious Composites and Ceramics*, pages 97–110. Springer, 2019.
- [43] H. Herrmann, O. Goidyk, H. Naar, T. Tuisk, and A. Braunbrück. The influence of fibre orientation in self-compacting concrete on 4-point bending strength. *Proceedings of the Estonian Academy of Sciences*, 68(3):337–346, 2019.
- [44] H. Herrmann and A. Lees. On the influence of the rheological boundary conditions on the fibre orientations in the production of steel fibre reinforced concrete elements. *Proceedings of the Estonian Academy of Sciences*, 65(4):408–413, 2016.
- [45] T. Jankun-Kelly and K. Mehta. Superellipsoid-based, real symmetric traceless tensor glyphs motivated by nematic liquid crystal alignment visualization. *IEEE Transactions on Visualization and Computer Graphics*, 12(5):1197–1204, 2006.
- [46] S.-T. Kang and J.-K. Kim. The relation between fiber orientation and tensile behavior in an Ultra High Performance Fiber Reinforced Cementitious Composites (UH-PFRCC). *Cement and Concrete Research*, 41(10):1001–1014, 2011.

- [47] D. Kartofelev, O. Goidyk, and H. Herrmann. A case study on the spatial variability of strength in a SFRSCC slab and its correlation with fibre orientation. *Proceedings of the Estonian Academy of Sciences*, 69(4):298–310, 2020.
- [48] A. Koenig. Analysis of air voids in cementitious materials using micro x-ray computed tomography (μ XCT). *Construction and Building Materials*, 244:118313, 2020.
- [49] T. Komarkova, P. Fiala, M. Steinbauer, and Z. Roubal. Testing an impedance non-destructive method to evaluate steel-fiber concrete samples. *Measurement Science Review*, 18(1):35, 2018.
- [50] H. Krenchel. Fibre spacing and specific fibre surface. *Fibre reinforced cement and concrete*, 1975:69–79, 1975.
- [51] R. Kumar and B. Bhattacharjee. Porosity, pore size distribution and in situ strength of concrete. *Cement and Concrete Research*, 33(1):155–164, 2003.
- [52] E. O. Lantsoght. How do steel fibers improve the shear capacity of reinforced concrete beams without stirrups? *Composites Part B: Engineering*, 175:107079, 2019.
- [53] E. S. Lappa. *High strength fibre reinforced concrete: static and fatigue behaviour in bending*. PhD thesis, Delft University of Technology, 2007.
- [54] F. Laranjeira de Oliveira. *Design-oriented constitutive model for steel fiber reinforced concrete*. PhD thesis, Universitat Politècnica de Catalunya, 2010.
- [55] H. Lashkarbolouk, A. M. Halabian, and M. R. Chamani. Simulation of concrete flow in V-funnel test and the proper range of viscosity and yield stress for SCC. *Materials and Structures*, 47(10):1729–1743, 2014.
- [56] J. Lataste, M. Behloul, and D. Breysse. Characterisation of fibres distribution in a steel fibre reinforced concrete with electrical resistivity measurements. *Ndt & E International*, 41(8):638–647, 2008.
- [57] P. Laure, L. Silva, T. Coupez, and F. Toussaint. Numerical modelling of concrete flow with rigid fibers. In *AIP Conference Proceedings*, volume 907, pages 1390–1395. American Institute of Physics, 2007.
- [58] V. C. Li. *Engineered cementitious composites (ECC): bendable concrete for sustainable and resilient infrastructure*. Springer, 2019.
- [59] J. Liu, C. Li, J. Liu, G. Cui, and Z. Yang. Study on 3D spatial distribution of steel fibers in fiber reinforced cementitious composites through micro-CT technique. *Construction and Building Materials*, 48:656–661, 2013.
- [60] L. Martinie and N. Roussel. Simple tools for fiber orientation prediction in industrial practice. *Cement and Concrete Research*, 41(10):993–1000, 2011.
- [61] N. Martys and C. F. Ferraris. Simulation of SCC flow. In J. N. L. S.P. Shah, Joseph A. Daczko, editor, *Proc. 1st North American Conf. on the design and use of Self-Consolidating Concrete*, Chicago, IL, pages 27–30. Citeseer, 2002.
- [62] N. S. Martys. A classical kinetic theory approach to Lattice Boltzmann. *International Journal of Modern Physics C*, 12(8):1169–1178, 2001.

- [63] N. S. Martys. Study of a dissipative particle dynamics based approach for modeling suspensions. *Journal of Rheology*, 49(2):401–424, 2005.
- [64] N. S. Martys, W. L. George, B.-W. Chun, and D. Lootens. A smoothed particle hydrodynamics-based fluid model with a spatially dependent viscosity: application to flow of a suspension with a non-Newtonian fluid matrix. *Rheologica acta*, 49:1059–1069, 2010.
- [65] I. Marzec, J. Tejchman, et al. Fracture evolution in concrete compressive fatigue experiments based on X-ray micro-CT images. *International Journal of Fatigue*, 122:256–272, 2019.
- [66] D. McCann and M. Forde. Review of NDT methods in the assessment of concrete and masonry structures. *Ndt & E International*, 34(2):71–84, 2001.
- [67] V. Mechtcherine, A. Gram, K. Krenzer, J.-H. Schwabe, S. Shyshko, and N. Roussel. Simulation of fresh concrete flow using Discrete Element Method (DEM): theory and applications. *Materials and Structures*, 47:615–630, 2014.
- [68] P. K. Mehta and P. J. Monteiro. *Concrete: microstructure, properties, and materials*. McGraw-Hill Education, 2014.
- [69] B. Miloud. Permeability and porosity characteristics of steel fiber reinforced concrete. *Asian Journal of Civil Engineering*, 6(4):317–330, 2005.
- [70] T. Mishurova, F. Léonard, T. Oesch, D. Meinel, G. Bruno, N. Rachmatulin, P. Fontana, I. Sevostianov, and B. für Materialforschung und prüfung. Evaluation of fiber orientation in a composite and its effect on material behavior. *e-Journal of Nondestructive Testing (eJNDT)*, 22:7–9, 2017.
- [71] M. Modigell, K. Vasilic, W. Brameshuber, and S. Uebachs. Modelling and simulation of the flow behaviour of self-compacting concrete. In G. D. Schutter and V. Boel, editors, *5th International RILEM Symposium on Self-Compacting Concrete*, pages 387–392. RILEM Publications SARL, 2007.
- [72] A. E. Naaman, T. Wongtanakitcharoen, and G. Hauser. Influence of different fibers on plastic shrinkage cracking of concrete. *ACI materials Journal*, 102(1):49–58, 2005.
- [73] S. Odaka. Flow simulation of fresh concrete by dynamic viscoplastic suspension element method. *Transactions of the Japan Concrete Institute*, 15:39–46, 1993.
- [74] N. Ozyurt, T. O. Mason, and S. P. Shah. Non-destructive monitoring of fiber orientation using AC-IS: An industrial-scale application. *Cement and Concrete Research*, 36(9):1653–1660, 2006.
- [75] N. Ozyurt, L. Y. Woo, T. O. Mason, and S. P. Shah. Monitoring fiber dispersion in fiber-reinforced cementitious materials: Comparison of AC-impedance spectroscopy and image analysis. *ACI Materials Journal*, 103(5):340–347, 2006.
- [76] E. Pastorelli. *Analysis and 3D Visualisation of Microstructured Materials on Custom-built Virtual Reality Environment*. PhD thesis, Tallinn University of Technology, 2015.
- [77] E. Pastorelli and H. Herrmann. Time-efficient automated analysis for fibre orientations in steel fibre reinforced concrete. *Proceedings of the Estonian Academy of Sciences*, 65(1):28–36, 2016.

- [78] Ö. Petersson. Simulation of self-compacting concrete-laboratory experiments and numerical modelling of testing methods, J-ring and L-box tests. In O. Wallevik and I. Nielsson, editors, *Proc. of the 3rd Int. Symp. on SCC*, pages 202–207. Reykjavik Iceland, 2003.
- [79] Ö. Petersson and H. Hakami. Simulation of SCC-laboratory experiments and numerical modeling of slump flow and L-box tests. In *Proc. of the 2nd Int. RILEM Symp. on SCC*, pages 79–88. Coms Engineering Corporation Tokyo, 2001.
- [80] S. Pieper, M. Halle, and R. Kikinis. 3D Slicer. In *2004 2nd IEEE international symposium on biomedical imaging: nano to macro (IEEE Cat No. 04EX821)*, pages 632–635. IEEE, 2004.
- [81] T. Ponikiewski and J. Katzer. X-ray computed tomography of fibre reinforced self-compacting concrete as a tool of assessing its flexural behaviour. *Materials and Structures*, 49(6):2131–2140, 2016.
- [82] T. Ponikiewski, J. Katzer, M. Bugdol, and M. Rudzki. Determination of 3d porosity in steel fibre reinforced scc beams using x-ray computed tomography. *Construction and Building Materials*, 68:333–340, 2014.
- [83] T. Ponikiewski, J. Katzer, M. Bugdol, and M. Rudzki. X-ray computed tomography harnessed to determine 3D spacing of steel fibres in self compacting concrete (SCC) slabs. *Construction and Building Materials*, 74:102–108, 2015.
- [84] M. Promentilla, T. Sugiyama, and K. Shimura. Three dimensional characterization of air void system in cement-based materials. In *3rd ACF International Conference ACF/VCA*, pages 940–947, 2008.
- [85] T. Rahmani, B. Kiani, M. Bakhshi, and M. Shekarchizadeh. Application of different fibers to reduce plastic shrinkage cracking of concrete. In A. Scarpas, N. Kringos, I. Al-Qadi, and A. Loizos, editors, *7th RILEM International Conference on Cracking in Pavements: Mechanisms, Modeling, Testing, Detection and Prevention Case Histories*, pages 635–642. Springer, 2012.
- [86] W. Ren, Z. Yang, R. Sharma, C. Zhang, and P. J. Withers. Two-dimensional X-ray CT image based meso-scale fracture modelling of concrete. *Engineering Fracture Mechanics*, 133:24–39, 2015.
- [87] K. Rokugo, T. Kanda, H. Yokota, and N. Sakata. Applications and recommendations of high performance fiber reinforced cement composites with multiple fine cracking (hpfrcc) in japan. *Materials and Structures*, 42:1197–1208, 2009.
- [88] N. Roussel. Three-dimensional numerical simulations of slump tests. In *Annual Transactions of the Nordic Rheology Society*, volume 12, pages 55–62. American Institute of Physics, 2004.
- [89] N. Roussel, A. Gram, M. Cremonesi, L. Ferrara, K. Krenzer, V. Mechtcherine, S. Shyshko, J. Skocec, J. Spangenberg, O. Svec, et al. Numerical simulations of concrete flow: A benchmark comparison. *Cement and Concrete Research*, 79:265–271, 2016.
- [90] N. Roussel, J. Spangenberg, J. Wallevik, and R. Wolfs. Numerical simulations of concrete processing: From standard formative casting to additive manufacturing. *Cement and Concrete Research*, 135:106075, 2020.

- [91] Severstal Metiz. Hendix prime 75/52 - hooked ends fiber. <http://www.severstalmetiz.ru/eng/catalogue/1930/document62190.shtml?6605,1>, 2018.
- [92] S. Shyshko and V. Mechtcherine. Continuous numerical modelling of concrete from fresh to hardened state. *IBAUSIL, internationale Baustofftagung Weimar, Germany*, pages 20–23, 2006.
- [93] SIS - Bygg och anläggning. SIS.: Fibre concrete-design of fibre concrete structures (Swedish standard SS 812310:2014). Technical report, Swedish Standards Institute, 2014.
- [94] Ł. Skarżyński and J. Suchorzewski. Mechanical and fracture properties of concrete reinforced with recycled and industrial steel fibers using Digital Image Correlation technique and X-ray micro computed tomography. *Construction and Building Materials*, 183:283–299, 2018.
- [95] Special Activity Group 5. *Fib.: Model Code 2010*. International Federation for Structural Concrete (fib), 2012.
- [96] P. Stähli, R. Custer, and J. G. van Mier. On flow properties, fibre distribution, fibre orientation and flexural behaviour of FRC. *Materials and Structures*, 41(1):189–196, 2008.
- [97] O. Sucharda, Z. Marcalikova, and R. Gandel. Microstructure, shrinkage, and mechanical properties of concrete with fibers and experiments of reinforced concrete beams without shear reinforcement. *Materials*, 15(16):5707, 2022.
- [98] J.-P. Suuronen, A. Kallonen, M. Eik, J. Puttonen, R. Serimaa, and H. Herrmann. Analysis of short fibres orientation in steel fibre-reinforced concrete (SFRC) by X-ray tomography. *Journal of Materials Science*, 48(3):1358–1367, 2013.
- [99] O. Svec. *Flow modelling of steel fibre reinforced self-compacting concrete*. PhD thesis, Technical University of Denmark, Department of Civil Engineering, 2014.
- [100] O. Svec, J. Skocek, J. F. Olesen, and H. Stang. Fibre reinforced self-compacting concrete flow simulations in comparison with l-box experiments using carbopol. In J. A. Barros, editor, *8th Rilem international symposium on fibre reinforced concrete: Challenges and Opportunities*, 2012.
- [101] O. Švec, J. Skoček, H. Stang, M. R. Geiker, and N. Roussel. Free surface flow of a suspension of rigid particles in a non-Newtonian fluid: A lattice Boltzmann approach. *Journal of Non-Newtonian Fluid Mechanics*, 179:32–42, 2012.
- [102] O. Svec, J. Skocek, H. Stang, J. F. Olesen, and P. N. Poulsen. Flow simulation of fiber reinforced self compacting concrete using Lattice Boltzmann method. In A. Palomo, editor, *13th International Congress on the Chemistry of Cement*, 2011.
- [103] O. Švec, G. Žirgulis, J. E. Bolander, and H. Stang. Influence of formwork surface on the orientation of steel fibres within self-compacting concrete and on the mechanical properties of cast structural elements. *Cement and Concrete Composites*, 50:60–72, 2014.

- [104] O. Švec, G. Žirgulis, J. E. Bolander, and H. Stang. Influence of formwork surface on the orientation of steel fibres within self-compacting concrete and on the mechanical properties of cast structural elements. *Cement and Concrete Composites*, 50:60–72, 2014.
- [105] K. T. Design guideline for structural applications of steel fibre reinforced concrete. Technical report, SFRC Consortium, 2014.
- [106] Y. Tanigawa and H. Mori. Analytical study on deformation of fresh concrete. *Journal of Engineering Mechanics*, 115(3):493–508, 1989.
- [107] Y. Tanigawa, H. Mori, K. Tsutsui, and Y. Kurokawa. Estimation of rheological constants of fresh concrete by slump test and flow test. *Transactions of the Japan Concrete Institute*, 8:65–72, 1986.
- [108] Y. Tanigawa, H. Mori, K. Tsutsui, and Y. Kurokawa. Simulation of deformation of fresh concrete by viscoplastic finite element analysis. *Transactions of the Japan Concrete Institute*, 8:57–64, 1986.
- [109] Technical Committee CEN/TC 229. EN 14651: Test method for metallic fibre concrete — Measuring the flexural tensile strength (limit of proportionality (LOP), residual). European Committee for Standardization, Brussels, 2005.
- [110] The OpenFOAM Foundation. OpenFOAM. <http://www.openfoam.org>, 2014. V. 2.3.0.
- [111] L. N. Thrane. *Form filling with self-compacting concrete*. PhD thesis, Technical University of Denmark, 2007.
- [112] L. N. Thrane, P. Szabo, M. Geiker, M. Glavind, and H. Stang. Simulation of the test method “L-box” for self-compacting concrete. *Annual Transactions of the NORDIC rheology society*, 12(1):47–54, 2004.
- [113] L. N. Thrane, P. Szabo, M. R. Geiker, H. Stang, and C. Pade. Simulation and verification of flow in test methods. In S. P. Shah, editor, *The Second North American Conference on the Design and Use of Self-Consolidating Concrete and the Fourth International RILEM Symposium on Self-Compacting Concrete*, pages 551–556. Hanley Wood, LLC, 2005.
- [114] J. M. Torrents, A. Blanco, P. Pujadas, A. Aguado, P. Juan-García, and M. Á. Sánchez-Moragues. Inductive method for assessing the amount and orientation of steel fibers in concrete. *Materials and Structures*, 45(10):1577–1592, 2012.
- [115] M. Torrijos, J. Tobes, B. Barragán, and R. Zerbino. Orientation and distribution of steel fibres in self-compacting concrete. In R. Gettu, editor, *7th RILEM Symposium on Fibre-Reinforced Concretes (FRC)-BEFIB*, pages 729–738, 2008.
- [116] K. Vasilic, A. Gram, and J. E. Wallevik. Numerical simulation of fresh concrete flow: insight and challenges. *RILEM Technical Letters*, 4:57–66, 2019.
- [117] M. A. Vicente, J. Mínguez, and D. C. González. Computed tomography scanning of the internal microstructure, crack mechanisms, and structural behavior of fiber-reinforced concrete under static and cyclic bending tests. *International Journal of Fatigue*, 121:9–19, 2019.

- [118] B. V. Volkov I.V., Gazin E.M. SNIP.: 52-104-2006 Steel fibre reinforced concrete structures design. Technical report, Research Institute of Reinforced Concrete Structures, 2007.
- [119] B. V. Volkov I.V., Gazin E.M. SNIP.: 52-104-2009 Steel fibre reinforced concrete structures design. Technical report, Research Institute of Reinforced Concrete Structures, 2010.
- [120] J. E. Wallevik. *Rheology of particle suspensions: fresh concrete, mortar and cement paste with various types of lignosulfonates*. PhD thesis, Department of Structural Engineering, The Norwegian University of Science and Technology (NTNU), 2003.
- [121] J. E. Wallevik and O. H. Wallevik. Analysis of shear rate inside a concrete truck mixer. *Cement and Concrete Research*, 95:9–17, 2017.
- [122] J. E. Wallevik and O. H. Wallevik. Concrete mixing truck as a rheometer. *Cement and Concrete Research*, 127:105930, 2020.
- [123] Y. Wang, D. Niu, and Z. Dong. Experimental study on carbonation of steel fiber reinforced concrete. In J. Olek and J. Weiss, editors, *Proceedings of the 4th International Conference on the Durability of Concrete Structures, ICDCS 2014*, pages 55–59, 07 2014.
- [124] S. Wansom and S. Janjaturaphan. Evaluation of fiber orientation in plant fiber-cement composites using AC-impedance spectroscopy. *Cement and Concrete Research*, 45:37–44, 2013.
- [125] S. Wansom, N. Kidner, L. Woo, and T. Mason. AC-impedance response of multi-walled carbon nanotube/cement composites. *Cement and Concrete Composites*, 28(6):509–519, 2006.
- [126] L. Woo, S. Wansom, N. Ozyurt, B. Mu, S. Shah, and T. Mason. Characterizing fiber dispersion in cement composites using AC-impedance spectroscopy. *Cement and Concrete Composites*, 27(6):627–636, 2005.
- [127] J. Wuest, E. Denarié, E. Brühwiler, L. Tamarit, M. Kocher, and E. Gallucci. Tomography analysis of fiber distribution and orientation in ultra high-performance fiber-reinforced composites with high-fiber dosages. *Experimental techniques*, 33(5):50–55, 2009.
- [128] Y. Yang, Y. Zhang, W. She, N. Liu, and Z. Liu. In situ observing the erosion process of cement pastes exposed to different sulfate solutions with x-ray computed tomography. *Construction and Building Materials*, 176:556–565, 2018.
- [129] N. Yousefieh, A. Joshaghani, E. Hajibandeh, and M. Shekarchi. Influence of fibers on drying shrinkage in restrained concrete. *Construction and Building Materials*, 148:833–845, 2017.
- [130] R. Zerbino, J. Tobes, M. Bossio, and G. Giaccio. On the orientation of fibres in structural members fabricated with self compacting fibre reinforced concrete. *Cement and Concrete Composites*, 34(2):191–200, 2012.

- [131] B. ZHOU and Y. UCHIDA. Fiber orientation in ultra high performance fiber reinforced concrete and its visualization. In J. Van Mier, G. Ruiz, C. Andrade, R. Yu, et al., editors, *Proceedings of the Eighth International Conference on Fracture Mechanics of Concrete and Concrete Structures*, 2013.
- [132] B. Zhou and Y. Uchida. Influence of flowability, casting time and formwork geometry on fiber orientation and mechanical properties of UHPFRC. *Cement and Concrete Research*, 95:164–177, 2017.
- [133] G. Žirgulis, M. R. Geiker, O. Švec, and T. Kanstad. Potential methods for quality control of fibre distribution in FRC SCC. In N. Roussel and H. Bessales-Bey, editors, *7th RILEM International Conference on Self-Compacting Concrete*, 2013.
- [134] G. Žirgulis, O. Švec, E. V. Sarmiento, M. R. Geiker, A. Cwirzen, and T. Kanstad. Importance of quantification of steel fibre orientation for residual flexural tensile strength in FRC. *Materials and Structures*, 49:3861–3877, 2016.
- [135] Österreichische Bautechnikvereinigung. Richtlinie Faserbeton. Technical report, Österreichische Vereinigung für Beton- und Bautechnik, 2008.

Acknowledgements

The research presented in this thesis was funded by the Estonian Research Council from PUT1146 "Rheology of short fibre reinforced cementitious composites and influence on the fracture behaviour". Gathering and expanding my skills in the numerical simulations in OpenFOAM was possible due to the SekMo Cross-Sectional Mobility Measure grant funded by the Estonian Research Council (ETAG).

First of all, I would like to thank my supervisor Heiko Herrmann for giving me the opportunity to work on this research project, for his support and ideas on how to improve the research, and for the valuable discussions we had over all these years.

I am grateful to E-Betoonielement OÜ for the cooperation and production of concrete slabs for full-scale experiments. I would also like to thank Tanel Tuisk and Mattias Põldaru for their technical assistance in preparing laboratory concrete samples and performing compression tests. Carrying out the bending tests of the concrete samples would not be possible without Hendrik Naar, Andres Braunbrück and Peeter.

I am also grateful to Dmitry Kartofelev and Mark Heinštein who provided me with strong support and fruitful discussions, who also co-authored some of my publications.

Special gratitude to Andrus Salupere, Kristi Juske and Mare Saago for their help with many bureaucratic issues and support during my studies.

Last but not least, I am very grateful to my family and friends, especially my parents Irina and Aleksandr Goidyk, my husband Anderoo and my beloved daughter Annika. Without their constant support and encouragement this work would not have been completed.

Abstract

Influence of the flow of fresh fiber concrete on the fiber orientations

This research is focused on studying the influence of the fresh fiber concrete flow on the fiber orientation distribution. Different alignment and fiber orientations demonstrate significant variability in the post-cracking behavior of the tested SFRSCC samples. The beneficial fiber orientations, when the fibers should be mostly aligned in the direction of the tensile stresses, provide better ductility and prevent crack propagation.

However, despite the obvious advantages of adding short fibers to the concrete matrix, some issues remain. One of the main challenges is to provide the most optimal conditions and factors of the casting procedure that ensure the obtaining of the beneficial fiber orientation distribution and can be precisely reproducible. Even existing standards and guidelines concerning fiber concrete do not provide strict rules for the manufacturing procedure and can be highly varying leading to different results. The current research is aimed to shed light on the importance of the casting procedure of SFRSCC samples. Moreover, the standards mostly propose the manufacturing and testing of relatively small specimens where the fiber orientations can be dominated by the wall effect resulting in the fiber's alignment in the direction of the tensile stresses which is quite different for the large structural elements used in practice. Experimental research presented in this thesis demonstrates that even little difference in the manufacturing procedure leads to changes in the fiber orientations that highly influence on the post-cracking behavior and the strength of the testing samples.

In addition, choosing a reliable and precise method for fiber orientation distribution estimation is another challenge in this research topic. In Publication II the application of the efficient non-destructive method of X-ray Computed Tomography analysis. The results of CT analysis are highly dependent on the size of the testing specimens and the resolution of the CT scanner. Therefore, to get more accurate outcomes for this research self-developed software was adapted and modified. The main challenge at this stage is related to the efficient filtering and cleaning process of the data. The implemented filters and parameters included in the analysis should ensure the accurate distinction of the voxels that belong to the fibers ignoring the concrete matrix objects (aggregates and air bubbles) together with noises and artefacts.

However, the experimental manufacturing and testing of large concrete specimens are highly time-, resource-consuming and expensive processes. Thus, the well-designed numerical simulations to predict and analyze the fiber orientations is a promising alternative. In Publication V we presented the comparison of the different casting methods of the fresh concrete flow by the numerical simulations using OpenFOAM software.

In Publications III and IV the obtained outcomes demonstrate the improved fracture behavior of all SFRSCC samples compared to the non-fibered ordinary concrete samples. However, the variation in the post-cracking behavior of fiber concrete samples is large and highly dependent on the place of the sample in the slab. The obtained post-cracking behavior of 40 beams ranges from strain-hardening to strain-softening, showing a clear correlation between the beam location in the slab. Namely, the beams that were cut out from the edges of the slab have shown the strain-hardening post-cracking behavior, while the beams located in the central (middle) part of the slab introduced the weak strain-softening post-cracking behavior.

The results of the experimental testing approximately coincide with the predicted fiber orientation and demonstrate that to achieve better ductility and strain-hardening post-

cracking behavior the fibers should be mostly aligned in a specific way: in the direction of the tensile stresses (Publications I, II, III, IV). In addition, numerical simulations of the different casting methods and various fluid viscosities demonstrate that even a little change in the casting procedure in combination with different transport properties can significantly change the results (Publication V).

The outcomes of this research emphasize the importance of the proper manufacturing process of fiber concrete elements and can contribute to the development of the European construction code.

Kokkuvõte

Vedela kiudbetooni voolamise mõju kiudude orientatsioonile

Töös uuritakse vedela betooni voolamise mõju selles sisalduvate kiudude jaotumisele. Eri-nev kiudude paiknemine ja orienteeritus põhjustab katsetes olulisi erinevusi isetihenduvast teraskiudbetoonist (lühend ingl. k. SFRSCC) katsekehade pragunemise järgses käitumises. Kiudude soodsaim orienteeritus, kus kiud on enamuses joondunud tõmbepingete sihis, võimaldab katsekeha paremat plastset käitumist ja takistab prao arengut. Siiski, vaatamata ilmsetele eelistele, mida lühikeste kiudude lisamine betoonile annab, jääb ka lahtisi küsimusi.

Üks põhilisi väljakutseid on optimaalsete tingimuste ja mõjurite väljapakkumine valutöödele, mis oleks täpselt korratavad ja tagaks soodsa kiudude orientatsioonilise jaotumise. Isegi olemasolevad kiudbetooni standardid ja juhendid ei paku tootmisprotsessile täpseid reegleid, vaid on oma soovitustes varieeruvad, mis võib viia erinevale lõpptulemusele. Käesoleva uurimistöö eesmärk on heita valgust SFRSCC katsekehade valuprotsessi olulisusele. Standardid pakuvad katsetamiseks suhteliselt väikesi katsekehi, kus kiudude orientatsioon võib olla mõjutatud seina efektist ja see tekitab kiudude joondumist tõmbepingete sihis, samas suurte detailide puhul, mida kasutatakse ehituspraktikas, võib olla pilt teistsugune.

Eksperimentaalsed tulemused, mida siin töös esitatakse näitavad, et isegi väikesed muutused tootmisprotsessis viivad muutusteni kiudude orientatsioonis, mis mõjutavad oluliselt katsekehade pragunemise järgset käitumist ja tugevust.

Lisa väljakutseks selles uurimisvaldkonnas on välja valida usaldusväärne ja täpne meetod kiudude orientatsioonilise jaotuse hindamiseks. Publikatsioonis II on kirjeldatud tõhusat mittepurustavat meetodit, mis põhineb röntgenkiirte arvutuslikul tomograafial (lühend ingl. k. CT). CT skaneeringu tulemused sõltuvad palju katsekeha mõõtmetest ja skanneri resolutsioonist. Paremate tulemuste saamiseks on siin töös kasutatud enda arendatud tarkvara, mida saab kohandada ja modifitseerida vastavalt vajadusele. Selle tegevuse põhiraskus on seotud andmete tõhusa filtreerimise ja puhastamisega. Töös kasutatud filtrid ja sellega seotud parameetrid peaksid tagama täpse mahuelemendi eristamise, mis on seotud kiuga ning välistama betooni kui maatriksi objektid (lisandid ja õhumullid) koos muu müra ja artefaktidega.

Publikatsioonides III ja IV saadud tulemused näitavad SFRSCC katsekehade paremat pragunemise järgset käitumist võrreldes ilma kiuta tavalise betooniga. Samas tulemused varieeruvad suuresti sõltudes sellest, mis kiudbetoonplaadi piirkonnast oli katsekeha pärit. 40 kiudbetoonplaadist väljalõigatud tala pragunemise-järgne käitumine varieerus plastsest tugevnemisest (kalestumine) plastse nõrgenemiseni olles selges korrelatsioonis tala asukohaga plaadis. Täpsemalt talad, mis olid pärit plaadi äärtest näitasid pragunemise järel plastset tugevnemist ja talad, mis lõigatud plaadi keskosast näitasid pragunemise järel vähest plastset nõrgenevat käitumist.

Samas suurte mõõtmetega betoonist katsekehade tootmine ja katsetamine eksperimentideks on aja- ja ressursimahukas ning kallis protsess. Siin on paljulubavaks alternatiiviks hästi kujundatud numbrilised simulatsioonid, mis ennustaksid ja analüüsiks kiudude orientatsiooni. Kasutades OpenFOAM tarkvara olen publikatsioonis V esitanud vedela betooni voolamise numbriliste simulatsioonide abil erinevate betooni valuprotsesside meetodite võrdluse.

Katsetulemused langevad ligikaudselt kokku ennustatud kiudude orientatsiooniga ja näitavad, et paremate pragunemise järgse plastsete omaduste ja kalestumise jaoks peaksid kiud olema orienteeritud kindlal moel, nimelt tõmbepingete sihis (publikatsioonid I, II, III, IV). Erinevate valumeetoditega ja erinevate vedeliku viskoossustega tehtud numbrilised

simulatsioonid on täiendavalt näidanud, et isegi väike muutus valuprotsessis kombineerituna erinevate omadustega edasikandumises võib tulemusi oluliselt muuta (publikatsioon V).

Selle uurimustöö väljundid rõhutavad kiudbetoonelementide tootmisprotsesside olulisust ja võivad anda oma panuse Euroopa ehitusnormide arendamisel.

Appendix 1

I

H. Herrmann, A. Braunbrück, T. Tuisk, O. Goidyk, and H. Naar. An initial report on the effect of the fiber orientation on the fracture behavior of steel fiber reinforced self-compacting concrete. In H. Herrmann and J. Schnell, editors, *Short fibre reinforced cementitious composites and ceramics*, pages 33–50. Springer, 2019

An Initial Report on the Effect of the Fiber Orientation on the Fracture Behavior of Steel Fiber Reinforced Self-Compacting Concrete



Heiko Herrmann, Andres Braunbrück, Tanel Tuisk,
Oksana Goidyk and Hendrik Naar

Abstract This paper presents a report about work in progress of research on the influence of the fiber orientations on the tensile strength of steel fiber concrete. Different fiber orientations in different parts of a structural element are caused by the casting process. Here, as an example, a small plate was cast of self-compacting concrete containing hooked-end steel fibers. The plate was cut into three beams, which in turn have been subjected to X-ray Computed Tomography scanning to obtain fiber orientations and to three-point bending test, to assess the tensile strength and fracture behaviour.

1 Introduction

During the past decades fiber concrete has become a material construction companies are more and more interested in, due to its potential to form a ductile concrete. This, in turn, has also created interest among researchers from different universities across the world to better understand the material. Due to the short fibers being introduced to the concrete mass at the mixing stage, the otherwise (mostly) homogeneous and isotropic concrete becomes inhomogeneous and anisotropic depending on the spatial and orientational distribution of the fibers [1–3]. For construction companies these effects are unpleasant companions in the “field use” of the material. Inhomogeneous

H. Herrmann (✉) · A. Braunbrück · O. Goidyk
Department of Cybernetics, Tallinn University of Technology, Tallinn, Estonia
e-mail: hh@cens.ioc.ee

A. Braunbrück · T. Tuisk · H. Naar
Department of Civil Engineering and Architecture, Tallinn University of Technology, Tallinn,
Estonia
e-mail: andres@cens.ioc.ee

H. Naar
e-mail: hendrik@mec.ee

T. Tuisk
e-mail: tanel.tuisk@ttu.ee

geneity and anisotropy make the material much more challenging to understand and introduce an additional level of complexity into the theoretical description.

In this paper, we present an ongoing study, similar to [4, 5], with the target of comparing the experimental behaviour of fiber concrete under bending load with different theoretical frameworks. Here, only the initial setup of the study and initial outcomes are presented, the comparison with theoretical models is future work.

1.1 Theoretical Work

So far, several theoretical models have been presented by researchers involving different levels of information about the fiber orientations [2, 3, 6–11]. In these, the level of fiber orientation information taken into account varies greatly, from only fiber amount, over average projected length (orientation number) [6], orientation profile [3] to orientation or alignment tensors and derived orientation parameters [2, 8, 9, 11, 12].

Some countries have developed (draft) guidelines for fiber concrete use in construction, among these Denmark [13], Germany [14], Sweden [15], USA [16, 17], Russia [18, 19] and Austria [20]; where the Austrian guideline is valid only against old national building code, and effectively defunct since Eurocode-2 was adopted. An international approach is [21].

The Swedish standard, for example, only allows the use of fiber concrete in load bearing structures with additional reinforcement. In general, the production method, i.e. the casting method, and its influence on fiber orientations is not taken into account in the standards. This shows, that there is still need for more research.

1.2 Overview of Testing Methods

Several non-destructive methods have been proposed that allow the estimation of the micro-structure, such as the fiber orientation and distribution inside the concrete matrix or damage. These methods include x-ray computed tomography scan (CT) [22–27], image analysis [28], conductometric (AC-IS) [29], electromagnetic [30, 31], ultrasonic [32] and acoustic analysis. However, these methods are not easily implemented in real life [22, 28, 33]. After successful application of non-destructive methods in medical research, they have been increasingly used in the investigation of cementitious composites due to their accuracy, efficiency and non-destructive nature [24].

Currently, assessment of the fiber distribution, its orientation inside the matrix and influence on the mechanical properties of concrete have been accepted as fundamental challenges because of the time- and resource-consuming processes [34, 35]. The majority of obstacles are connected with inability to observe the fiber orientation and distribution within concrete mass immediately after casting.

The appearance and widespread use of steel fiber concrete have aroused interest to investigate the material by new non-destructive testing (NDT) methods for inner microstructure analysis and evaluation of the bonds between aggregates, cement paste and steel fibers. NDT techniques are used widely for a long time, but specifically to be applied in civil engineering not too many are available [36]. These methods have been used during more than three decades to evaluate the condition of a structure and to acquire precise information about the concrete samples. Their main advantages are higher reliability, effectiveness and avoidance of material damage during testing.

The majority of researchers have pointed out that it is essential to apply different NDT methods to fiber cementitious materials. These methods vary from very simple to technically complicated depending on the purpose, including CT, conductometric (AC-IS), electromagnetic, ultrasonic, and acoustic emission methods. This section reviews the main NDT methods applied on concrete structures.

Propagation and reflection of various rays, such as CT scan, through a structure, may be also used to study the amount of damage experienced by concrete structures [22, 23, 28, 37]. An in-depth analysis by Liu et al. [24] using micro-CT technique proves that the influence of size and quantity of aggregate on fiber orientation in cementitious materials is more significant than the influence on spacial distribution of fibers. According to Ponikiewski et al. [22], there is an exponential distribution of the fiber angles with respect to the beam main axis. Moreover, CT scan allows the automatic air pore segmentation, provides data on the position and shape properties and evaluation of orientation of steel fibers. Promentilla et al. [23] demonstrate the use of CT technique in the microstructure studies of cement-based materials in relation to the durability performance of these materials.

Another method for detection of fiber density and orientation is the Alternating Current Impedance Spectroscopy (AC-IS) that make use of the electromagnetic properties of steel fibers with a probe designed for this purpose. Ferrara et al. [29] report that the local average concentration and orientation of the steel fibers can be assessed by measuring the variation of the probe inductance. According to his study, the method is easy to implement: a probe is brought in contact with the specimen, without any particular care about the quality of the contact, nevertheless the test results are repeatable with low uncertainties.

Among other electromagnetic testing methods for steel fiber concrete is surface electromagnetic sensor technique [38]. This method requires access to one surface and uses a radio wave system that is able to measure steel fiber distribution, concentration and orientation in the concrete [38].

In Electrical Resistance Tomography (ERT) several electrodes are connected to the specimen surface, that both send alternating currents to the specimen and also record the resulting voltages from the specimen. The measured data allows to recreate this conductivity distribution of the whole specimen volume [30]. Steel reinforcement bars or metallic fibers, cracks, air voids, changes in moisture, distribution of chloride, all influence conductivity [30].

The main idea of the inductive method proposed by Torrents et al. [31] is to measure the variation in self-induction while the specimen is turned with respect to

three orthogonal axes. As a rough estimate, the average of the three measurements is considered independent of the fiber orientation [31].

With regard to concrete structures, ultrasound has been used for the detection of cracks and corrosion and also for thickness measurements [36]. Schickert et al. [32] have reported about Ultrasonic Synthetic Aperture Focusing Technique (SAFT). From many pulse-echo measurements a tomographic image is constructed [32]. For concrete with distributed damage a nonlinear ultrasonic technique is developed [39]. Ultrasound attenuation and the appearance of the second harmonic are used to characterise distributed damage [39]. These techniques can be used not only to investigate the microstructure of the material but with recent developments like direct-sequence spread-spectrum ultrasonic evaluation (DSSSUE) changes in properties after damage of the material like shape, density, homogeneity and acoustic velocity may be detected in large and complicated structures [36].

The working principle of acoustic emission (AE) is that a crack is detected the moment it appears, because a propagating crack generates high frequency sound waves and if these waves are extracted from the background noise, the condition of the structure is monitored [36]. AE is very sensitive technique and is able to pick up microscopic changes in the material [36]. During monitoring, the AE sensors of AE work continuously but passively. Unlike other NDE techniques—like radiography, ultrasound, eddy current—AE does not need much preparation time to be set up and is therefore cost-efficient.

In addition, Grosse et al. [40] have pointed out that AE gives us the complete timeline of the damage process without any additional manipulations to the specimen, AE is able to determine the fracture type, size, energy and crack orientation.

The presented various NDT methods are based on different theories, principles and applications, with their advantages and disadvantages. NDT methods have been shown to play a significant role in the assessment and investigation of the microstructure of building materials. Generally, the main advantage of the NDT techniques is the ability to examine the matrix of cementitious materials and reveal hidden defects and acquire data about fiber orientation and distribution without causing damage to the specimen. To achieve better assessment and precise results, it is required to combine several methods. Based on experience, theory and purposes, the best combination of the NDT techniques can be selected for diagnostics of concrete structures.

2 Materials and Methods

To investigate the influence of fiber orientations on the fracture behaviour of fiber concrete, three beam specimen have been prepared by casting a small plate of self-compacting fiber concrete and cutting it into beams. The beams have been subjected to x-ray computed tomography scanning to obtain information about fiber placement and orientation, and to three point bending tests to obtain the stress-strain diagrams. The methods are described in detail below.

Table 1 Data of used fibers:
Sentu WireFib 80/60;
amount used 25kg/m³

Length	60 mm
Diameter	0.75 mm
Aspect ratio	80
Number of fibers/kg n.	4600
Tensile strength	> 1000 MPa
Coating	Uncoated
Steel quality	EN 10016-2 C9

Table 2 Concrete data

Casting day		30.09.16
Slump (diameter) of concrete		750 mm
Temperature		20 °C
Density and Compressive strength at 3 day	2470 kg/m ³	48.2 MPa
Density and Compressive strength at 7 day	2460 kg/m ³	61.1 MPa
Density and Compressive strength at 28 day	2470 kg/m ³ 2470 kg/m ³	71.2 MPa 67.5 MPa

2.1 Fresh Concrete

A self-compacting concrete mix was prepared according to a recipe by the producer. Steel fibers of 60 mm length and 0.75 mm diameter with hooked ends (see Table 1) have been added at the mixing stage and mixed with the concrete according to the data sheet.

Cubes for compression tests have been prepared according to the usual procedure, the test results are presented in Table 2.

2.2 Casting of a Small Plate

To test the influence of the fiber orientation on the mechanical properties of the fiber concrete, especially on the peak load and post-cracking behaviour, a small plate has been cast. The size of the plate was ($L \times W \times H$) 90 cm \times 60 cm \times 20 cm.

The plate was cast from one end with a 10 cm wide inlet and flow directed along the length of the plate. This casting was chosen to enable comparison with the fluid simulations and “simulation experiments” (see [41, 42]). As mentioned before, the concrete was self-leveling concrete and the slump-test had a diameter of 75 cm.

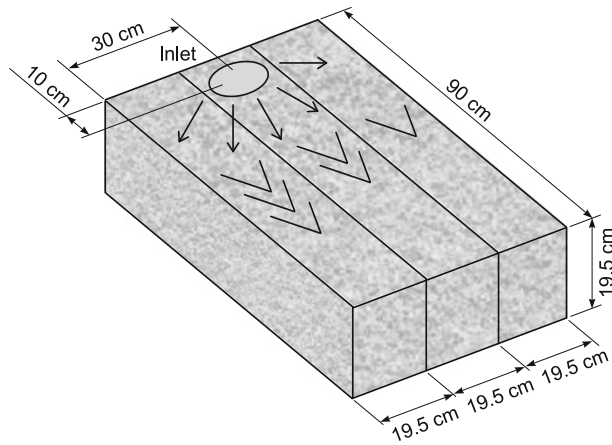


Fig. 1 Cutting beams from the plate

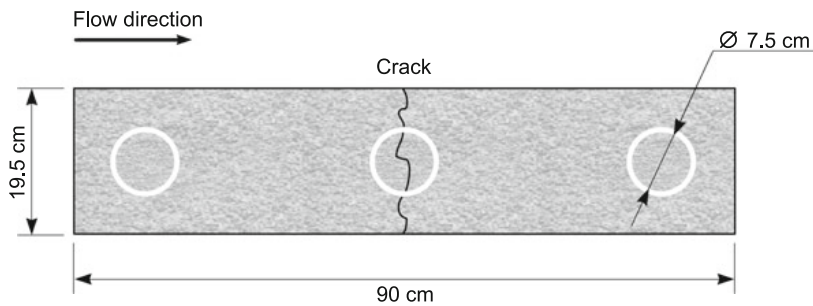


Fig. 2 Position of cylinders

2.3 Preparing Beams from the Plate

This plate has been cut into three beams of size ($L \times W \times H$) 90 cm \times 19.5 cm \times 19.5 cm (see Fig. 1). According to the computer simulations and “simulation experiments” (see [41, 42]) the outer beams should have the fibers mostly oriented along the main axis of the beam, while in the middle beam the fibers should be mostly perpendicular to the main axis.

2.4 Drilling of Cylinders

After the mechanical testing of the beams, cylinder samples were drilled out of the beams (see Fig. 2), to enable a better tomography scanning of some areas, especially of the crack area, and also to perform split-tests (see Sect. 4.2).

3 Fiber Orientations Measurement by X-Ray Computed Tomography

X-ray computed tomography has become an efficient and reliable method to obtain information about the inner structure of materials. It can be used on the macro and down to the nano scale, depending on the sample size and x-ray attenuation of the scanned objects. Previous studies have used x-ray computed tomography to obtain information about aggregates, porosity [43, 44] and fiber positions and orientations [25–27, 42, 45–48].

In this study, fiber orientations in a small plate are of interest. The plate was cut into beams and later, after bending tests, cylinders have been drilled from the beams. The beams and cylinders have been subjected to x-ray computed tomography scanning using medical scanners. The devices used and results are discussed in the following.

3.1 X-Ray CT of the Beams

The beams have been scanned using a GE Medical Systems “Discovery STE”, the reconstruction of the volume was performed with 0.6 mm resolution, Table 3 summarizes the parameters. The size of the beams (cross section 19.5 cm × 19.5 cm) turned out to be slightly above the attenuation limit for this scanner, fibers can only be clearly identified close to the surfaces of the beam, not in the inner region. The fibers in the bottom layer of the beams can be seen in Fig. 3. Visually the fiber orientations coincide with the expectations from a casting into a slippery formwork [4, 41, 42].

From the orientation ellipses shown in Fig. 4d, f one can see, that the orientation is more favourable to take tension stresses in the outer regions of the plate, namely the left side of beam 3 and the right side of beam 1, while in the center region of the plate (beam 2) the fiber orientation distribution is more isotropic with a tendency to alignment perpendicular to the tension stress.

The numbers of fibers per beam segment and per cell in the beams differ from 11 to 29, with the highest numbers in the central beam (beam 2), see Fig. 4g, h, i.

3.2 X-Ray CT of the Cylinders

Due to the problems with separating fibers from the matrix in the CT scans of the beams, cylinders have been drilled from the beams after the bending tests, to identify fiber orientations in the bulk and in the crack plane. The scans were again performed using a medical CT scanner, but this time a GE Medical Systems “Discovery CT750 HD” was used. The parameters of the scan are summarized in Table 4.

Table 3 Scanning and reconstruction parameters used for beams

Manufacturer	GE MEDICAL SYSTEMS
Manufacturers model name	Discovery STE
Full fidelity	CT_LIGHTSPEED
Acquisition group length	412
Scan options	HELICAL MODE
Slice thickness	0.625000
Data collection diameter	500.000000
Reconstruction diameter	317.000000
X Ray tube current	400
Filter type	BODY FILTER
Convolution kernel	BONEPLUS
Single collimation width	0.625
Total collimation width	40
Table feed per rotation	20.625
Spiral pitch factor	0.515625
Rows	512
Columns	512
Pixel spacing	0.619141/0.619141
Bits allocated	16
Bits stored	16
High bit	15
Pixel representation	Signed

An example of the data received from the CT scan is given in Fig. 5. The volume image is thresholded to show only the greylevel corresponding to fibers, but as one can see, some aggregate particles have almost the same attenuation, and therefore greylevel, as the fibers.

4 Strength Experiments and Results

Two types of mechanical tests have been performed: three-point bending tests of the beam specimen and splitting tests on cylinders drilled from the beams after the bending tests.

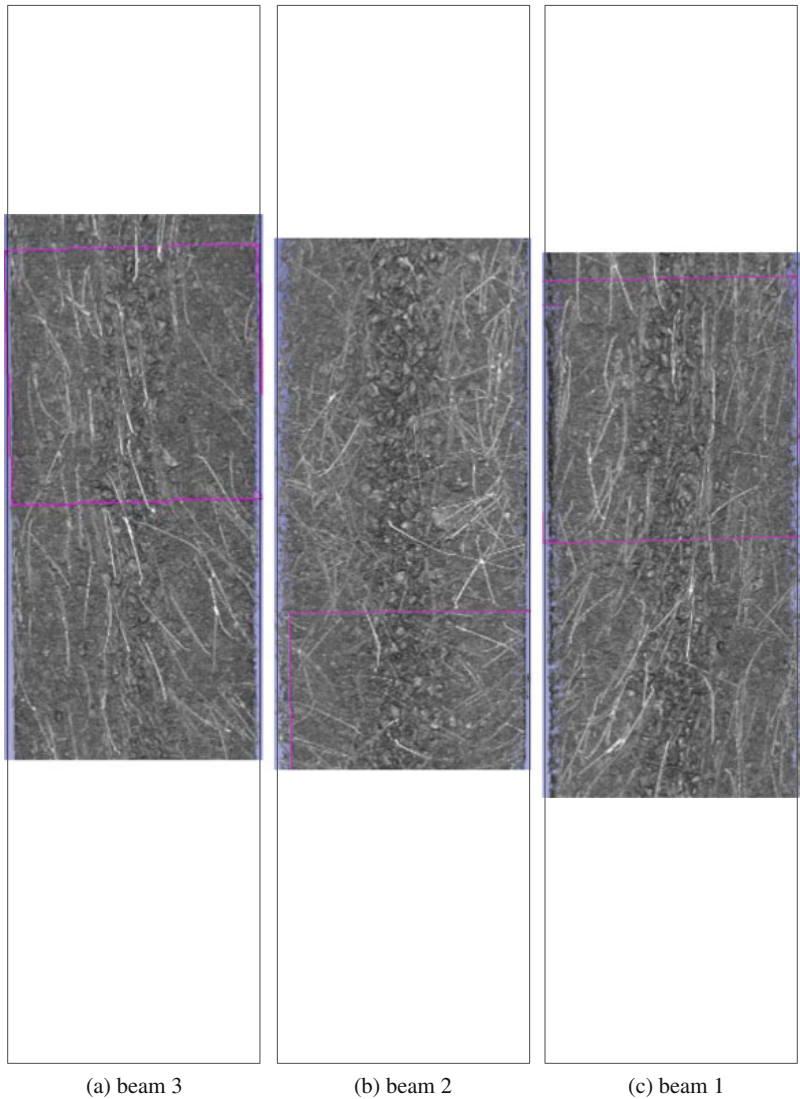
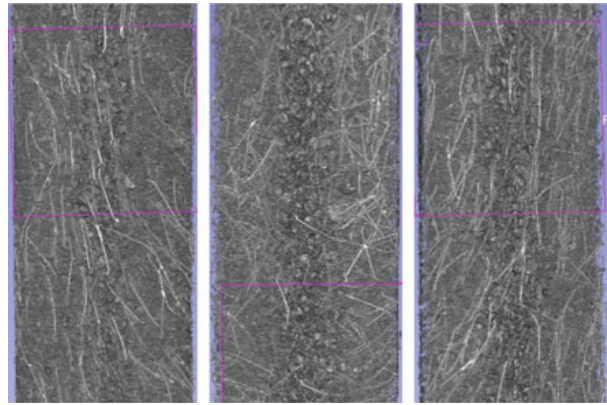


Fig. 3 Bottom layer of the central section of the beams in x-ray CT, the volume image is thresholded to show the fibers in the bottom layer

4.1 Bending Test

The three-point bending tests of the fiber-concrete beam specimens was performed on *Zwick Roell z250* strength testing machine. Three beams with dimensions $90 \times 19.5 \times 19.5$ cm were tested. The two vertical supports *A* and *B* were $L = 0.78$ m apart, each being positioned 6 cm inward from the end of the beam, Fig. 6. The line-load *F* was applied at the mid cross-section *C* (Fig. 7).

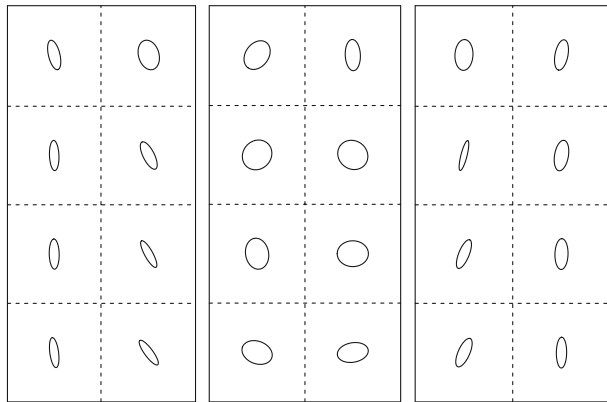
Fig. 4 CT image of center parts of beams thresholded to show fibers in bottom layer, fiber orientation ellipses and fiber amount per cell in the three beams; beam 1: 137 fibers; beam 2: 198; beam 3: 156



(a) CT, beam 3

(b) CT, beam 2

(c) CT, beam 1



(d) orientation, beam 3

(e) orientation, beam 2

(f) orientation, beam 1

19	23	24	29	16	17
20	15	24	28	17	11
20	16	23	26	21	15
20	23	21	23	20	20

(g) amount, beam 3

(h) amount, beam 2

(i) amount, beam 1

Table 4 Scanning and reconstruction parameters used for cylinders

Manufacturer	GE MEDICAL SYSTEMS
Rows	512
Columns	512
Bits allocated	16
Bits stored	16
High bit	15
Pixel representation	Signed
X Ray tube current in micro amps	300000.00
Acquisition type	SPIRAL
Single collimation width	0.62
Total collimation width	40
Spiral pitch factor	0.52

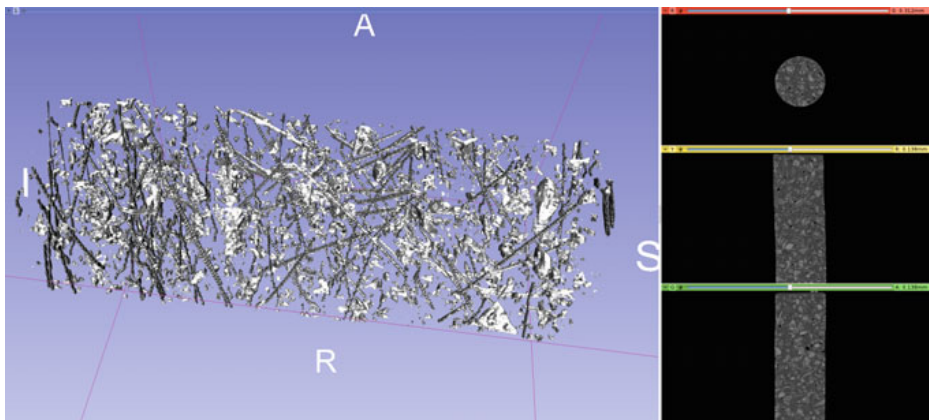


Fig. 5 Volume and slice images of a CT scanned cylinder

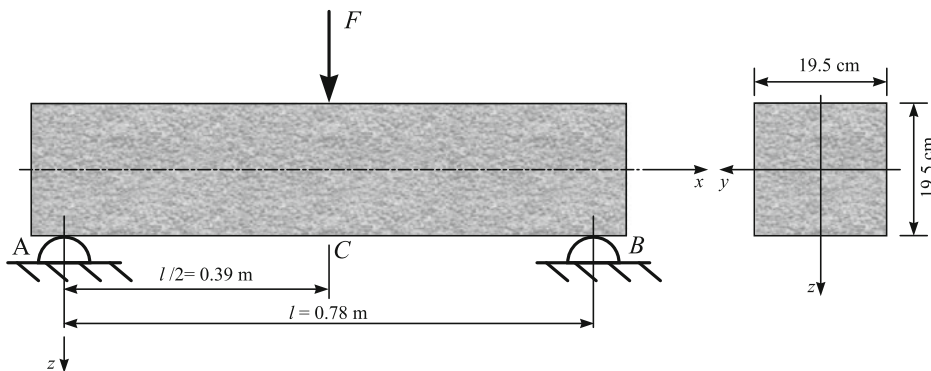


Fig. 6 Bending test setup

Fig. 7 Photo of the bending test showing a beam sample in the testing machine with the frame for displacement measurements and displacement sensors



The recorded force-displacement curves are presented in Fig. 8 where the maximum force value before cracking is $F_1 = 45.36$ kN, $F_2 = 44.06$ kN and $F_3 = 43.18$ kN for beams 1, 2, and 3, respectively. The formula to calculate the maximum bending stresses in a cross-section is $\sigma^{M_y} = \frac{M_y}{W_y}$ that we apply in the cross-section C where the bending moment is given by $M_y = FL/4$ and the section modulus is given by $W_y = (wh^2)/6$.

Flexural fracture strength (in MPa):

$$\sigma^{M_y} = \frac{M_y}{W_y} = \frac{FL}{4} \frac{6}{w * h^2} \quad (1)$$

$$\sigma_{fs} = \frac{1.5 * F * L}{w * h^2} \quad (2)$$

with F maximum force at cracking (in N), L length between supports (in mm), w the width of the sample (in mm) and h the height of the sample (in mm).

Fig. 8 Force displacement curves for the three-point bending test of the three beams

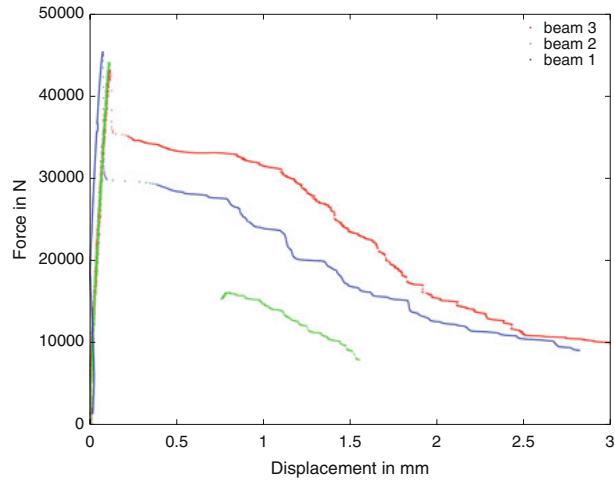


Table 5 Flexural fracture strength of the three beams; the average was $\bar{\sigma}^{M_y} = 6.97$ with a standard-deviation of 0.18

Beam	max. force in N	FFS in MPa
1	45364.7	7.16
2	44058.4	6.95
3	43178.6	6.81

For a cross-section of 19.5×19.5 cm the maximum stress is $\sigma_1^{M_y} = 7.16$ MPa, $\sigma_2^{M_y} = 6.95$ MPa, $\sigma_3^{M_y} = 6.81$ MPa for beams 1, 2, and 3, respectively, see Table 5. Over the three experiments we get the averaged maximum stress $\bar{\sigma}^{M_y} = 6.97$ MPa.

Comparing the results of the bending test with the number and orientation of fibers in the immediate bottom layer, one can note the following: (1) the peak-strength shows no obvious correlation with the fiber amount in/near the crack-region, (2) though beam 2 has the highest number of fibers in the cells next to the crack, it shows the weakest post-cracking, (3) though having the highest number of fibers, their orientations is the least beneficial in beam 2, this seems to show correlation with the post-cracking behaviour. Taking both fiber amount and orientation into account one can note: beam 1 and 3 have both similar orientation distributions and beam 3 has a higher number of fibers, beam 3 also shows the best post-cracking behaviour of the three beams.

4.2 Split Test

The split test was performed with a *Matest IT Tech Cyber Plus Evolution* testing machine on a single specimen that was drilled out from the intact part of the beam

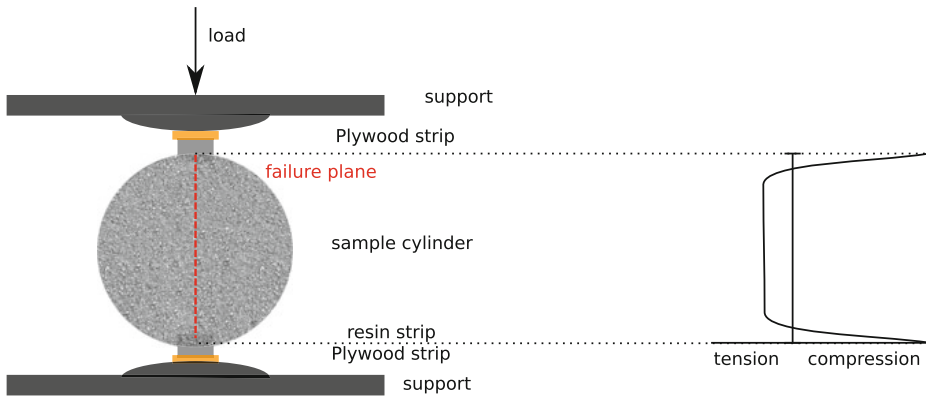


Fig. 9 Schematic of split test



Fig. 10 Split test

sample after the three-point bending test. The cylinder specimen had the average diameter $d = 74$ mm and height $l = 195$ mm. In addition to the regular setup of a concrete split test a special epoxy glue interlayer was prepared on two opposite sides of the cylinder to facilitate a smoother distribution of loads over the cylinder surface, Fig. 9.

The maximum force during the split test was $P = 126160$ N, Fig. 10. The splitting tensile strength σ in MPa may be calculated as [49]:

$$\sigma = \frac{2P}{\pi ld} = \frac{2 \cdot 126160}{\pi \cdot 74 \cdot 195} \frac{N}{mm^2} = 5.57 \text{ MPa} \quad (3)$$

with P the maximum applied load in N, l the length in mm and d the diameter in mm.

For our sample a splitting tensile strength $\sigma = 5.57$ MPa resulted.

5 Future Work

The casting of a larger plate, from which more beams with similar to identical fiber orientation distributions can be cut, is underway. Also, for this casting at the same time more reference samples for compression tests of pure concrete and fiber concrete will be cast, additionally a reference plate out of pure concrete will be cast to produce reference beams for the bending tests. This will improve statistics and provide error margins.

6 Conclusion

In this preliminary study the contribution of fiber orientation on the strength of steel fiber reinforced concrete was investigated. Three-point bending tests have been performed on beam samples and special attention has been paid to the fiber amount and orientation distribution in the bottom layer. While the results give no conclusive evidence that the peak strength depends on the amount or orientation of fibers, the post-cracking behaviour shows dependence on fiber orientations and amount. The following has been noted: the beam with the highest amount of fibers in the bottom layer (highest tensile stress) showed the weakest post-cracking behaviour, it had also the least beneficial fiber orientation distribution. Two beams with similar beneficial fiber orientation distributions showed better post-cracking behaviour, the one with a slightly higher fiber count was the stronger one among the two in the post-cracking regime.

Acknowledgements The authors gratefully acknowledge the funding by the Estonian Research Council by the exploratory research grant PUT1146.

We also thank Maria Kremsreiter who helped during her Erasmus+ internship at the Institute of Cybernetics. Therefore: With the support of the Erasmus+ programme of the European Union. Thanks to E-Betoonement, especially Aare Lessuk, Rasmus-R. Marjapuu and Sergej Graf, for preparing the experiment plate.

References

1. Eik, M., Löhmus, K., Tigasson, M., Listak, M., Puttonen, J., Herrmann, H.: DC-conductivity testing combined with photometry for measuring fibre orientations in SFRC. *J. Mater. Sci.* **48**(10), 3745–3759 (2013)
2. Herrmann, H.: An improved constitutive model for short fibre reinforced cementitious composites (SFRC) based on the orientation tensor. In: *Generalized Continua as Models for Classical and Advanced Materials*, pp. 213–227. Springer International Publishing, Cham (2016)
3. Laranjeira, F., Grünewald, S., Walraven, J., Blom, K., Molins, C., Aguado, A.: Characterization of the orientation profile in fiber reinforced concrete. *Mater. Struct.* **44**(6), 1093–1111 (2011)
4. Žirgulis, G., Švec, O., Sarmiento, E.V., Geiker, M.R., Cwirzen, A., Kanstad, T.: Importance of quantification of steel fibre orientation for residual flexural tensile strength in FRC. *Mater. Struct.* 1–17 (2015)
5. Švec, O., Žirgulis, G., Bolander, J.E., Stang, H.: Influence of formwork surface on the orientation of steel fibres within self-compacting concrete and on the mechanical properties of cast structural elements. *Cement Concr. Compos.* **50**, 60–72 (2014)
6. Grünewald, S.: Performance-based design of self-compacting fibre reinforced concrete. Ph.D. thesis, Technische Universiteit Delft (2004)
7. Eik, M., Puttonen, J., Herrmann, H.: An orthotropic material model for steel fibre reinforced concrete based on the orientation distribution of fibres. *Compos. Struct.* **121**, 324–336 (2015)
8. Eik, M., Herrmann, H., Puttonen, J.: Orthotropic constitutive model for steel fibre reinforced concrete: linear-elastic state and bases for the failure. In: Kouhia, R., Mäkinen, J., Pajunen, S., Saksala, T. (eds.) *Proceedings of the XII Finnish Mechanics Days: 4–5 June 2015, Tampere, Finland*, pp. 255–260 (2015)
9. Herrmann, H., Eik, M., Berg, V., Puttonen, J.: Phenomenological and numerical modelling of short fibre reinforced cementitious composites. *Meccanica* **49**(8), 1985–2000 (2014)
10. Krasnikovs, A., Kononova, O., Khabbaz, A., Machanovsky, E., Machanovsky, A.: Post-cracking behaviour of high strength fiber concrete prediction and validation. *World Acad. Sci. Eng. Technol.* **59**, 988–992 (2011)
11. Eik, M., Puttonen, J., Herrmann, H.: The effect of approximation accuracy of the orientation distribution function on the elastic properties of short fibre reinforced composites. *Compos. Struct.* **148**, 12–18 (2016)
12. Herrmann, H., Beddig, M.: Tensor series expansion of a spherical function for use in constitutive theory of materials containing orientable particles. *Proc. Est. Acad. Sci.* **67**(1), 73–92 (2018) (Open-Access CC-BY-NC 4.0)
13. Kasper, T., Tvede-Jensen, B., Stang, H., Mjoernell, P., Slot, H., Vit, G., Thrane, L.N., Reimer, L.: Design guideline for structural applications of steel fibre reinforced concrete. Technical report, SFRC Consortium (2014)
14. Deutscher Ausschuss für Stahlbeton: DAFStb-Richtlinie. Beuth Verlag GmbH, Berlin (2010)
15. SIS.: Fibre concrete-design of fibre concrete structures (Swedish standard – SS 812310:2014) (2014)
16. ACI Committee 544.: 544.4r-88 design considerations for steel fiber reinforced concrete. Technical report, American Concrete Institute (2002)
17. ACI Committee 544.: 544.5r-10: Report on the physical properties and durability of fiber-reinforced concrete. Technical report, American Concrete Institute (2010)
18. SNIP.: 52-104-2006–steel fibre reinforced concrete structures design. Technical report, SNIP, Moskau (2007)
19. SNIP.: 52-104-2009–steel fibre reinforced concrete structures design. Technical report, SNIP, Moskau (2010)
20. Österreichische Bautechnikvereinigung. Richtlinie faserbeton, 2008. Österreichische Vereinigung für Beton- und Bautechnik
21. Fib.: Model Code 2010. International Federation for Structural Concrete (fib) (2012)

22. Ponikiewski, T., Gołaszewski, J., Rudzki, M., Bugdol, M.: Determination of steel fibres distribution in self-compacting concrete beams using x-ray computed tomography. *Arch. Civil Mech. Eng.* **15**, 558–568 (2015)
23. Promentilla, M.A.B., Sugiyama, T., Shimura, K.: Threedimensional imaging of cement-based materials with x-ray tomographic microscopy: visualization and quantification. In: *International Conference. Microstructure Relat Durab Cem Compos*, vol. 61, pp. 1357–1366 (2008)
24. Liu, J., Li, C., Liu, J., Cui, G., Yang, Z.: Study on 3D spatial distribution of steel fibers in fiber reinforced cementitious composites through micro-ct technique. *Constr. Build. Mater.* **48**, 656–661 (2013)
25. Pastorelli, E., Herrmann, H.: Time-efficient automated analysis for fibre orientations in steel fibre reinforced concrete. *Proc. Est. Acad. Sci.* **65**(1), 28–36 (2016)
26. Herrmann, H., Pastorelli, E., Kallonen, A., Suuronen, J.-P.: Methods for fibre orientation analysis of x-ray tomography images of steel fibre reinforced concrete (SFRC). *J. Mater. Sci.* **51**(8), 3772–3783 (2016)
27. Suuronen, J.-P., Kallonen, A., Eik, M., Puttonen, J., Serimaa, R., Herrmann, H.: Analysis of short fibres orientation in steel fibre reinforced concrete (SFRC) using x-ray tomography. *J. Mater. Sci.* **48**(3), 1358–1367 (2013)
28. Liu, J., Sun, W., Miao, C., Liu, J., Li, C.: Assessment of fiber distribution in steel fiber mortar using image analysis. *J. Wuhan Univ. Technol. Mater. Sci. Ed.* **27**, 166–171 (2012)
29. Ferrara, L., Faifer, M., Toscani, S.: A magnetic method for non destructive monitoring of fiber dispersion and orientation in steel fiber reinforced cementitious composites—Part 1: method calibration. *Mater. Struct.* 1–15 (2011)
30. Karhunen, K., Seppänen, A., Lehtikoinen, A., Monteiro, P.J.M., Kaipio, J.P.: Electrical resistance tomography imaging of concrete. *Cement Concr. Res.* **40**, 137–145 (2010)
31. Torrents, J.M., Blanco, A., Pujadas, P., Aguado, A., Juan-García, P., Sánchez-Moragues, M.Á.: Inductive method for assessing the amount and orientation of steel fibers in concrete. *Mater. Struct.* **45**(10), 1577–1592 (2012)
32. Schickert, M.: Progress in ultrasonic imaging of concrete. *Mater. Struct.* **38**, 807–815 (2005)
33. Grigaliunas, P., Kringelis, T.: SCC flow induced steel fiber distribution and orientation, non-destructive inductive method. In: *11th European Conference on Non-Destructive Testing*. Prague, Czech Republic (2014)
34. Zhou, B., Uchida, Y.: Fiber orientation in ultra high performance fiber reinforced concrete and its visualization. In: *8th International Conference on Fracture Mechanics of Concrete and Concrete Structures* (2013)
35. Svec, O., Skocek, J., Olesen, J.F., Stang, H.: Fibre reinforced self-compacting concrete flow simulations in comparison with l-box experiments using carbopol. In: *8th Rilem International Symposium on Fibre Reinforced Concrete* (2012)
36. Rens, K.L., Wipf, T.J., Klaiber, F.W.: Review of nondestructive evaluation techniques of civil infrastructure. *J. Perform. Constr. Facil.* **11**, 152–160 (1997)
37. Akhtar, S.: Review of nondestructive testing methods for condition monitoring of concrete structures. *J. Constr. Eng.* (2013)
38. Al-Mattarneh, H.: Electromagnetic quality control of steel fiber concrete. *Constr. Build. Mater.* **73**, 350–356 (2014)
39. Shah, A.A., Hirose, S.: Nonlinear ultrasonic investigation of concrete damaged under uniaxial compression step loading. *J. Mater. Civil Eng.* **11**, 476–484 (2009)
40. Grosse, C.U., Reinhardt, H.W., Finck, F.: Signal-based acoustic emission techniques in civil engineering. *J. Mater. Civil Eng.* **15**, 274–279 (2003)
41. Herrmann, H., Lees, A.: On the influence of the rheological boundary conditions on the fibre orientations in the production of steel fibre reinforced concrete elements. *Proc. Est. Acad. Sci.* **65**(4), 408–413 (2016) (Open-Access CC-BY-NC 4.0)
42. Herrmann, H., Goidyk, O., Braunbrück, A.: Influence of the flow of self-compacting steel fiber reinforced concrete on the fiber orientations, a report on work in progress. In: *Short Fiber Reinforced Cementitious Composites and Ceramics*. Springer (2018)

43. Ponikiewski, T., Katzer, J., Bugdol, M., Rudzki, M.: Determination of 3D porosity in steel fibre reinforced SCC beams using x-ray computed tomography. *Constr. Build. Mater.* **68**, 333–340 (2014)
44. du Plessis, A., le Roux, S.G., Guelpa, A.: Comparison of medical and industrial x-ray computed tomography for non-destructive testing. *Case Stud. Nondestruct. Test. Eval.* **6**, 17–25 (2016)
45. Vicente, M.A., González, D.C., Mínguez, J.: Determination of dominant fibre orientations in fibre-reinforced high-strength concrete elements based on computed tomography scans. *Nondestruct. Test. Eval.* **29**(2), 164–182 (2014)
46. Ponikiewski, T., Katzer, J., Bugdol, M., Rudzki, M.: Steel fibre spacing in self-compacting concrete precast walls by x-ray computed tomography. *Mater. Struct.* **48**(12), 3863–3874 (2015)
47. Ponikiewski, T., Katzer, J., Bugdol, M., Rudzki, M.: X-ray computed tomography harnessed to determine 3D spacing of steel fibres in self compacting concrete (SCC) slabs. *Constr. Build. Mater.* **74**, 102–108 (2015)
48. Mínguez, M.A.V.J., Gonzalez, D.C.: Image data processing to obtain fibre orientation in fibre-reinforced elements using computed tomography scan. In *Short Fiber Reinforced Cementitious Composites and Ceramics*. Springer (2018)
49. ASTM International.: Standard test method for splitting tensile strength of cylindrical concrete specimens. Technical report, ASTM, 2004. Designation: C 496/C 496M – 04

Appendix 2

II

H. Herrmann, O. Goidyk, and A. Braunbrück. Influence of the flow of self-compacting steel fiber reinforced concrete on the fiber orientations, a report on work in progress. In H. Herrmann and J. Schnell, editors, *Short Fibre Reinforced Cementitious Composites and Ceramics*, pages 97–110. Springer, 2019

Influence of the Flow of Self-Compacting Steel Fiber Reinforced Concrete on the Fiber Orientations, a Report on Work in Progress



Heiko Herrmann, Oksana Goidyk and Andres Braunbrück

Abstract This paper presents a report about work in progress of research on the influence of the flow of SCFRC on the fiber orientations. Mechanical properties of the short steel fiber reinforced cementitious materials mostly depend on the fiber orientation and spatial dispersion. Many studies have shown that it is possible to achieve the desired fiber orientation by optimizing the parameters of rheological properties or the casting process. In order to improve the key mechanical properties, multiple statistical experiments with various factors are needed. This paper analyzes the influence of casting velocity and formwork surface quality on the fiber distribution and orientation. A suitable technique for our method was to replace Steel Fiber Reinforced Self-Compacting Concrete (SFRSCC) by a transparent polymer with similar rheological properties as SFRSCC. Preliminary analysis of the experimental results shows that the fibers tend to orient mostly perpendicular to the flow direction and turn their orientation longitudinally near the walls. Experiments showed that the fiber spatial distribution was affected by the casting velocity. Faster casting velocities provided more preferable homogeneous distribution. Moreover, the roughness of the bottom of the formwork demonstrated some influence on the fiber orientations but no significant impact on the spatial dispersion. In addition, we used the image analysis method to estimate fiber orientation and distribution.

1 Introduction

Steel fiber reinforced self-compacting concrete (SFRSCC) is increasingly used in today's building industry because of its alleged advantages over ordinary concrete, however, the use in load-bearing structures requires additional reinforcement. Self-compacting concrete (SCC) itself simplifies the casting process significantly due to

H. Herrmann (✉) · O. Goidyk · A. Braunbrück
Department of Cybernetics, Tallinn University of Technology, Tallinn, Estonia
e-mail: hh@cens.ioc.ee

A. Braunbrück
e-mail: andres@cens.ioc.ee

© Springer Nature Switzerland AG 2019
H. Herrmann and J. Schnell (eds.), *Short Fibre Reinforced Cementitious Composites and Ceramics*, Advanced Structured Materials 95,
https://doi.org/10.1007/978-3-030-00868-0_7

the compacting capacity to entirely fill the formwork under own weight. The essential advantage of using SCC is that it produces materials free of air voids and honeycombs without using additional vibration [1, 2]. According to many studies, the use of short steel fibers for reinforcing concrete has some advantages in the properties of the material, for example, reduced brittleness, improved ductility, flexural and shear strength of the material. Moreover, the fibers reduce cracking, drying shrinkage and permeability of concrete and bridge cracks during loading and transfer of the load [3–8].

Many studies have attempted to estimate the significance of fibers inside the concrete matrix [7–10]. To evaluate this significance properly, it is essential to take into account many factors. The properties of the short steel fiber concrete largely depend on the full cycle of stages of producing SFRSCC from the mixing to the hardening state. Firstly, the recipe of a mixture, the fiber content, fiber aspect ratio, type, geometry and sizes of fibers are crucial. Secondly, it is required to consider the rheological properties of concrete in a fresh state before casting (flowability, viscosity, compacting ability, etc.). Thirdly, the casting and flow parameters, velocity, possible vibrations and fiber orientations inside the concrete matrix after casting have major influence on the properties of concrete [1, 9, 11–14]. In its turn, the fiber orientations are also largely influenced by the flow of concrete, which depends on the formwork geometry and formwork surface quality. Supposedly, a rough and sticky formwork surface produces a different fiber distribution and orientation compared to a smooth and non-sticky one [12, 15].

To obtain the desired fiber orientation that provides the improved mechanical properties of material, the optimization of casting process is needed. For this purpose, to detect the defects of the internal structure of the materials and to evaluate the fiber orientation and distribution inside the cementitious composites, large variety of non-destructive and destructive methods have been proposed. The current research mostly focuses on the non-destructive methods for estimation of fiber orientation and distribution due to some significant benefits. The crucial advantages of non-destructive methods in comparison with destructive are accuracy, reliability, efficiency, cost saving and safety. The last benefit is extremely important, because of most tests are completely harmless to people and all testing methods leave examined samples totally undamaged. The most popular and frequently applicable in practice in the testing of cementitious materials are x-ray Computed Tomography scanning [9, 16–20], image analysis [10], conductometric (AC-IS) [21], electromagnetic [22, 23], ultrasonic [24] and acoustic [25–27] methods.

Together with non-destructive fiber orientation control methods, numerical simulations of fiber concrete and modeling the cracking behavior are widely used in cementitious materials research.

Computational fluid dynamics (CFD) simulations are starting to become used in the planning of SCC castings to investigate if the SCC flows around reinforcement bars and can fill the complete formwork. CFD simulations need to be calibrated to benchmark cases, to make sure the numerical scheme works. For SCC those benchmark cases have been proposed in [28]. However, only the final result, not the filling velocity was compared. For SFRSCC the situation is much more

complex and factors that influence the fiber orientation and spatial distribution need to be determined in order to propose relevant benchmark cases. Promising simulations have been performed by Svec et al. [12], using a Lattice-Boltzmann approach and immersed particles, and by Herrmann and Lees [15], using a Finite Volume scheme for a Bingham-plastic and a tensorial equation for the fiber orientation distribution. However, before these methods can be used on an everyday basis in production it must be certain that the influential parameters in the casting process are identified. The main purpose of the current research is to identify those parameters by analyzing experimentally the fiber orientation under different casting factors and establish the correlation between the fiber orientation, formwork surface quality and casting velocity; moreover, to compare different casting methods and conditions.

Therefore, in this study numerical and experimental “simulations” of the fibers inside of concrete mass are compared to real castings. The essence of this approach is that the opaque concrete is replaced by a transparent and viscous polymer solution that is similar to the rheological properties and parameters of the fresh self-compacting concrete. For an initial comparison a small concrete plate was produced and subjected to x-ray Computed Tomography to evaluate the fiber distribution and orientation. The results obtained from the casting experiments with the transparent polymer matrix in this research and those from the experiments with a concrete sample will be compared.

2 Materials and Methods

In this section we will describe two different approaches to estimate the fiber orientation and distribution: the first one is focused on the experiments with SFRSCC specimens and further x-ray computed tomography technique (Sect. 2.1), the second approach are “simulation experiments” and are concerned with a transparent polymer mixture as replacement for the opaque concrete (Sect. 2.2).

2.1 Concrete Experiments: Fresh Concrete

In this study, we examined a slab of steel fiber reinforced self-compacting concrete (SFRSCC) of dimensions 90 cm × 60 cm × 20 cm. The casting process was conducted from a hopper positioned in the middle of the edge of the formwork. The point of slump was located at one of the 60 cm edges, see Fig. 1. The formwork was sprayed with a thin layer of oil before casting to simplify the further demolding process. One side of the form was equipped with lifting anchors to simplify the lifting of the slab.

The mix proportion of self-compacting concrete have been chosen by the producer. Hooked end steel fibers were gradually added to the self-compacting concrete and mixed. The fiber volume ratio was 0.5%. The fiber length and the fiber diameter were

Fig. 1 Casting of a small plate using a bucket and half-funnel



Table 1 Fiber concrete data

Casting day		30.09.16
Slump (diameter) of concrete		75 cm
Temperature		20°C
Density and Compressive strength at 3 day	2470 kg/m ³	48.2 MPa
Density and Compressive strength at 7 day	2460 kg/m ³	61.1 MPa
Density and Compressive strength at 28 day	2470 kg/m ³ 2470 kg/m ³	71.2 MPa 67.5 MPa

60 mm and 0.75 mm, respectively; the fiber properties are summarized in Table 2. The properties of the hardened concrete are given in Table 1.

After hardening in order to make an orientation analysis with x-ray CT possible, the slab was cut into three beams of 90 cm × 19.5 cm × 19.5 cm using a diamond saw, as indicated in Fig. 2. The arrows represent the flow direction of concrete. One of the beams contains the lifting anchors.

Table 2 Data of used fibers:
Sentu WireFib 80/60;
amount used 25 kg/m^3

Length	60 mm
Diameter	0.75 mm
Aspect ratio	80
Number of fibers/kg n	4600
Tensile strength	> 1000 MPa
Coating	uncoated
Steel quality	EN 10016-2 C9

2.2 Simulation Experiments: Transparent Replacement Matrix

The method used in this research is similar to that in [8, 29]. It is based on replacing of SFRSCC by transparent polymer mixture, allowing observation of fiber orientation and distribution during and immediately after the casting process. For this experiment, a mixture was produced according to the manufacturer's guidelines of the Sodium PVM/MA Stabilizer. The experimental mixture consists of a stabilizer powder, water and sodium hydroxide (NaOH). The mixture is produced in two main stages. In the first stage, the stabilizer powder is dissolved in the water at room temperature and the obtained mixture is neutralized with NaOH. The mixture should be regularly shaken/stirred to achieve a better homogeneity and dispersion with minimal amount of air voids and bubbles. The second stage ensures higher transparency and gel viscosity of the experimental fluid. Finally, after multiple adding of NaOH and frequent shaking, the PH of the obtained mixture was equal to 7. Then the mixture was left for a couple of days to achieve better viscosity and transparency.

Before the casting experiments, the rheological properties of the mixture were tested by means of the standardized slump flow test. The suitable mixture should represent a homogeneous and visco-plastic fluid (shows Bingham plastic behavior).

Fig. 2 Layout of beam-cutting of small plate

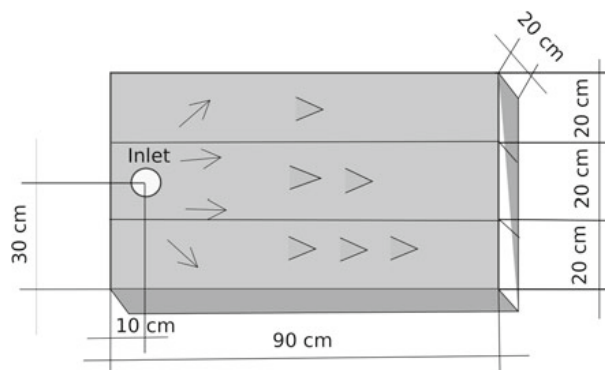
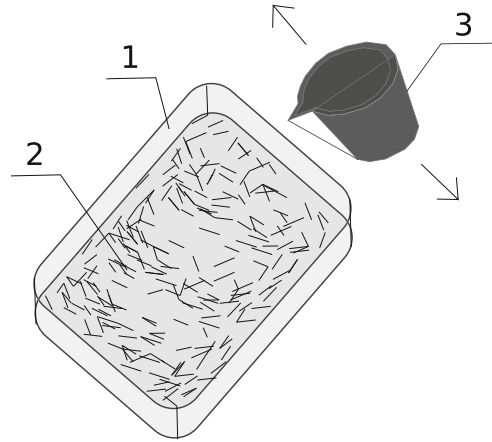


Fig. 3 Casting using a bucket. 1: plastic box, 2: polymer with fibers, 3: 12 l bucket



When the mixture was ready, the matchsticks fibers were gradually added in a proportion of 3%. The length of the matchstick fibers was 50 mm and the aspect ratio (fiber length/fiber diameter) was 25.

The main aim of the casting experiments was to investigate the correlation between the casting conditions—e.g. formwork surface quality—fiber orientation and distribution experimentally. For that purpose, the following series of experiments with different casting conditions and formwork surface quality was performed:

1. Experiment with rough formwork surface and using a fixed pipe located in the middle of the formwork edge;
2. Experiment with smooth formwork surface and using a fixed pipe located in the middle of the formwork edge;
3. Experiment with rough formwork surface and using a bucket located in the middle of the formwork edge;
4. Experiment with smooth formwork surface and using a bucket located in the middle of the formwork edge;
5. Experiment with smooth formwork surface and using a bucket moving back and forth along the formwork edge;
6. Experiment with rough formwork surface and using a bucket moving back and forth along the formwork edge (Fig. 3).

2.3 Fiber Position and Orientation Measurement

Fiber position and orientations in real world are 3D, but here we only consider a thin layer, the bottom layer and therefore use a 2D description, namely x and y coordinates, and one angle θ , the angle between the fiber and the x -axis, counted counter-clockwise.

To describe the fiber orientation¹ and alignment² mathematically, several measures are common, the orientation factor, orientation number which are closely related and based on a pre-set cross-section or preference direction. Mathematically more sophisticated measures exist in the form of the orientation or alignment tensor and the scalar order parameter [30–32].

The orientation factor relates the average fiber orientation to the number of fibers crossing a given cross-section, e.g. a crack-plane:

$$\alpha = \frac{N_f A_f}{A_c v_f}, \quad (1)$$

where A_c is the cross-section area of the concrete under consideration, N_f is the number of fibers in the cross-section A_c , A_f is the fiber cross-section and v_f is the volume fraction of the fibers.

The orientation number calculates the average projected length of a fiber onto a given direction, e.g. the normal to the crack-plane:

$$\eta = \frac{1}{N} \sum_{i=1}^N \cos \theta_i, \quad (2)$$

where θ_i is the angle between the i -th fiber and a given axis, e.g. the x -axis.

The tensor-based orientation and alignment measures are based on the use of spherical harmonical functions and an orientation *distribution* on a unit sphere, for details, see [30–32]. The scalar order parameter is given as:

$$S = \frac{\langle d \cos^2(\phi_i) - 1 \rangle_i}{d - 1}, \quad (3)$$

$$\text{in 3D: } S = \frac{\langle 3 \cos^2(\phi_i) - 1 \rangle_{i=1 \dots N}}{2}, \quad (4)$$

$$\text{in 2D: } S = \frac{\langle 2 \cos^2(\phi_i) - 1 \rangle_{i=1 \dots N}}{1}, \quad (5)$$

where $\langle \cdot \rangle$ denotes the ensemble average over all N fibers, d is the space dimension and ϕ_i is the angle between the i -th fiber and the average orientation. The average orientation can be obtained from the eigenvectors and eigenvalues of the second order orientation tensor.

The scalar order parameter is independent of a pre-defined direction, as it describes how well the fibers are aligned with each other. The eigenvectors of the alignment tensor describe in which direction the fibers are oriented.

Fiber orientations and their alignment can be visualized by orientation ellipses, whose major axes are oriented according to the eigenvectors and the scaling of the

¹Orientation as in oriented in a (certain) direction.

²Alignment as in aligned with each other.

axes is according to the eigenvalues of the second order orientation or alignment tensor.

$$\frac{(e_1^T x)^2}{\left(\frac{1}{\sqrt{\lambda_1}}\right)^2} + \frac{(e_2^T x)^2}{\left(\frac{1}{\sqrt{\lambda_2}}\right)^2} = 1 \quad (6)$$

or, with all ellipses having the same major axis (assuming λ_1 is the smaller eigenvalue)

$$\frac{(e_1^T x)^2}{1} + \frac{(e_2^T x)^2}{\left(\sqrt{\frac{\lambda_2}{\lambda_1}}\right)^2} = 1. \quad (7)$$

3 Results of Casting Experiments

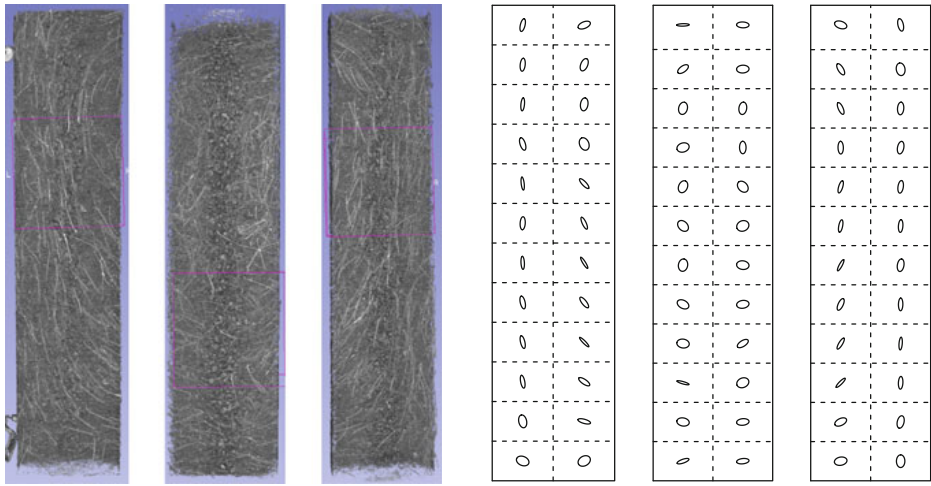
In this section the results of the analysis of the spatial and orientational distribution of the fibers for the SFRC and for the “simulation” experiments with the polymer matrix will be presented. The fiber orientations have been obtained from images of the cast material. In the case of the SFRC, this has been x-ray CT images, and in the case of the polymer matrix, photos have been taken after the casting. In both cases, the fibers have been analyzed using the measurement tool from ImageJ [33].

3.1 Casting of a Small SFRC Plate: Fiber Orientations and Spatial Distribution

The three beams have been scanned using a medical x-ray CT scanner. The bottom layer of the volume images was then thresholded to show the fibers. In the resulting image, the fibers were measured using the measurement tool of ImageJ with manual identification of the fibers. This was necessary, as automatic fiber analysis was difficult due to the low resolution of the scanner compared to the fiber diameter and the large sample diameter, which had caused noise and artifacts together with a strong cupping effect.

The orientation and position analysis of the received data was performed using self-developed scripts [34] in R [35] calculating the orientation tensor and its eigenvalues and eigenvectors and finally plotting [36] the orientation ellipses.

Figure 4 shows the results of the orientation and spatial distribution analysis. As can be seen, the orientation distribution resembles one predicted for a slippery formwork [15]. Especially the fibers are oriented mostly perpendicular to the flow velocity.



(a) Beam 3 (b) beam 2 (c) Beam 1 (d) Beam 3 (e) Beam 2 (f) Beam 1

21	9
15	14
7	9
19	14
15	7
15	13
16	11
14	13
12	14
11	15
9	14
4	5

7	12
13	13
21	19
14	18
16	17
16	20
16	14
13	16
13	14
9	18
11	12
9	7

18	15
18	11
6	9
13	11
11	9
18	8
14	10
17	15
14	12
13	15
13	12
7	8

(g) Beam 3 (h) Beam 2 (i) Beam 1

Fig. 4 Bottom layer of the beams in x-ray CT. Casting point was at the top of the middle beam. The fibers are mostly oriented parallel to the flow front, meaning perpendicular to the flow velocity

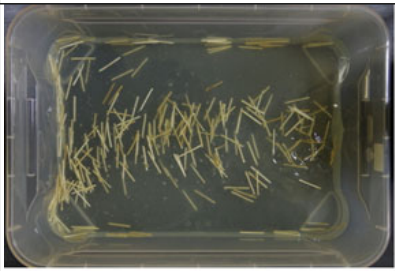
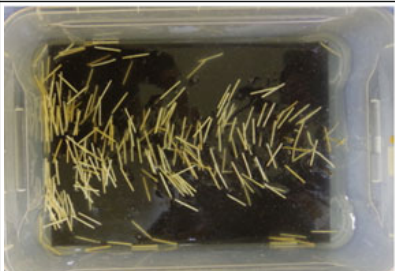
3.2 Replacement Castings: Fiber Orientations and Spatial Distribution

Preliminary observations were obtained immediately after each experiment, which show that the fiber orientation is mainly perpendicular to the flow direction but their spatial distribution is quite different.

After each series of experiments, we obtained the images from above, which were subjected to further image analysis. A typical image obtained during the experiment is presented in Table 3.

The results of the spatial and orientational analysis for the different casting schemes are presented in Figs. 5, 6, 7 and 8. As can be seen, the fibers are mainly oriented perpendicular to the flow direction. The dependence of the orientational

Table 3 Matrix of experiments

	slow	fast
bottom		
smooth dry		
smooth wet		
rough dry		

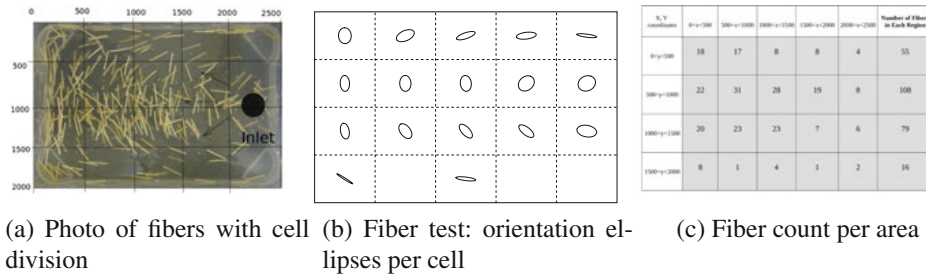


Fig. 5 Fiber orientations, smooth bottom, fast casting

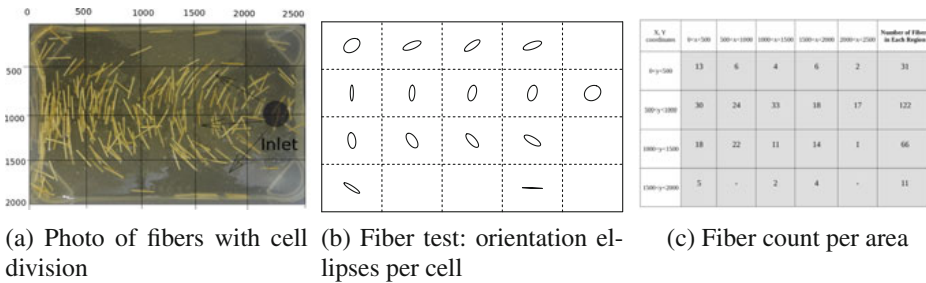


Fig. 6 Fiber orientations, smooth bottom, slow casting

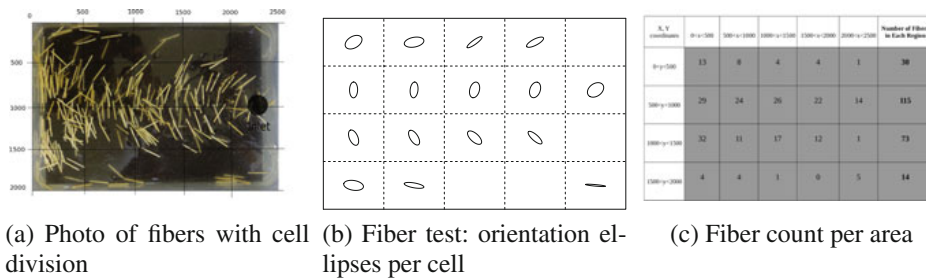


Fig. 7 Fiber orientations, rough bottom, slow casting

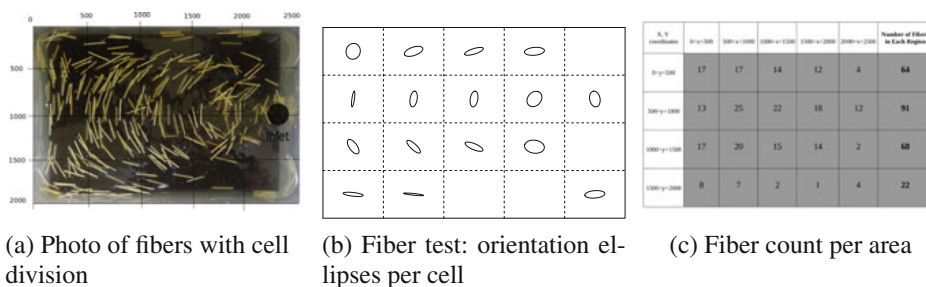


Fig. 8 Fiber orientations, rough bottom, fast casting

distribution on the smoothness of the formwork bottom is inconclusive. The spatial distribution show a dependence on the casting velocity, with the fibers concentrating in a narrower channel in cases of very slow casting.

4 Conclusion

Several factors influencing the fiber orientations and placement in fiber reinforced materials have been experimentally investigated. The experiments showed a surprising influence of the casting velocity on the spatial distribution of fibers, while only small influence on the orientational distribution. The roughness of the formwork bottom showed some influence on the fiber orientations but no significant influence on the spatial dispersion. While some influences have been identified in this initial study, further investigations are necessary.

Acknowledgements The authors gratefully acknowledge the funding by the Estonian Research Council by the exploratory research grant PUT1146.

We also thank Maria Kremsreiter who helped during her Erasmus+ internship at the Institute of Cybernetics. Therefore: With the support of the Erasmus+ programme of the European Union. Thanks to E-Betoonement, especially Aare Lessuk, Rasmus-R. Marjapuu and Sergei Graf, for preparing the experiment plate.

References

1. Beissel, R.A., Lim, H.: Self Compacting Concrete: Modern Concrete and Admixture Technology, pp. 607–612 (2000)
2. Brouwers, H.J.H., Radix, H.J.: Self-compacting concrete: theoretical and experimental study. *Cem. Concr. Res.* **35**(11), 2116–2136 (2005)
3. Nawy, E.G., Edward, G.: *Fundamentals of High-performance Concrete*. Wiley (2001)
4. Balaguru, P.N., Shah, S.P.: *Fiber-reinforced cement composites* (1992)
5. Lawler, J.S., Zampini, D., Shah, S.P.: Permeability of cracked hybrid fiber-reinforced mortar under load. *Mater. J.* **99**(4), 379–385 (2002)
6. Voigt, T., Van Bui, K., Shah, S.P.: Drying shrinkage of concrete reinforced with fibers and welded-wire fabric. *Mater. J.* **101**(2), 233–241 (2004)
7. Mesbah, H.A., Buyle-Bodin, F.: Efficiency of polypropylene and metallic fibres on control of shrinkage and cracking of recycled aggregate mortars. *Constr. Build. Mater.* **13**(8), 439–447 (1999)
8. Boulekbache, B., Hamrat, M., Chemrouk, M., Amziane, S.: Flowability of fibre-reinforced concrete and its effect on the mechanical properties of the material. *Constr. Build. Mater.* **24**(9), 1664–1671 (2010)
9. Ponikiewski, T., Gołaszewski, J., Rudzki, M., Bugdol, M.: Determination of steel fibres distribution in self-compacting concrete beams using x-ray computed tomography. *Arch. Civ. Mech. Eng.* **15**, 558–568 (2015)
10. Liu, J., Sun, W., Miao, C., Liu, J., Li, C.: Assessment of fiber distribution in steel fiber mortar using image analysis. *J. Wuhan Univ. Technol. Mater. Sci. Ed.* **27**, 166–171 (2012)
11. Stähli, P., Custer, R., van Mier, J.G.M.: On flow properties, fibre distribution, fibre orientation and flexural behaviour of FRC. *Mater. Struct.* **41**(1), 189–196 (2008)
12. Švec, O., Žirgulis, G., Bolander, J.E., Stang, H.: Influence of formwork surface on the orientation of steel fibres within self-compacting concrete and on the mechanical properties of cast structural elements. *Cem. Concr. Compos.* **50**, 60–72 (2014)
13. Soroushian, P., Lee, C.-D.: Distribution and orientation of fibers in steel fiber reinforced concrete. *Mater. J.* **87**, 433–439 (1990)

14. Grigaliunas, P., Kringelis, T.: SCC flow induced steel fiber distribution and orientation. Non-destructive inductive method. In: 11th European Conference on Non-Destructive Testing, Prague, Czech Republic (2014)
15. Herrmann, H., Lees, A.: On the influence of the rheological boundary conditions on the fibre orientations in the production of steel fibre reinforced concrete elements. *Proc. Est. Acad. Sci.* **65**(4), 408–413 (2016). Open-Access CC-BY-NC 4.0
16. Promentilla, M.A.B., Sugiyama, T., Shimura, K.: Threedimensional imaging of cement-based materials with x-ray tomographic microscopy: visualization and quantification. In: International Conference on Microstructure Related Durability of Cementitious Composites, vol. 61, pp. 1357–1366 (2008)
17. Liu, J., Li, C., Liu, J., Cui, G., Yang, Z.: Study on 3D spatial distribution of steel fibers in fiber reinforced cementitious composites through micro-CT technique. *Constr. Build. Mater.* **48**, 656–661 (2013)
18. Pastorelli, E., Herrmann, H.: Time-efficient automated analysis for fibre orientations in steel fibre reinforced concrete. *Proc. Est. Acad. Sci.* **65**(1), 28–36 (2016)
19. Herrmann, H., Pastorelli, E., Kallonen, A., Suuronen, J.-P.: Methods for fibre orientation analysis of x-ray tomography images of steel fibre reinforced concrete (SFRC). *J. Mater. Sci.* **51**(8), 3772–3783 (2016)
20. Suuronen, J.-P., Kallonen, A., Eik, M., Puttonen, J., Serimaa, R., Herrmann, H.: Analysis of short fibres orientation in steel fibre reinforced concrete (SFRC) using x-ray tomography. *J. Mater. Sci.* **48**(3), 1358–1367 (2013)
21. Ferrara, L., Faifer, M., Toscani, S.: A magnetic method for non destructive monitoring of fiber dispersion and orientation in steel fiber reinforced cementitious composites—Part 1: method calibration. *Mater. Struct.*, 1–15 (2011)
22. Karhunen, K., Seppänen, A., Lehikoinen, A., Monteiro, P.J.M., Kaipio, J.P.: Electrical resistance tomography imaging of concrete. *Cem. Concr. Res.* **40**, 137–145 (2010)
23. Torrents, J.M., Blanco, A., Pujadas, P., Aguado, A., Juan-Garcia, P., Sánchez-Moragues, M.Á.: Inductive method for assessing the amount and orientation of steel fibers in concrete. *Mater. Struct.* **45**, 1577–1592 (2012)
24. Schickert, M.: Progress in ultrasonic imaging of concrete. *Mater. Struct.* **38**, 807–815 (2005)
25. Aggelis, D.G., Soulioti, D., Barkoula, N.M., Paipetis, A.S., Matikas, T.E., Shiotani, T.: Acoustic emission monitoring of steel-fiber reinforced concrete beams under bending. *Prog AE* **14**, 287–294 (2008)
26. Keru, W., Chen, B., Yao, W.: Study on the ae characteristics of fracture process of mortar, concrete and steel-fiber-reinforced concrete beams. *Cem. Concr. Res.* **30**(9), 1495–1500 (2000)
27. Soulioti, D., Barkoula, N.M., Paipetis, A., Matikas, T.E., Shiotani, T., Aggelis, D.G.: Acoustic emission behavior of steel fibre reinforced concrete under bending. *Constr. Build. Mater.* **23**(12), 3532–3536 (2009)
28. Roussel, N., Gram, A., Cremonesi, M., Ferrara, L., Krenzer, K., Mechtcherine, V., Shyshko, S., Skocec, J., Spangenberg, J., Svec, O., Thrane, L.N., Vasilic, K.: Numerical simulations of concrete flow: a benchmark comparison. *Cem. Concr. Res.* **79**, 265–271 (2016)
29. Svec, O., Skocec, J., Olesen, J.F., Stang, H.: Fibre reinforced self-compacting concrete flow simulations in comparison with l-box experiments using carbopol. In: 8th Rilem International Symposium on Fibre Reinforced Concrete (2012)
30. Ehrentraut, H., Muschik, W.: On symmetric irreducible tensors in d-dimensions. *ARI Int. J. Phys. Eng. Sci.* **51**(2), 149–159 (1998)
31. Herrmann, H., Beddig, M.: Tensor series expansion of a spherical function for use in constitutive theory of materials containing orientable particles. *Proc. Est. Acad. Sci.* **67**(1), 73–92 (2018). Open-Access CC-BY-NC 4.0
32. Eik, M., Puttonen, J., Herrmann, H.: The effect of approximation accuracy of the orientation distribution function on the elastic properties of short fibre reinforced composites. *Compos. Struct.* **148**, 12–18 (2016)
33. Abràmoff, M.D., Magalhães, P.J., Ram, S.J.: Image processing with ImageJ. *Biophotonics Int.* **11**(7), 36–42 (2004)

34. Herrmann, H.: Alignment tensor package for R (2016). <http://bitbucket.org/vispar/alignment>
35. R Development Core Team: R: A Language and Environment for Statistical Computing. R Foundation for Statistical Computing, Vienna, Austria (2011). ISBN 3-900051-07-0
36. Lemon, J.: Plotrix: a package in the red light district of R. R-News **6**(4), 8–12 (2006)

Appendix 3

III

H. Herrmann, O. Goidyk, H. Naar, T. Tuisk, and A. Braunbrück. The influence of fibre orientation in self-compacting concrete on 4-point bending strength. *Proceedings of the Estonian Academy of Sciences*, 68(3):337–346, 2019



The influence of fibre orientation in self-compacting concrete on 4-point bending strength

Heiko Herrmann^{a*}, Oksana Goidyk^a, Hendrik Naar^b, Tanel Tuisk^b, and Andres Braunbrück^a

^a Department of Cybernetics, Tallinn University of Technology, Akadeemia tee 21, 12618 Tallinn, Estonia

^b Department of Civil Engineering and Architecture, Tallinn University of Technology, Ehitajate tee 5, 19086 Tallinn, Estonia

Received 13 December 2018, accepted 2 March 2019, available online 15 August 2019

© 2019 Authors. This is an Open Access article distributed under the terms and conditions of the Creative Commons Attribution-NonCommercial 4.0 International License (<http://creativecommons.org/licenses/by-nc/4.0/>).

Abstract. This contribution presents the performed experiments and experimental setup in detail for future reference and the results of bending tests performed on steel fibre concrete beam specimen, which have been cut out of a larger plate. These beams have different fibre orientation distributions, due to being taken from different parts of the plate and with different orientation with respect to the flow of the fresh concrete.

Key words: mechanics, fibre orientation, bending test, fibre concrete, strength analysis.

1. INTRODUCTION

With the shortage of sand and gravel in many areas [1] and the global concern about carbon dioxide emissions, it becomes necessary to reduce the environmental impact of concrete construction. Concrete is an ubiquitous building material, it is also essential for wind farms [2], which are the main providers of renewable energy. One possibility to achieve this is to create stronger concrete that behaves ductile. The addition of short fibres to the concrete mix can introduce ductility to concrete. However, the results of strength tests on small test-specimen show great variability and the test results of large elements do not match the results of the strongest small specimen. The probable causes for the variability are the spatial fibre distribution and the orientational fibre distribution, which can both vary between small specimen and also within a large element [3,4]. Fibre pullout tests have shown, that the pullout force depends on the inclination angle of the fibre. The angle between fibre and crack therefore influences the post-cracking behaviour [5,6]. Theoretical approaches that model the dependence of the mechanical properties and take the fibre orientations into account

have been proposed by several research teams, the used methods range from orientation numbers over orientation profile to orientation tensors [7–12]. Both, for comparison of experiments and for application of the theories it is necessary to know the fibre orientations. Fibre orientation measurements can be performed using X-ray computed tomography [3,13–23], which gives the orientations and positions of individual fibres, and by electro-magnetic methods, which give tendencies of fibre alignment. A comparison of different measurement techniques can be found in [24].

The spatial variation of fibre density and orientation distribution within a structural element is largely due to the flow of the fresh concrete mass when filling the formwork [25–30]. In this study the experiments to determine the local strength characteristics of a large plate are presented. The aim is to correlate the strength characteristics with fibre orientations expected from casting simulations. To achieve this, a large plate was cast with documented casting procedure and the plate was cut into beams, which have been subjected to four-point bending tests. The post-cracking behaviour of beams has also been studied by other researchers, e.g., using three-point bending tests of unnotched specimen

* Corresponding author, hh@cens.ioc.ee

[30–32]. This paper focuses on the description of experiments and the presentation of the raw results from the bending tests. The detailed analysis of the measurements is left for a future paper.

2. EXPERIMENTS

In this section the experiment setup is described, first a description of the casting of the fibre concrete and reference plates including the concrete mix is given, then the setting of the four-point bending tests is described, followed by digital image correlation and acoustic emission measurements, that have been performed during some of the bending tests.

2.1. Casting of plates, materials and mix design

For this study, two different mixtures: an ordinary self-compacting concrete (SCC) and steel fibre reinforced self-compacting concrete (SFRSCC), were produced according to the recipe by the manufacturer. The composition of the mixtures is presented in Table 1. The constituent materials were mixed according to normal factory procedure in a production-line mixer with a capacity of 1–2 t.

The consistency and viscosity of the concrete mixture was measured by means a slump-flow test, according to EN12350-8. The spread of the slump was 700 mm, which satisfied the requirement of 650–800 mm.

In the end, the obtained mixture was placed into the previously prepared film coated plywood mould, whose bottom was covered with plastic foil. As filling method a moving bucket was used, the pouring position was moved in the longitudinal direction.

For the second mixture the same recipe and procedure were used. However, this time hooked-end steel fibres were added. Table 2 provides the characteristics and properties of used steel fibres, a photo of a fibre is presented in Fig. 1. To avoid clustering of fibres the mixture was mixed for a couple of minutes. The fibre dosage was 1% per volume of concrete. To achieve the required rheological properties of the concrete mixture, the water dosage was slightly increased. After the slump flow test (spread of the slump was 650 mm), the same casting procedure was performed. To provide the accurate surface leveling the surface was treated with a roller immediately after the casting process. After both casting processes lifting anchors were put into the fresh concrete, to be able to transport the plate safely after hardening. The videos of both casting processes were recorded with a camera for further visual observation and analysis. Then both slabs were stored in the manufacturing hall at room temperature and left to harden.

Standard compression tests have been performed on separately cast cubic test specimen, the concrete for these was taken out of the mass for the plates during casting.

Table 1. Composition of SCC mix, amount mixed: 1 m³

Cement, kg	330
Sand (0–2 mm), kg	398
Sand (0–4 mm), kg	505
Crushed stone (2–5), kg	336
Crushed stone (8–11), kg	539
Filler, kg	80
Admixture, kg	5.1
Water, kg	175
Fibres (SFRSCC only), kg	50
Extra water (SFRSCC only), kg	~10

Table 2. Data of the steel fibres, according to [33]

Manufacturer	Severstal Metiz
Model	Hendix prime 75/52
Type	Hooked end
Length, mm	52 ± 2.0
Diameter, mm	0.75 ± 0.04
Hook length, mm	2.0 – 1.0 / + 2.0
Hook height, mm	2.1 + 0.5 / – 0.0
Bend angle, degrees	40 ± 5
Tensile strength, MPa	1500
Elastic modulus, MPa	≥ 190 000
Number of fibres per kg, pcs.	~ 5 545



Fig. 1. Photo of a fibre.

2.2. Preparation of beam specimen

After hardening and demoulding both slabs had dimensions of ($L \times W \times H$) 400 cm × 100 cm × 10 cm. From the slab of SCC 10 beams of size 100 cm × 10 cm × 10 cm have been cut. The slab of SFRSCC has been cut into 40 beams of size 100 cm × 10 cm × 10 cm. A principal layouts of the specimens cut out of the cast slabs is presented in Fig. 2. The cutting of both plates took place twenty days after the casting.

2.3. The bending test set-up

The main goals of 4-point bending test are to evaluate the tensile and post-cracking behaviour of SFRSCC, determine the peak load, the mid-span deflections, crack mouth opening displacement and the contribution of fibres in the strength of fibre concrete. The basic idea to carry out 4-point bending test with unnotched specimens is concerned with the evaluation of the

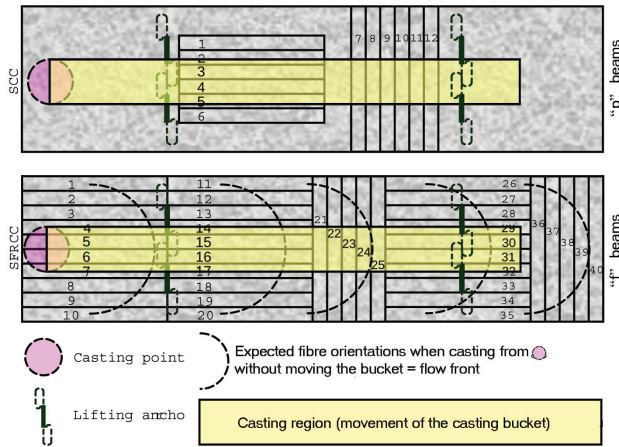


Fig. 2. Beam layout of specimens cut out of the cast plates; SFRCC beams are referred to with “f” and their number, non-fibre beams with “p” and their number.

influence of fibre distribution on independent crack formation/propagation and post-cracking behaviour, since generally, the existence of the notch in the midspan section would modify the stress pattern and anticipates the formation and further growing of the crack.

All the 50 beams were subjected to 4-point bending test in order to analyse and compare the mechanical properties and the post-cracking behaviour of concrete.

The 4-point bending test of specimens was performed on a universal electro-mechanic/hydraulic testing machine *EU100*. The testing machine was connected to an *HBM QuantumX MX840A* universal measuring amplifier module to acquire the data and a laptop to record the experimental data and control the testing procedure. For the data collection and visualization the *CatmanEasy DAQ* software was used.

The experimental equipment and the concrete specimen mounted in the testing machine is depicted in Fig. 3a (photo) and Fig. 3b (drawing).

The beams were maintained by means of two supports with the metal rollers at the edges with a diameter of 5 cm. Two metal plates were located on the top of the rollers in order to fix and eliminate any movements of the testing specimens. The distance between supports was 90 cm, and 5 cm from each supports to the edges of the beams. The experimental beams were correctly centered with the supports of the testing machine. The load was applied through two metal cylinders of 1.5 cm diameter located between two metal plates of size 2 cm × 1 cm and length 15 cm in order to ensure the stability and evenly distribute of the loading force. The loading points were located at the distance

(a)



(b)

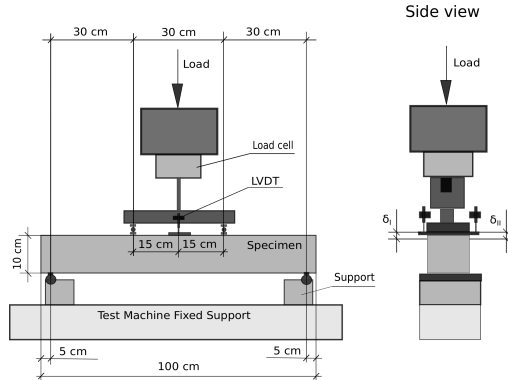


Fig. 3. Four point bending test: (a) photo of the setup, (b) sketch.

of 30 cm from each other (approximately 1/3 of total range). To measure the loading force during the test, the load cell *HBM U10M* with a capacity of 50 kN was used. The displacement was continuously increased until the displacements achieved specific values. The maximum load for all specimens was in the range 6–8 kN.

The accurate measurements and recording of the mid-span deflections during the bending test were arranged. To determine the vertical displacements under the load, the displacement sensors *HBM W1/10mm-T* were applied. The displacement sensors were located on a metal plate at half-length on the top surface of the specimen and fixed on two opposite sides of specimen (δ_I , δ_{II}). The displacement transducers have to be carefully mounted in order to exclude the rotation. The schematic illustration of the displacement transducers is shown in Fig. 3b.

In order to get the accurate measurements it is important before the test to make sure that the surface of the specimens are clean and free of the industrial dust and other extraneous materials. At the time of the bending tests the samples have been between 23 weeks and 28 weeks old. This means that all specimen have been over five months old at the time of testing and the effect of the difference in age at the time of testing should be negligible.

2.4. The digital image correlation set-up

Digital image correlation (DIC) method is an effective optical and non-contact measuring technique that employs the comparing, tracking the changes and visualization of deformations in the digital images of the specimen surface. The main principle of this method is based on digital image processing and numerical computing that involves monitoring and identifying transformations in a surface pattern of objects under the loading [34–37].

The most important step during the experimental setup is the appropriate arrangement of the specimen, camera and light sources. Since the obtained results strongly depend on the quality of the images, the equipment disposition should be organized quite thoroughly. Primarily, the camera should be positioned exactly in front of the specimen at sufficient distance and perpendicularly to the main axis of the specimen. The light sources (white or natural day light can be used) play a significant role because it enhances the contrast and therefore, the quality of the final images.

In the research, to record the video and images of the testing beams a digital camera with a photo-resolution of 4608×3456 pixels and a HD video-resolution of 1280×720 pixels was used. The digital camera was mounted on a tripod, perpendicular to one side of the specimen and accurately directed to the area of interest. The distance from the camera to the testing specimen was approximately 60 cm. The schematic illustration of the experimental setup for DIC is presented in Fig. 4.

For DIC analysis the software package *pydic* [38] was used. *Pydic* is a free and easy-to-use software for

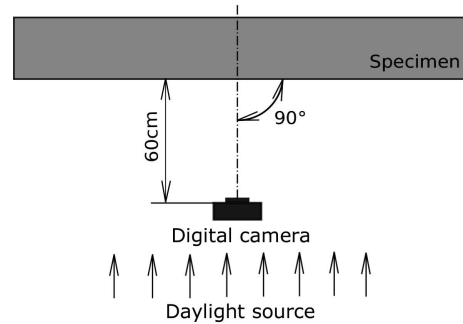


Fig. 4. The typical experimental setup for digital image correlation (top view).

computing the displacement and the strain fields inside a region of interest, that is based on Python packages. The testing images were obtained as screen-shots from the video. Generally, DIC analysis involves the comparison of the images that were taken upon the bending test, before, during and after the deformation process caused by the applied force. In other words, DIC software computes and traces the position changes of each image point by comparing several images of object surface in various moment in time. For DIC analysis each experimental image was converted from RGB colour to grayscale (eight-bit digital images). Moreover, it is required that among the testing images the first one should be taken in undeformed state and another during deformed state.

Figures 5a and 5b show the typical images used for DIC in different states of the specimen.

2.5. The acoustic emission set-up

The acoustic emission (AE) method is widespread non-destructive technique assigned to investigate the internal and external damages in the materials.

Under the applied load the localized stress energy causes the crack appearance and growing/propagation that induces sound waves. These waves can be extracted and recorded by using transducers (sensors) or microphones, mounted on the surface of the testing specimens [39]. As a result, AE signal parameters, such as amplitude, counts, energy, duration time, rise time are obtained by the measurement system and further used for the post-processing analysis [40,41].

The intention to use record AE was to try to identify which crack appeared first in case of multi-cracking and to possibly identify fibre-rupture events.

The schematic experimental setup and positions of microphones that were used for the AE technique are presented in Fig. 6.

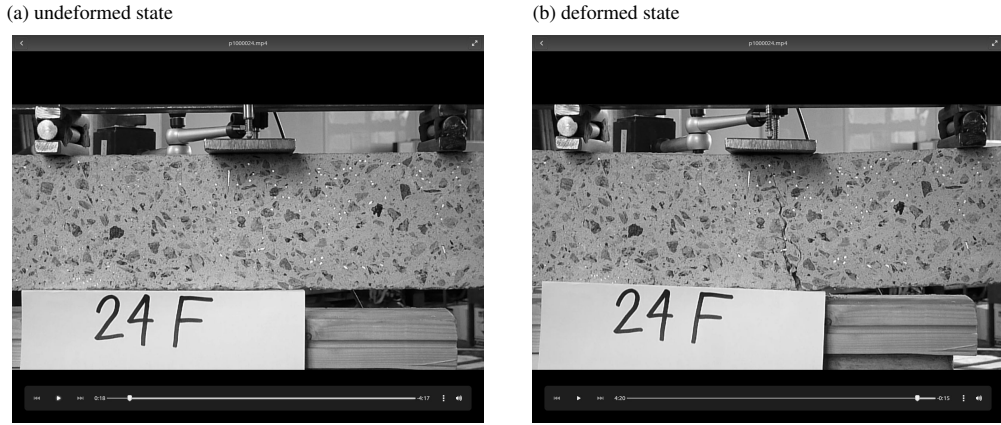


Fig. 5. Typical photos used for digital image correlation (undeformed and deformed state).

Two piezo clip-on contact microphones were attached to the metal plates, located between bottom of the specimen and rollers of supports. It is worth to note, that the economic contact microphones were not matched and their sensitivity varied considerably. This was compensated by the level setting of the microphone pre-amps in the audio interface. A matched stereo pair of compact condenser microphones was mounted on two tripods at the distance about 10 cm from the opposite side of the specimen. The AE signals were recorded with a four-channel USB Audio Interface, the amplitude resolution was 24 bit and time resolution for the initial recordings 192 kHz and later reduced to 96 kHz because of the file size and software crashes. The audio interface was connected to a Linux laptop (Debian Linux stretch) running the JACK audio daemon [42] and Ardour5.5.0 [43] recording software. The JACK daemon

proved superior to using Ardour5.5.0 with ALSA [44], because in the case of xrums (buffer under/over-runs) the recording continued when using the JACK daemon, while it was stopped when using the Ardour5.5.0 ALSA driver. For later recordings only the contact microphones were used, as these have been resistant to ambient noise and due to other experiments in the same hall, the ambient noise level had increased over the duration of the experiments.

To synchronize the audio recording with the load-displacement measurements, after switching all recordings on, the plate on which the displacement sensors where in contact with the beam was hit slightly with a metal rod. This caused a very small temporary displacement and an audible ping. Both were recorded and can be used for synchronization.

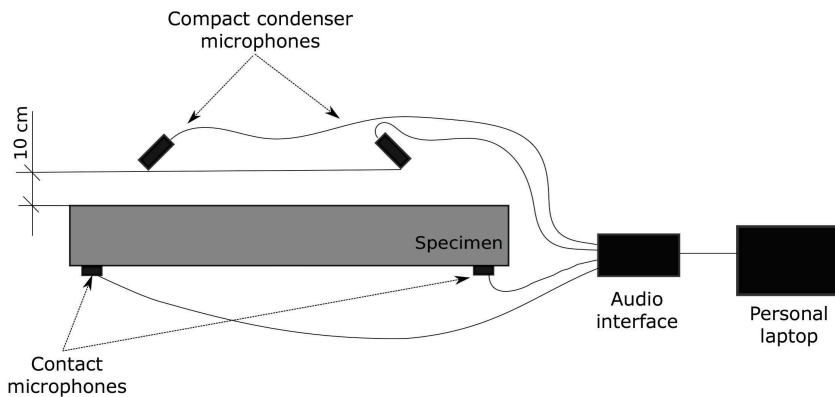


Fig. 6. An experimental setup for acoustic emission monitoring.

3. RESULTS

In the following, the results of the experiments are presented. In particular, the load-displacement curves for all beams are given, and a proof-of-concept for the digital image correlation and acoustic emission measurements. A detailed analysis of the results is ongoing and will be presented elsewhere.

3.1. The compression tests

The results of the compression tests are presented in Table 3. It is notable, that the normal concrete without fibres shows higher strength at all ages compared to the fibre concrete. This can partly be explained by the higher water-cement ratio of the fibre concrete.

3.2. The bending tests

Here the load-displacement diagrams of the four-point bending test are presented in Fig. 7. One can notice that the variation between the different beams is large, though in all cases the presence of the fibres introduced some ductility into the concrete. The range of post-cracking behaviour included strain hardening cases, where the

maximum load is higher than the load at the first crack, but also strain-softening, where the residual strength is only a quarter of the load at first crack. Some correlation between the position of the beam in the plate and the post-cracking behaviour can be observed, for example the beams taken from the edges of the plate are strain-hardening, while the middle beams show weak post-cracking strength. Many of these results are in accordance with expectations with respect to fibre orientations, however there are also cases that do not seem to agree. The analysis of these is ongoing and will be presented in a future paper.

3.3. The digital image correlation

To obtain the strain distribution images, at first, the region of interest was specified as a virtual computational grid. Further, the program calculates the displacements at the each point of this virtual grid. After the execution of the full cycle of DIC analysis, the program writes the typical series of results' files, that include the folder with images of displacements' field, the folder with images of displacements' grids, the folder with images of the displacements of the correlated windows and CSV results files that are needed for post-processing.

Table 3. Results of compression tests for SCC and SFRSCC

	Age at test in days	4	4	4	7	7	7	28	28	28	28	28	28	28	28	28	28
SCC	ρ , kg/m ³	2330	2330	2330	2310	2340	2370	2380	2380	2370	2380	2360	2380	2390	2380	2380	2390
	β , kg/m ³	2330	2330		2340	2340						2379					
	stdev, kg/m ³		0		30	30						9					
	$\sigma_{u,c}$, MPa	55.4	54.5	52.3	54.7	54.5	56.8	67.6	66.4	70.9	66.3	68.8	69	69.9	72.1	66	69
	$\sigma_{u,c}$, MPa		54.1		55.3	55.3						68.6					
	stdev, MPa		2		1	1						2					
SFRSCC	ρ , kg/m ³	2350	2350	2370	2380	2360	2370	2390	2370	2380	2380	2410	2390	2370	2390	2360	2380
	β , kg/m ³	2350	2357		2370	2370						2382					
	stdev, kg/m ³		12		10	10						14					
	$\sigma_{u,c}$, MPa	45.1	45	44.5	46.1	45.3	45.1	55.7	55	57.2	58.1	57.3	57.4	56.9	55.9	58.1	54.9
	$\sigma_{u,c}$, MPa		44.9		45.5	45.5						56.6					
	stdev in MPa		0		1	1						1					

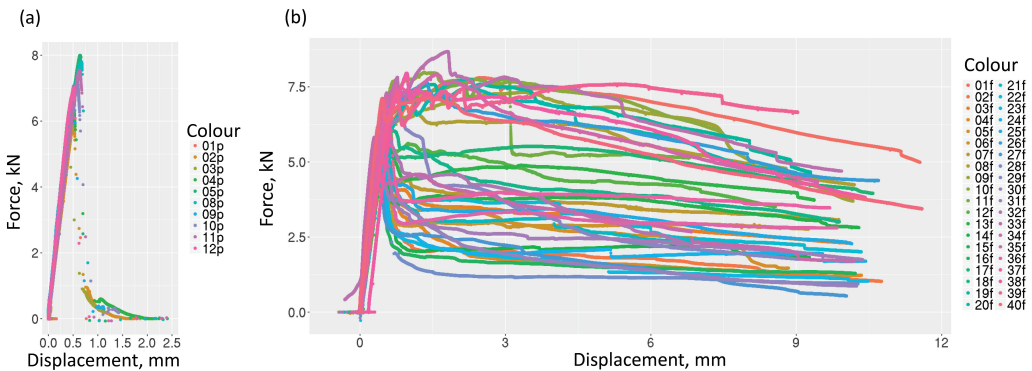


Fig. 7. Load-displacement diagrams for the tested beams: (a) SCC, (b) SFRSCC.

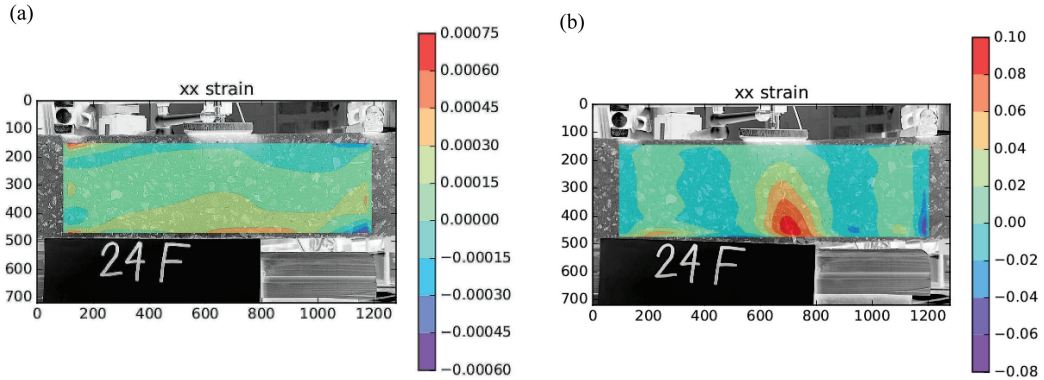


Fig. 8. Horizontal strain in beam 24f: (a) analysis just before the crack, (b) analysis after the crack.

Finally, the software allows to create plots of the strain field interactively with matplotlib, a Python library for plotting [45], see Fig. 8. Additionally, the program automatically computes the Young’s modulus from strain fields and meta-data.

3.4. The acoustic emission

The setup for recording acoustic emissions during the bending experiments was successful. Despite some

software instability, many crack events could be recorded acoustically. An example of such a recording is presented in Fig. 9. The figure shows the amplitudes over time recorded by the four microphones. As the figure shows, the noise level is very low for all microphones and the crack events can be clearly identified without further filtering techniques.

A detailed analysis of the recorded events is still under way and will be presented in a different publication.

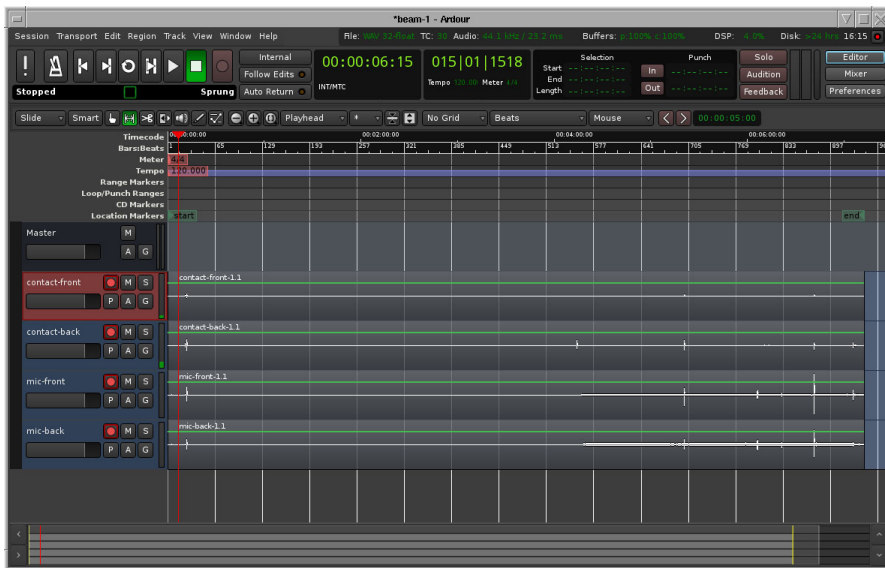


Fig. 9. An example recording of the 4 microphones shown is the entire recording for a fibre-beam (f01). At the beginning of the recording the synchronization click is visible, all other peaks belong to crack events.

4. DISCUSSION OF RESULTS

The initial results are, that in all beams fibres improve the fracture behaviour compared to SCC, although the actual post-cracking performance shows a large variability and depends on the position within the plate where the sample was taken from. Beams taken from the edges (side or end) show strain-hardening, while centre beams show strain-softening. The results coincide (roughly) with expectations from predicted fibre orientation distribution in samples, meaning that the samples where according to flow simulations the fibres should be mostly aligned in tensile stress direction, the beams show strain-hardening [28,46,47]. The high variability of results seems to be typical for small samples, where stochastic variations of density or orientation distribution matter. This means a more samples should be tested compared to non-fibre SCC. In large samples the variability should be smaller. Several draft guidelines suggest to obtain constitutive parameters from either three-point of four-point bending tests of relatively small samples, e.g., [48]. Also, in small samples the fibre orientations can be dominated by the wall-effect, leading to alignment of the fibres in the direction of tensile stresses, like in the side-edge beams taken from the plate. This could result in a strain-hardening post-cracking behaviour. If these material parameters would be chosen to design a plate, the performance of the plate could be severely overestimated.

5. ONGOING AND FUTURE INVESTIGATIONS

The analysis of fibre orientations by use of X-ray computed tomography (CT) of the tested beams has begun. Selected beams will be scanned using CT and the fibre positions and orientations will be extracted from the volume image. Special attention will be paid to the cracked region. The results of the fibre orientation measurements will be compared to computational fluid dynamics simulations of the fibre orientations. The detailed analysis regarding post-crack behaviour with respect to the location in plate is still ongoing. The relation between post-cracking strength and fibre orientations will be investigated. Comparison of peak strength and post-cracking behaviour with existing theoretical models will be performed.

6. CONCLUSIONS

In this paper the results of four-point bending tests performed on forty beam specimens cut out of a large plate have been presented. Special focus has been paid to describe the experimental setting in detail. The initial results are, that in all beams fibres improve the fracture behaviour compared to SCC, although the actual post-cracking performance depends on the

position within the plate where the sample was taken from. The results coincide (roughly) with expectations from predicted fibre orientation distribution in samples, which seems to confirm that the flow of the fresh concrete mass influences the fibre orientations. In particular, the edge beams are strain-hardening while the centre beams are strain-softening, which coincides with fibres aligned in tensile direction for the edge beams and non-aligned fibres for the centre beams. It also leads to the conclusion, that the bending results are very sensitive to the casting procedure. From this follows, that for fibre concrete specifically produced small laboratory samples may not be representative for large structural elements, this is in contrast to the case of ordinary concrete. Further, one can conclude that special care is needed to design casting technologies which will produce consistent fibre orientation distributions and that on-site casting may be problematic.

ACKNOWLEDGEMENTS

Funding by the Estonian Research Council by the exploratory research grant PUT1146 is gratefully acknowledged. Thanks to AS E-Betoonement, especially Aare Lessuk, Sergei Graf and Borys Zavadski, for preparing the experiment plates, space for cutting the beams and their general support of the research, also thanks to Ekaterina Pronyuk for being our “tourguide” on the cutting day. We also thank Elmar-Jaan Just and Peeter Linnas of the Department of Civil Engineering and Architecture, School of Engineering, for letting us use the equipment in the Mäepealse lab. The publication costs of this article were covered by the Estonian Academy of Sciences.

REFERENCES

1. Torres, A., Brandt, J., Lear, K., and Liu, J. A looming tragedy of the sand commons. *Science*, 2017, **357**(6355), 970–971.
2. Damme, H. V. Concrete material science: past, present, and future innovations. *Cem. Concr. Res.*, 2018, **112**, 5–24.
3. Suuronen, J.-P., Kallonen, A., Eik, M., Puttonen, J., Serimaa, R., and Herrmann, H. Analysis of short fibres orientation in steel fibre reinforced concrete (SFRC) using x-ray tomography. *J. Mat. Sci.*, 2012, 1–10.
4. Svec, O., Zirgulis, G., Bolander, J. E., and Stang, H. Influence of formwork surface on the orientation of steel fibres within self-compacting concrete and on the mechanical properties of cast structural elements. *Cem. Concr. Compos.*, 2014, **50**(0), 60–72.
5. Krasnikovs, A., Kononova, O., Khabbaz, A., Machanovsky, E., and Machanovsky, A. Post-cracking behaviour of high strength fiber concrete prediction and validation. *WASET*, 2011, **59**, 988–992.
6. Macanovskis, A., Lusiš, V., and Krasnikovs, A. Crack opening investigation in fiberconcrete. *WASET*, 2014, **8**(4), 430–438.

7. Laranjeira, F., Grünewald, S., Walraven, J., Blom, K., Molins, C., and Aguado, A. Characterization of the orientation profile of steel fiber reinforced concrete. *Mat. Struct.*, 2011, **44**(6), 1093–1111.
8. Mishurova, T., Léonard, F., Oesch, T., Meinel, D., Bruno, G., Rachmatulin, N., et al. Evaluation of fiber orientation in a composite and its effect on material behavior. In *Proceedings of the 7th Conference on Industrial Computed Tomography (ICT)*, Vol. 22(03), Leuven, Belgium, February 7–9, 2017. <http://www.ndt.net/?id=20818>.
9. Eik, M., Herrmann, H., and Puttonen, J. Orthotropic constitutive model for steel fibre reinforced concrete: linear-elastic state and bases for the failure. In *Proceedings of the XII Finnish Mechanics Days, Tampere, Finland, June 4–5* (Kouhia, R., Mäkinen, J., Pajunen, S., and Saksala, T., eds). Finnish Association for Structural Mechanics, 2015, 255–260.
10. Eik, M., Puttonen, J., and Herrmann, H. The effect of approximation accuracy of the orientation distribution function on the elastic properties of short fibre reinforced composites. *Comp. Struct.*, 2016, **148**, 12–18.
11. Herrmann, H. An improved constitutive model for short fibre reinforced cementitious composites (SFRC) based on the orientation tensor. In *Generalized continua as models for classical and advanced materials* (Altenbach, H. and Forest, S., eds). Springer International Publishing, Switzerland, 2016, 213–227.
12. Herrmann, H. and Beddig, M. Tensor series expansion of a spherical function for use in constitutive theory of materials containing orientable particles. *Proc. Est. Acad. Sci.*, 2018, **67**(1), 73–92.
13. Vicente, M., Mínguez, J., and González, D. The use of computed tomography to explore the microstructure of materials in civil engineering: from rocks to concrete. In *Computed Tomography – Advanced Applications* (Halefoglou, D. A. M., ed.). InTech, 2017, 207–230.
14. Schnell, J., Schladitz, K., and Schuler, F. Richtungsanalyse von Fasern in Betonen auf basis der computer-tomographie. *Beton-Stahlbetonbau*, 2010, **105**(2), 72–77.
15. Ponikiewski, T., Katzer, J., Bugdol, M., and Rudzki, M. X-ray computed tomography harnessed to determine 3D spacing of steel fibres in self compacting concrete (SCC) slabs. *Constr. Build. Mater.*, 2015, **74**(0), 102–108.
16. Ponikiewski, T., Katzer, J., Bugdol, M., and Rudzki, M. Steel fibre spacing in self-compacting concrete precast walls by X-ray computed tomography. *Mater. Struct.*, 2015, **48**(12), 3863–3874.
17. Pittino, G., Geier, G., Fritz, L., Hadwiger, M., Rosc, J., and Pabel, T. Computertomografische untersuchung von stahlfaserspritzbeton mit mehrdimensionalen transferfunktionen. *Beton-Stahlbetonbau*, 2011, **106**(6), 364–370.
18. Vicente, M. A., Gonzalez, D. C., and Mínguez, J. Determination of dominant fibre orientations in fibre-reinforced high-strength concrete elements based on computed tomography scans. *Nondestr. Test. Eval.*, 2014, **29**(2), 164–182.
19. Oesch, T. S., Landis, E. N., and Kuchma, D. A. Conventional concrete and uhpc performance–damage relationships identified using computed tomography. *J. Eng. Mech.*, 2016, **142**(12), 04016101.
20. Oesch, T. In-situ CT investigation of pull-out failure for reinforcing bars embedded in conventional and high-performance concretes. In *Proceedings of the 6th Conference on Industrial Computed Tomography, Wels, Austria, February 9–12, 2016*. http://www.ndt.net/article/ctc2016/papers/ICT2016_paper_id83.pdf
21. Oesch, T. S. *Investigation of fiber and cracking behavior for conventional and ultra-high performance concretes using X-ray computed tomography*. PhD thesis. University of Illinois, Urbana-Champaign, 2015.
22. Pastorelli, E. and Herrmann, H. Time-efficient automated analysis for fibre orientations in steel fibre reinforced concrete. *Proc. Est. Acad. Sci.*, 2016, **65**(1), 28–36.
23. Pastorelli, E. and Herrmann, H. Virtual reality visualization for short fibre orientation analysis. In *Proceedings of the 14th Biennial Baltic Electronic Conference (BEC)*, Tallinn, Estonia, October 6–8, 2014. Institute of Electrical and Electronics Engineers, 2014, 201–204.
24. Zhang, S., Liao, L., Song, S., and Zhang, C. Experimental and analytical study of the fibre distribution in SFRC: a comparison between image processing and the inductive test. *Compos. Struct.*, 2018, **188**, 78–88.
25. Eiduks, M., Krasnikovs, A., Dunskis, E., and Kononova, O. Investigation of fibre orientation in viscous fluid. *Sci. J. Riga Tech. Univ.*, 2010, **33**, 98–102. <https://ortus.rtu.lv/science/lv/publications/8346>.
26. Kononova, O., Krasnikovs, A., Lapsa, V., Kalinka, J., and Galushchak, A. Internal structure formation in high strength fiber concrete during casting. In *International Conference on Applied Mechanics and Mechanical Engineering (ICAMME 2011) Venice, Italy, November 28–30, 2011*, 1864–1867.
27. Zirgulis, G., Svec, O., Geiker, M. R., Cwirzen, A., and Kanstad, T. Influence of reinforcing bar layout on fibre orientation and distribution in slabs cast from fibre-reinforced self-compacting concrete (FRSCE). *Struct. Concr.*, **17**(2), 245–256.
28. Herrmann, H. and Lees, A. On the influence of the rheological boundary conditions on the fibre orientations in the production of steel fibre reinforced concrete elements. *Proc. Est. Acad. Sci.*, 2016, **65**(4), 408–413.
29. Herrmann, H., Goidyk, O., and Braunbrück, A. Influence of the flow of self-compacting steel fiber reinforced concrete on the fiber orientations, a report on work in progress. In *Short fiber reinforced cementitious composites and ceramics* (Herrmann, H. and Schnell, J., eds). Springer, 2019, 97–110.
30. Herrmann, H., Braunbrück, A., Tuisk, T., Goidyk, O., and Naar, H. An initial report on the effect of the fiber orientation on the fracture behavior of steel fiber reinforced self-compacting concrete. In *Short fiber reinforced cementitious composites and ceramics*

- (Herrmann, H. and Schnell, J., eds). Springer, 2019, 33–50.
31. González, D. C., Vicente, M. A., and Ahmad, S. Effect of cyclic loading on the residual tensile strength of steel fiber-reinforced high-strength concrete. *J. Mat. Civ. Eng.*, 2015, **27**(9), 04014241.
 32. González, D. C., Moradillo, R., Mínguez, J., Martínez, J. A., and Vicente, M. A. Post-cracking residual strengths of fiber-reinforced high-performance concrete after cyclic loading. *Struct. Concr.*, 2018, **19**(2), 340–351.
 33. Severstal Metiz. Hendix prime 75/52 – hooked ends fiber. <http://www.severstalmetiz.ru/eng/catalogue/1930/document62190.shtml?6605,1>
 34. Pan, B., Qian, K., Xie, H., and Asundi, A. Two-dimensional digital image correlation for in-plane displacement and strain measurement: a review. *Meas. Sci. Technol.*, 2009, **20**(6), 062001.
 35. Shi, X., Pang, H., Zhang, X., Liu, Q., and Ying, M. In-situ micro-digital image speckle correlation technique for characterization of materials' properties and verification of numerical models. *IEEE Trans. Compon. Packag. Technol.*, 2004, **27**(4), 659–667.
 36. Chu, T. P. and Poudel, A. Digital image correlation techniques for aerospace applications. In *ASNT Annual Conference 2014*, 37–44.
 37. Hild, F. and Roux, S. Digital image correlation: from displacement measurement to identification of elastic properties – a review. *Strain*, **42**(2), 69–80.
 38. Andre, D. Pydic. <https://gitlab.com/damien.andre/pydic>, 2018.
 39. Grosse, C. U., Reinhardt, H. W., and Finck, F. Signal-based acoustic emission techniques in civil engineering. *J. Mater. Civ. Eng.*, 2003, **15**(3), 274–279.
 40. Wu, K., Chen, B., and Yao, W. Study on the AE characteristics of fracture process of mortar, concrete and steel-fiber-reinforced concrete beams. *Cem. Concr. Res.*, 2000, **30**(9), 1495–1500.
 41. Zhou, J. *A study of acoustic emission technique for concrete damage detection*. MSc thesis. Michigan Technological University, Department of Civil and Environmental Engineering, 2011. <https://digitalcommons.mtu.edu/etds/726>.
 42. JACK audio connection kit. <http://jackaudio.org/>
 43. Ardour5.5.0. <https://ardour.org/>
 44. Advanced Linux Sound Architecture (ALSA). <https://www.alsa-project.org>
 45. The Matplotlib Development Team. Matplotlib. <https://matplotlib.org/>
 46. Herrmann, H., Eik, M., Berg, V., and Puttonen, J. Phenomenological and numerical modelling of short fibre reinforced cementitious composites. *Meccanica*, 2014, **49**(8), 1985–2000.
 47. Eik, M., Puttonen, J., and Herrmann, H. An orthotropic material model for steel fibre reinforced concrete based on the orientation distribution of fibres. *Comp. Struct.*, 2015, **121**(0), 324–336.
 48. Walraven, J., Bigaj-van Vliet, A., et al. *fib. Model code for Concrete Structures 2010*. Wilhelm Ernst & Sohn, Verlag für Architektur und Technische Wissenschaften GmbH & Co. KG, Berlin, 2013.

Kiudude orientatsiooni mõju isetiheneva betooni 4 punkti paindetugevusele

Heiko Herrmann, Oksana Goidyk, Hendrik Naar, Tanel Tuisk ja Andres Braunbrück

Ristkülikukujuline kiudbetoonplaat lõigati neljakümneks väiksemaks talaks, millega tehti purustav 4 punkti paindekats. Katsel mõõdeti elektroonselt koormust, keskristlõike siiret ja purunemisel tekkivat akustilist emissiooni. Paralleelselt sooritati võrdluskatsed ainult betoonplaadist lõigatud katsekehadega.

Kiudbetooni katsetel täheldatud tulemuste varieeruvus paindetugevuse ja peale prao teket jääva tugevuse osas on seostatav kiudude jaotustiheduse ning orientatsioonilise jaotumisega plaadi eri piirkondades. Viimased omakorda on mõjustatud vedela kiudbetooni valuprotsessist ja -vormist.

Toodud esmaste analüüsiandmete põhjal saab väita, et laboris valatud väikeste mõõtmetega katsekehade baasil ei saa konstruktsiooniliste kiudbetoonielementide kohta järeldusi teha. Samuti vajab erilist tähelepanu kiudbetooni valuprotseduur, mille tõttu kandvate kiudbetoon-konstruktsioonide valu ehitusplatsil võib problemaatiline olla.

Appendix 4

IV

D. Kartofelev, O. Goidyk, and H. Herrmann. A case study on the spatial variability of strength in a SFRSCC slab and its correlation with fibre orientation. *Proceedings of the Estonian Academy of Sciences*, 69(4):298–310, 2020



A case study on the spatial variability of strength in a SFRSCC slab and its correlation with fibre orientation

Dmitri Kartofelev^a, Oksana Goidyk^a, and Heiko Herrmann^{a*}

^a Department of Cybernetics, Tallinn University of Technology, Akadeemia tee 21, 12618 Tallinn, Estonia

Received 23 March 2020, accepted 29 June 2020, available online 16 October 2020

© 2020 Authors. This is an Open Access article distributed under the terms and conditions of the Creative Commons Attribution-NonCommercial 4.0 International License (<http://creativecommons.org/licenses/by-nc/4.0/>).

Abstract. This paper presents the results of an experimental investigation into the effects of the fibre orientation and the concrete casting method on the flexural strength and fracture toughness of steel fibre reinforced self-compacting concrete (SFRSCC). A destructive four-point bending testing is used to measure the flexural strength at the main cracking, the accepted mean post-cracking loading, and the energy absorption capacity (toughness) of the concrete. It is shown that a *favourable* fibre orientation increases flexural strength up to 25%, the accepted mean post-cracking loading up to 65%, and the toughness up to 65% for the specific concrete mixture and concrete beams used. The presented results and analysis demonstrate the importance of the spatial fibre orientation and distribution on the final strength and durability of hardened concrete. The main findings and conclusions of this paper can also be extended to other fibre reinforced composite materials.

Key words: open pour concrete casting, material strength, free-surface flow, fibre orientation, four-point bending test, concrete reinforcement, concrete cracking, crack control, structural concrete elements.

1. INTRODUCTION

Concrete is one of the most widely used building materials that has developed considerably in the last 40 years, during which time its worldwide use has significantly increased [1]. It is first and foremost due to the use of fibre reinforced composites as construction materials that have improved many important aspects of modern buildings. Composites have decreased overall construction times and at the same time increased overall structural durability, impact, fire and corrosion resistance. They allow for higher strength at lower weight and lift various restrictions on previously non-feasible designs [2,3]. One such composite material is steel fibre reinforced self-compacting concrete (SFRSCC). It is often believed that in addition to time savings it also reduces the amount of skilled labour required on building sites, and as a result, is a source of financial savings [4,5].

Previous studies of SFRSCC have established that favourable mechanical properties of SFRSCC depend strongly on the average fibre orientation. Superior strength is achieved when fibres are oriented mostly in the dominant direction of tensile stresses present in a final product, which has been shown experimentally [6–12] and is in accordance with various theories [13–16]. The final orientation of the fibres within the hardened concrete is influenced by several factors: most importantly, the so-called “wall effects” of the

* Corresponding author, hh@cens.ioc.ee

casting formwork/molds [17,18]; pouring of the concrete and other nuances of the casting method used [19]; geometry and size of formwork [20,21]. Additionally, the amount and type of fibre have an impact on the post-cracking behaviour of SFRSCC. In particular, hooked-end fibres can show deflection-hardening behaviour, while straight fibres demonstrate the deflection-softening response [22]. Similarly, a low fibre amount leads to strain-softening while a higher fibre dosage is necessary to achieve strain-hardening. Different fibre materials, fibre geometry, and fibre amounts change the mechanical properties and post-cracking dynamics. For instance, the addition of medium or high strength steel fibres significantly increases the tensile and flexural strength of SFRSCC [23,24], whereas polyolefin fibres are chemically inert, able to control micro cracking occurring at the initial shrinkage stage of concrete hardening, and strengthen thus the interfacial bonds between the fibres and the concrete matrix [25]. Several research groups [26,27] have also considered hybrid fibre concretes that contain a mixture of different fibre types and materials, where each type of fibres has its own function and contribution to the cracking control. Some research has been done on the effect of the fibre content and fibre orientation on concrete fatigue under static and cyclic bending tests [28].

In order to predict or estimate the fibre orientation and dispersion, both during and after concrete casting, computational fluid dynamics modelling has been used. Kang and Kim [29] have analysed the dynamics of the flow-dependent fibre orientation, where for the sake of simplicity the interactions between fibres were neglected. They show that the fibres tend to align/orient in parallel with respect to the main flow direction in the case of shear flow, and perpendicular in the case of radial flow. This was shown to be especially true for increased distances from the casting point. Svec et al. [30] have presented a modified method that combines the lattice Boltzmann modelling with the corrected immersed boundary methods and a mass tracking algorithm allowing to simulate the SFRSCC flow as a non-Newtonian fluid. Herrmann and Lees [17] have performed the simulations of multiphase free-surface flow by using OpenFOAM 2.3.0 library [31]. They show that the influence of the surface properties of a casting formwork should be taken into account when modelling SFRSCC casting.

The aim of this case study is to present the quantitative results of an experimental investigation into the effects of the fibre orientation and the concrete casting method on the flexural strength and fracture toughness of SFRSCC. This paper is organized as follows. Section 2 describes in detail the experimental methodology applied. Section 3 presents the main findings: comparison of SFRSCC to standard self-compacting concrete (SCC) (Sec.3.1); effects of the fibre orientation on flexural strength (Sec.3.2); effects of the fibre orientation on the accepted mean post-cracking loading (Sec.3.3); effects of the fibre orientation on post-cracking absorbed energy (Sec.3.4); relationships between SFRSCC strength and crack positions (Sec.3.5). Section 4 analyses the results of the experimental investigation and Section 5 presents a summary of the findings along with recommendations based on the analysed data.

2. EXPERIMENTAL METHODOLOGY

2.1. Main approach, theoretical and working assumptions

Two flat slabs with dimensions of $1.0 \text{ m} \times 0.1 \text{ m} \times 4.0 \text{ m}$ are cast, using SCC and SFRSCC. After hardening, the SCC slab is cut by hand-held water-cooled diamond saw into 12 beams in the size of $0.1 \text{ m} \times 0.1 \text{ m} \times 1.0 \text{ m}$, approximately. The SFRSCC slab is cut into 40 beams in the size of $b \times h \times 1.0 \text{ m}$, where the average beam cross-section width $b = 0.096 \text{ m}$ with the standard deviation of 0.0027 m and the average beam cross-section height $h = 0.105 \text{ m}$ with the standard deviation of 0.0014 m (normal and non-correlated distribution of beam cross-section dimensions is assumed). The layout and position of the cut-out beams with respect to the original slab is shown in Fig. 1.

The concrete casting process of the slabs used in this study is no different from the ordinary casting procedure implemented in civil engineering when creating similar structural concrete elements. The wet SFRSCC mixture is poured directly from a casting bucket into a formwork. The pouring and the consequent free-surface flow is initiated at the *casting point* (see Fig. 1) near one end of the slab. The casting point is

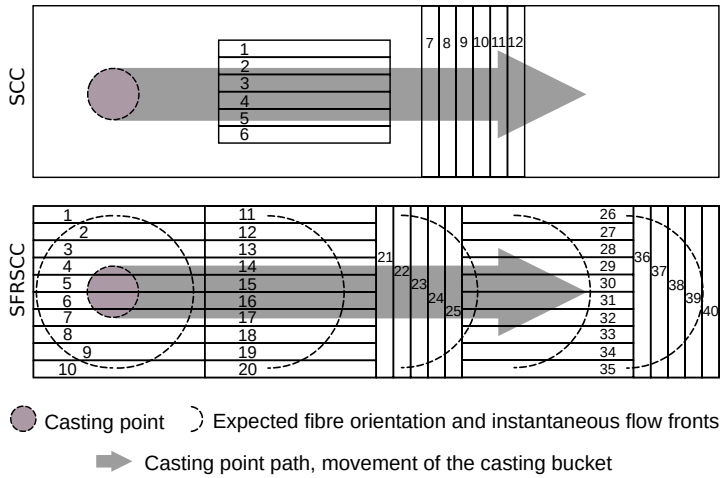


Fig. 1. Schematic drawing of the top view of the studied concrete slabs. Segmentation of the slab into smaller beams totalling 12 in the case of SCC and 40 in the case of SFRSCC.

then progressively moved along the centerline towards the other end of the slab, filling the formwork in its path. This concrete casting process is schematically depicted in Fig. 1, marked by the gray region/arrow. A more detailed overview of the casting and curing procedures is given in [32] and a micro-structure analysis in [33]. We proceeded from the assumption that the aforementioned casting process would ensure a symmetric fibre orientation that is qualitatively similar to the one shown in Fig. 1, i.e., the fibres that would eventually be closer to the longer edges of the slab (formwork walls) tend to align more in the direction of the casting point path (centerline), and the fibres that would be closer to the casting point path tend to orient more perpendicularly to it [34,35].

Each created beam is subjected to destructive four-point bending test (described below). The test determines the beam loading history as a function of the beam deflection s registered at the beam midpoint $F(s)$. The main cracking, i.e. the first major crack, is defined by the following condition

$$R(s) = \frac{dF(s)}{ds} = 0, \tag{1}$$

where $F(s)$ is the measured beam loading history and $R(s)$ is the history of flexural rigidity (stiffness). The flexural strength at the moment of cracking is given as

$$\sigma = \frac{F_f L}{bh^2}, \tag{2}$$

where $F_f \equiv F(s_f)$ is the fail load and s_f is the beam midpoint deflection corresponding to the main cracking; L is the effective length of the beam, see Fig. 3, b and h are the width and height of the beam cross-section mentioned above. Energy absorption history is presented as

$$E(s) = \int F(s) ds. \tag{3}$$

Pre-cracking absorbed energy is defined by

$$E|_{s \in [0, s_f]} = \int_0^{s_f} F(s) ds, \tag{4}$$

and post-cracking absorbed energy by

$$E|_{s \in (s_f, s_s)} = \int_{s_f}^{s_s} F(s) ds, \quad (5)$$

where $s_s \approx 7$ mm is the maximum deflection achieved/allowed during a bending test. Total absorbed energy is expressed as

$$E|_{s \in [0, s_s]} = \int_0^{s_s} F(s) ds. \quad (6)$$

Numeric integration of definite integrals, Eqs (4), (5), and (6), in the case of discretized $F(s)$ values is performed numerically by using the trapezoidal integration rule. Discretized samples F_i of force history $F(s)$ are defined as follows: $F_i = F(s_i)$, $s_i = i\Delta s$, and $\Delta s = s_s/N$, where i is the sample index and N is the total number of measured samples. In the current study $N \gtrsim 700$ for all the SFRSCC beams measured. The accepted mean pre-cracking load \bar{F} , for $s \in [0, s_f]$ is defined by

$$\bar{F}|_{s \in [0, s_f]} = \frac{1}{s_f} \int_0^{s_f} F(s) ds. \quad (7)$$

The accepted mean post-cracking load \bar{F} for $s \in (s_f, s_s]$ is expressed as

$$\bar{F}|_{s \in (s_f, s_s]} = \frac{1}{s_s - s_f} \int_{s_f}^{s_s} F(s) ds. \quad (8)$$

In the case of discretized load history values F_i , it is possible to use the following formula for the arithmetic average:

$$\bar{F}|_{s \in [s_a, s_b]} = \frac{1}{N_{\text{span}}} \sum_{i=a}^b F_i, \quad (9)$$

where N_{span} is the number of samples in the span/range over which the average is calculated, a is the index of the discretized deflection value corresponding to the beginning of the range s_a , so that $s_a = a\Delta s$, and b is the index of the last sample of the range s_b , so that $s_b = b\Delta s$.

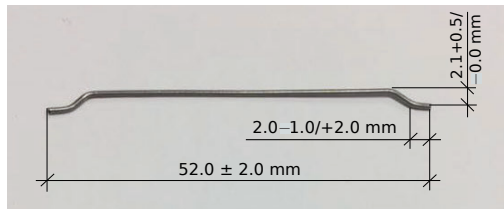
2.2. Concrete mixture and steel fibres

The SFRSCC mixture is prepared by using a regular off-the-shelf concrete mixer with a capacity of 2 m³ and the SCC mix specified in Table 1. SCC is turned into SFRSCC via a gradual addition of a small amount of extra water and hooked-ended steel fibres, shown in Fig. 2 (single fibre). The fibres are added gradually in small batches to prevent possible fibre clustering until fibre content of 0.64% by volume is reached, corresponding to 50 kg/m³. The geometric, physical and other properties of the fibres are shown in Table 2. The slump flow test of the wet SFRSCC mixture results in the slump diameter of 0.65 m.

The compressive strength after 28 days in the case of SCC was 68.6 MPa (stdev 2 MPa) and in the case of SFRSCC 56.6 MPa (stdev 1 MPa), the individual test results are available in [32].

Table 1. Composition of SCC and SFRSCC, the amount mixed 1.0 m³

Ingredient	Amount (kg)
Cement	330
Sand (0–2 mm)	398
Sand (0–4 mm)	505
Crushed Stone (2–5)	336
Crushed Stone (8–11)	539
Filler	80
Admixture	5.1
Water	175
Fibres (SFSCC only)	50
Extra water (SFSCC only)	≈ 10

**Fig. 2.** Steel fibre used in the wet SFRSCC mix.**Table 2.** Information on the steel fibres as provided by the manufacturer [36]

Manufacturer	Severstal Metiz
Model	Hendix prime 75/52
Type	Hooked end
Length	52 ± 2 mm
Diameter	0.75 ± 0.04 mm
Bend angle	(40 ± 5)°
Tensile strength	1.5 GPa
Elastic modulus	≥ 190 GPa
Number of fibres	≈ 5.5 · 10 ³ kg ⁻¹

2.3. Destructive four-point bending test

The four-point bending test set-up is shown schematically in Fig. 3. The beams are deformed by means of the universal electro-mechanical/hydraulic testing machine “EU100”, manufactured by VEB Werkstoffprüfmaschinen Leipzig. The mechanical load F accepted by a beam is measured by piezoelectric force sensors “HBM U10M” with a measuring range up to 50 kN and a measurement uncertainty of 50 N. The midspan beam deflection s is measured with the help of displacement sensors “HBM WI/10mm-T” that have the measurement uncertainty of 0.2 mm. Additionally, the universal amplifier/analog-to-digital converter “HBM QuantumX MX840A” is used, manufactured by HBM Hottinger Baldwin Messtechnik GmbH that connects to the aforementioned measurement sensors. Digital data capture and the initial on-the-spot data visualization are performed with the software “CatmanEasy DAQ” which was included in the package of the HBM QuantumX.

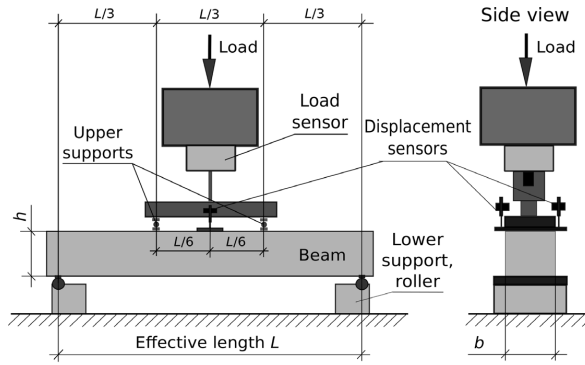


Fig. 3. Schematic drawing of the four-point bending test set-up, where the effective length L is 0.9 m. The zero point for the displacement is on top of a thin plate which is placed across the top of the beam in the centre, at the beginning of the test the displacement gauges are compressed.

3. EXPERIMENTAL RESULTS AND ANALYSIS

3.1. Comparison of SCC beams with SFRSCC beams

Figure 4 illustrates the load history of the selected SCC beams (see Fig. 1). The beams display elastic, mostly constant pre-cracking behaviour with the mean flexural rigidity $\bar{R}|_{s \in [0, \bar{s}_f]} \approx 12.7$ kN/mm, and the post-cracking mean flexural rigidity $\bar{R}|_{s \in (\bar{s}_f, s_s]} \approx -9.5$ kN/mm.

Figure 5 shows: the load history data $F(s)$ for all the 40 beams (see Fig. 1); the average pre-cracking and post-cracking load, and the absorbed energy values; the average load history graph $\bar{F}(s)$; and the absorbed energy history graphs $E(s)$. The following characteristics of the average load history $\bar{F}(s)$ are not indicated in Fig. 5: the mean pre-cracking flexural rigidity $\bar{\bar{R}}|_{s \in [0, \bar{s}_f]} = 12.05 \pm 1.89$ kN/mm, where the uncertainty is understood as a standard deviation of \bar{R} values; the mean post-cracking flexural rigidity $\bar{\bar{R}}|_{s \in (\bar{s}_f, s_s]} = -0.39 \pm 0.20$ kN/mm. These results are calculated slightly differently in comparison to the previous definition of mean values, cf. Eqs (7) and (8). The mean (or more precisely the mean of a mean) pre-cracking flexural rigidity $\bar{\bar{R}}$ is expressed as

$$\bar{\bar{R}}|_{s \in [0, \bar{s}_f]} = \frac{1}{40} \sum_{j=1}^{40} (\bar{R}|_{s \in [0, s_f]})_j, \quad (10)$$

where $j \in [1, 40]$ is the beam number and

$$\bar{R}|_{s \in [0, s_f]} = \frac{1}{s_f} \int_0^{s_f} R(s) ds. \quad (11)$$

And, the mean post-cracking flexural rigidity $\bar{\bar{R}}$ is defined by

$$\bar{\bar{R}}|_{s \in (\bar{s}_f, s_s]} = \frac{1}{40} \sum_{j=1}^{40} (\bar{R}|_{s \in (s_f, s_s]})_j, \quad (12)$$

where

$$\bar{R}|_{s \in (s_f, s_s]} = \frac{1}{s_s - s_f} \int_{s_f}^{s_s} R(s) ds. \quad (13)$$

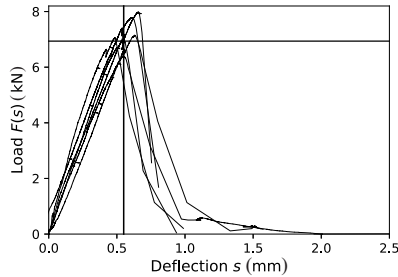


Fig. 4. Load history $F(s)$ for the selected SCC beams, shown in Fig. 1. The average deflection corresponding to the main cracking $\bar{s}_f = 0.55$ mm is depicted by the vertical line. The mean cracking load $\bar{F}_f \equiv \bar{F}(\bar{s}_f) \approx 7.0$ kN corresponding to the selected load history graphs is indicated by the horizontal line.

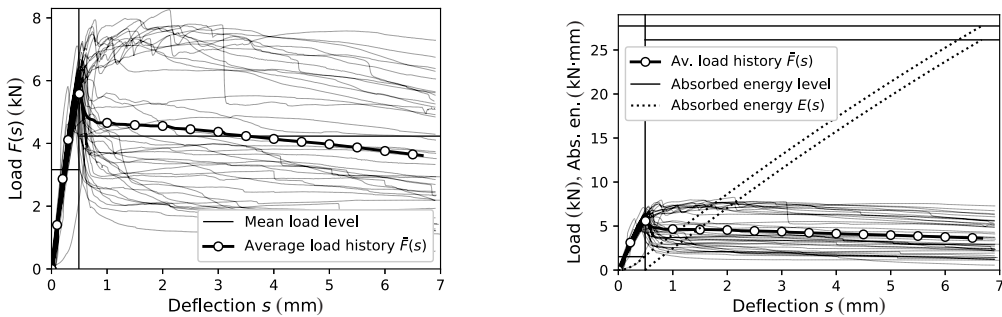


Fig. 5. Load history graphs $F(s)$ for SFRSCC beams No. 1–40 are represented by the thin continuous lines. The load history graph that is shown by the marked thick line is the mean load history $\bar{F}(s)$ averaged over all the 40 measured beam histories. Left: the mean pre-cracking load $\bar{F}|_{s \in [0, \bar{s}_f]} = 3.2$ kN, where $\bar{s}_f = 0.50$ mm (indicated by the vertical line), and the mean post-cracking load $\bar{F}|_{s \in (\bar{s}_f, s_s]} = 4.2$ are represented by the horizontal continuous lines. Right: the pre-cracking absorbed energy level $E|_{s \in [0, \bar{s}_f]} = 1.5$ kN-mm, the post-cracking absorbed energy level $E|_{s \in (\bar{s}_f, s_s]} = 26.1$ kN-mm, and the total absorbed energy level $E|_{s \in (0, s_s]} = 27.7$ kN-mm are shown by the horizontal continuous lines. The corresponding energy absorption histories $E(s)$ are depicted by the dotted lines.

The comparison of the results shown in Figs 4 and 5 demonstrates clearly that the addition of the fibres changes the post-cracking dynamics of SFRSCC significantly. SFRSCC is capable of accepting significant loading even after cracking of a beam has occurred. The mean pre-cracking flexural rigidity $\bar{R}|_{s \in [0, \bar{s}_f]}$ in the case of SCC and $\bar{R}|_{s \in [0, \bar{s}_f]}$ in the case of SFRSCC are approximately equal, which is expected since as regards small deflections, both materials should behave according to the linear theory. The comparison of the mean cracking loads reveals that in relation to SCC $\bar{F}_f \approx 7.0$ kN and in relation to SFRSCC $\bar{F}_f \approx 5.5$ kN. This counter-intuitive observation can likely be explained by the slightly different water contents in the wet concrete mixtures, see Table 1.

At the first glance the results for SFRSCC beams shown in Fig. 5 seem random. One can observe the beam load histories $F(s)$ with deflection-hardening dynamics and with the opposite, as well. Also, the highly fluctuating mean post-cracking load values can be detected that span from 1.0 to 7.0 kN, approximately. In the following sections the presented data will be analysed and attempted to be organized.

3.2. Effect of dominant fibre orientation on flexural strength

Figure 6 shows the flexural strength σ , Eq. (2), against the beam number. The results are divided into four groups/regions of the original slab: beams 1–10, 11–20, 26–35, and the *centerline* beams. Figure 7 presents

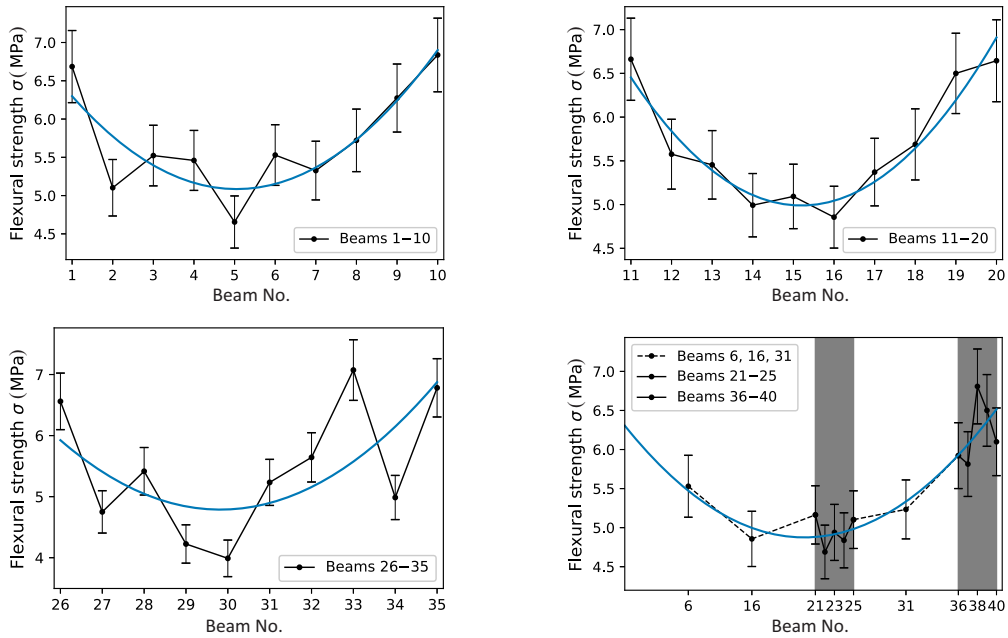


Fig. 6. Flexural strength σ as a function of the beam number. Least square fit graphs of the dominant trends are indicated by using the continuous lines. The lower-right plot corresponds to the centerline results highlighted in Fig. 7.

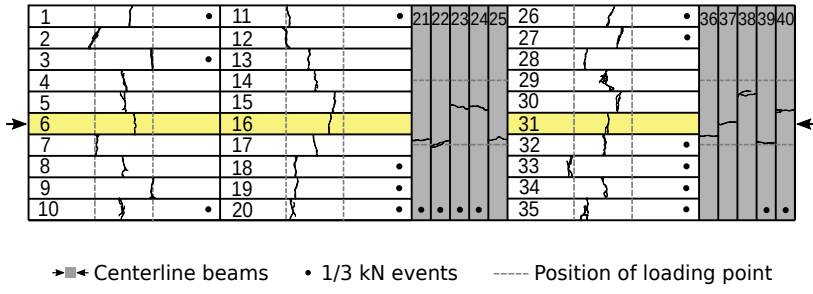


Fig. 7. Centerline beams numbered 6, 16, 21–25, 31, 36–40 are highlighted by the coloured backgrounds and bold arrows. The positions and shapes (bottom view) of the cracks sustained at the main cracking are shown based on the realistic crack patterns.

the numbering and positions of all the 40 beams (the same as in Fig.1), as well as the four groups of interest, including the centerline beams. The centerline beams represent a cross-section of the original slab in its lengthwise direction. The other groups are cross-sections perpendicular to the longer dimension of the slab.

All the presented results, shown in Fig. 6, feature a parabolic trend. The trend is detected by least square fitting of a second-order polynomial to the shown data points. The beams and thus the slab is stronger near its edges. The relative increase in flexural strength σ near the edges is approximately 20–25% in comparison to the regions closer to the middle. The change in flexural strength σ is relatively gradual and continuous, considering the stochastic and anisotropic nature of the material worked with.

The reason for this strength increase must be related to the fibre orientation [33]. A SFRSCC beam with a favourable dominant fibre orientation is able to better resist the bending. The results presented here serve as a justification/proof to the assumption given in Sec. 2.1 regarding the dominant fibre orientation, see Fig. 1. When even a small fraction of fibres are aligned along the direction of the length of a beam (direction of the tensile stress), they will effectively start to perform similarly to regular steel rebars increasing the effective/average tensile strength of the concrete.

3.3. Effect of dominant fibre orientation on mean post-cracking load

Figure 8 demonstrates the accepted mean post-cracking load $\bar{F}|_{s \in (s_f, s_s)}$ against the beam number. The results presented here are qualitatively identical to the ones shown in Fig. 6. This means that the post-cracking strength and durability characteristic are also governed by the dominant fibre orientation. The beams closer to the edges of the slab accept approximately 50–65% more load compared to the middle region of the slab.

3.4. Effect of dominant fibre orientation on post-cracking absorbed energy

Figure 9 presents the post-cracking absorbed energy $E|_{s \in (s_f, s_s)}$ against the beam number. Once again the parabolic trends are present. SFRSCC located near the edges of the slab is capable of absorbing approximately 45–65% more energy compared to the concrete located in the middle of the slab. The ability of the material to absorb energy is referred to as its toughness.

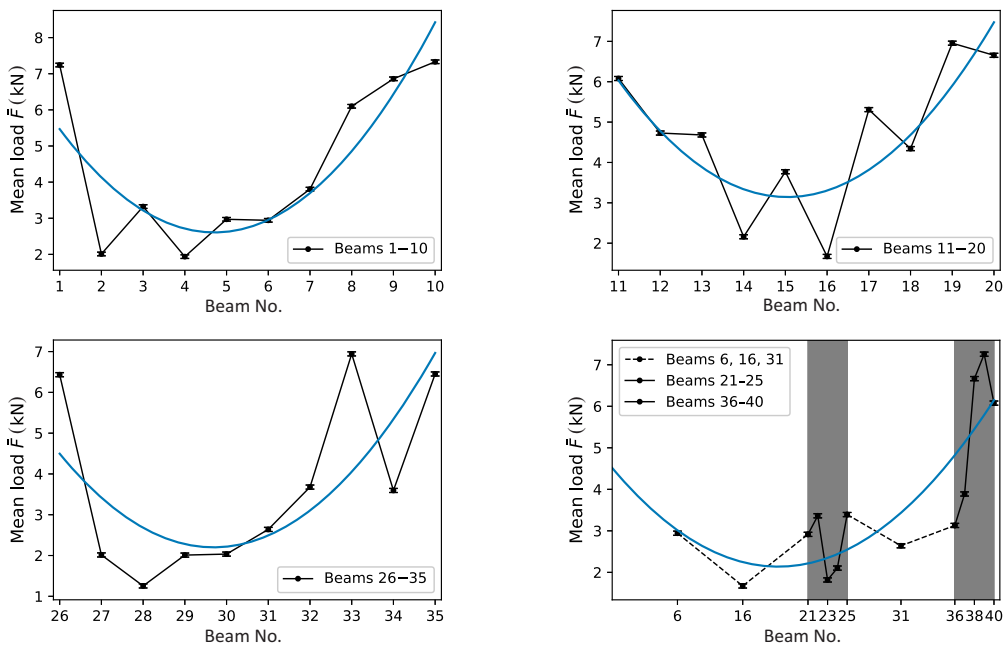


Fig. 8. The accepted mean post-cracking load $\bar{F}|_{s \in (s_f, s_s)}$ as a function of the beam number. Least square fit graphs of the dominant trends are indicated by the continuous lines. The lower-right plot corresponds to the centerline results highlighted in Fig. 7. The uncertainty of the displayed accepted mean load values $\delta \bar{F}|_{s \in (s_f, s_s)} = \pm 50$ N.

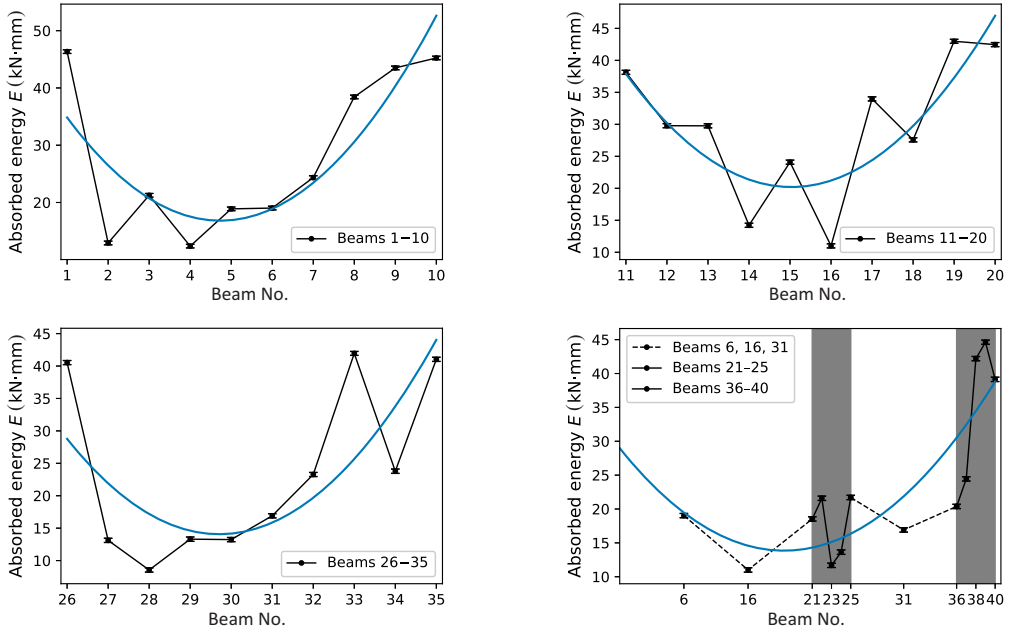


Fig. 9. Post-cracking absorbed energy $E|_{s \in (s_f, s_s)}$ as a function of the beam number. Least square fit graphs of the dominant trends are indicated by the continuous lines. The lower-right plot corresponds to the centerline results highlighted in Fig. 7. The calculated uncertainty of the displayed energy values $\delta E|_{s \in (s_f, s_s)} = \pm \xi$ kN·mm, where $\xi \in [0.30, 0.33]$.

3.5. Dominant fibre orientation and crack position

Figure 7 demonstrates the position and shape of the cracks associated with the main cracking of the beams. The cracks are shown for all the 40 beams. A visual inspection of beams 11–20 seems to suggest that the stronger beams, located closer to the edges of the slab, tend to crack near the upper support points of the four-point bending machine shown in Fig. 3. This may be explained by the interplay of shear stresses and bending moments. The normal force introduced by the support simply cuts through/pushes itself into the material. In the other regions of the slab this phenomenon is less observable, being harder to distinguish from a random chance.

4. DISCUSSION

In addition to the post-cracking results discussed in Secs 3.3 and 3.4, the authors of this paper also considered the mean pre-cracking accepted load $\bar{F}|_{s \in [0, s_f]}$, the total mean load $\bar{F}|_{s \in [0, s_s]}$, the pre-cracking absorbed energy $E|_{s \in [0, s_f]}$, and the total absorbed energy $E|_{s \in [0, s_s]}$ values. It was established that all of these values when plotted against the beam numbers and for the four regions of interest discussed in Sec. 3.2 have graphs qualitatively similar to the ones shown in Figs 8 and 9. The results regarding the mean pre-cracking load $\bar{F}|_{s \in [0, s_f]}$ and the pre-cracking absorbed energy $E|_{s \in [0, s_f]}$ mean that in a linear regime of loading the SFRSCC strength depends also on the dominant fibre orientation. The intact and loaded SFRSCC is stronger when the fibres are oriented in the direction of the tensile stresses.

While analysing the data presented in this paper, an interesting observation was made. The load history $F(s)$ curves of the individual beams feature step-shaped cracking events that are temporally highly located.

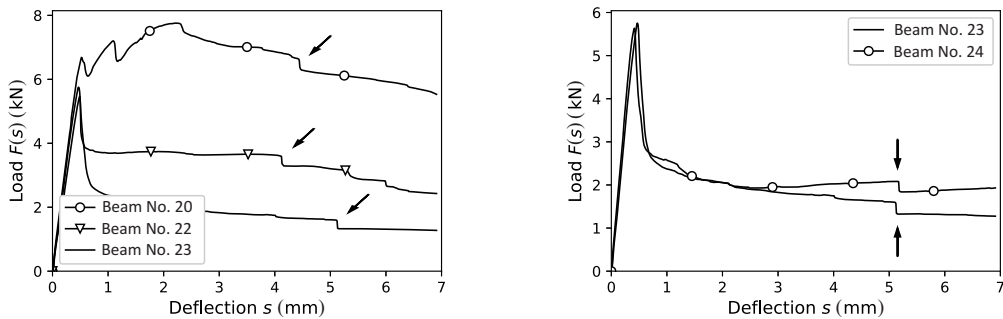


Fig. 10. Left: Examples of 1/3 kN events. The events are indicated by the bold arrows. Right: An example of neighbouring beams where the 1/3 kN events occurred almost precisely at the same beam deflection value s .

What is interesting about these events is the fact that the drop in the accepted load F is consistently almost precisely 1/3 kN. The examples regarding the 1/3 kN events are presented in Fig.10. The beams featuring in the events are shown in Fig.7. Almost half (47.5%) of the beams feature in at least one 1/3 kN event. In one instance an event spans two neighbouring beams, beams 23 and 24, see Fig.10. A satisfactory explanation supported by evidence regarding the cause/source of the 1/3 kN events has not been identified by the authors.

5. CONCLUSIONS

This paper presents the results of an experimental investigation into the effects of the fibre orientation on the flexural strength and fracture toughness of SFRSCC. The destructive four-point bending testing was used to measure the flexural strength at the main cracking (Sec. 3.2), the accepted mean post-cracking loading (Sec. 3.3), and energy absorption capacity (toughness) of the concrete (Sec. 3.4)

It was shown that a *favourable* fibre orientation, where the fibres are oriented in the direction of tensile stresses, would increase the flexural strength of the SFRSCC beams with dimensions of 0.1 m \times 0.1 m \times 1.0 m, up to 25% (approximately 20–25%), the accepted mean post-cracking loading up to 65% (approximately 50–65%), and the absorbed energy levels up to 65% (approximately 45–65%) for the specific concrete mixture used, see Table 1.

The presented results and analysis demonstrate the importance of the dominant fibre orientation on the final strength and toughness characteristics of hardened SFRSCC. If a concrete slab with uniform and isotropic strength characteristics is required, one needs to ensure a random fibre orientation throughout the material. Open pour casting, where the concrete mix is subjected to a free-surface flow, as was described in Sec. 2.1, can – and often will – result in an uneven strength distribution, see Figs 6, 8, and 9. This uneven strength and toughness distribution should be taken into consideration in construction guidelines and specially trained staff may be required for the casting of SFRSCC to ensure the desired properties.

CREDIT AUTHORSHIP CONTRIBUTION STATEMENT

Dmitri Kartofelev: Investigation, Formal analysis, Writing – Original draft. **Oksana Goidyk:** Investigation – Conducting experiments, Formal analysis, Writing – Original draft. **Heiko Herrmann:** Conceptualization, Methodology, Investigation – Planning and conducting experiments, Writing – Review and editing, Project administration, Funding acquisition.

ACKNOWLEDGEMENTS

This work was supported by the Estonian Research Council grant (PUT1146 and IUT33-24). The authors express their gratitude to Elmar-Jaan Just and Peeter Linnas of the Department of Civil Engineering and Architecture, for the opportunity to use the equipment in the Mäepealse Lab. The authors also thank Tanel Tuisk and Andres Braunbrück, Department of Civil Engineering and Architecture, as well as E-Betoonelement OÜ for their help with the experiments. The publication costs of this article were covered by the Estonian Academy of Sciences.

REFERENCES

1. Brandt, A. M. Fibre reinforced cement-based (FRC) composites after over 40 years of development in building and civil engineering. *Compos. Struct.*, 2008, **86**(1–3), 3–9.
2. Błaszczyszki, T. and Przybylska-Fałek, M. Steel fibre reinforced concrete as a structural material. *Procedia Eng.*, 2015, **122**, 282–289.
3. Naaman, A. E. High performance fiber reinforced cement composites: classification and applications. In *CBM-CI international workshop, Karachi, Pakistan*, 2007, 389–401.
4. Di Prisco, M., Plizzari, G., and Vandewalle, L. Fibre reinforced concrete: new design perspectives. *Mater. Struct.*, 2009, **42**(9), 1261–1281.
5. Domone, P. L. Self-compacting concrete: an analysis of 11 years of case studies. *Cem. Concr. Compos.*, 2006, **28**(2), 197–208.
6. Vicente, M. A., Gonzalez, D. C., and Mínguez, J. Determination of dominant fibre orientations in fibre-reinforced high-strength concrete elements based on computed tomography scans. *Nondestr. Test. Eval.*, 2014, **29**(2), 164–182.
7. Laranjeira, F., Aguado, A., Molins, C., Grunewald, S., Walraven, J., and Cavalaro, S. H. P. Framework to predict the orientation of fibers in FRC: a novel philosophy. *Cem. Concr. Res.*, 2012, **42**(6), 752–768.
8. Vandewalle, L., Heirman, G., and Van Rickstal, F. Fibre orientation in self-compacting fibre reinforced concrete. In *Proc. of the 7th Int. RILEM Symp. on Fibre Reinforced Concrete: Design and Applications (BEFIB2008)*. 2008, 719–728.
9. Zerbino, R., Tobes, J. M., Bossio, M. E., and Giaccio, G. On the orientation of fibres in structural members fabricated with self compacting fibre reinforced concrete. *Cem. Concr. Compos.*, 2012, **34**(2), 191–200.
10. Michels, J. and Gams, M. Preliminary study on the influence of fibre orientation in fibre reinforced mortars. *Gradevinar*, 2016, **68**(8), 645–655.
11. Mínguez, J., González, D. C., and Vicente, M. A. Fiber geometrical parameters of fiber-reinforced high strength concrete and their influence on the residual post-peak flexural tensile strength. *Constr. Build. Mater.*, 2018, **168**, 906–922.
12. González, D. C., Mínguez, J., Vicente, M. A., Cambroner, F., and Aragón, G. Study of the effect of the fibers' orientation on the post-cracking behavior of steel fiber reinforced concrete from wedge-splitting tests and computed tomography scanning. *Constr. Build. Mater.*, 2018, **192**, 110–122.
13. Eik, M., Puttonen, J., and Herrmann, H. An orthotropic material model for steel fibre reinforced concrete based on the orientation distribution of fibres. *Compos. Struct.*, 2015, **121**, 324–336.
14. Eik, M., Puttonen, J., and Herrmann, H. The effect of approximation accuracy of the orientation distribution function on the elastic properties of short fibre reinforced composites. *Compos. Struct.*, 2016, **148**, 12–18.
15. Herrmann, H. An Improved Constitutive Model for Short Fibre Reinforced Cementitious Composites (SFRC) Based on the Orientation Tensor. In *Generalized Continua as Models for Classical and Advanced Materials* (Altenbach, H. and Forest, S., eds), Springer International Publishing, Cham, 2016, 213–227.
16. Laranjeira, F., Grunewald, S., Walraven, J., Blom, C., Molins, C., and Aguado, A. Characterization of the orientation profile of steel fibre reinforced concrete. *Mater. Struct.*, 2011, **44**(6), 1093–1111.
17. Herrmann, H. and Lees, A. On the influence of the rheological boundary conditions on the fibre orientations in the production of steel fibre reinforced concrete elements. *Proc. Estonian Acad. Sci.*, 2016, **65**(4), 408–413.
18. Martinie, L. and Roussel, N. Simple tools for fiber orientation prediction in industrial practice. *Cem. Concr. Res.*, 2011, **41**(10), 993–1000.
19. Torrijos, M. C., Barragán, B. E., and Zerbino, R. L. Placing conditions, mesostructural characteristics and post-cracking response of fibre reinforced self-compacting concretes. *Constr. Build. Mater.*, 2010, **24**(6), 1078–1085.
20. Dupont, D. and Vandewalle, L. Distribution of steel fibres in rectangular sections. *Cem. Concr. Compos.*, 2005, **27**(3), 391–398.
21. Zhou, B. and Uchida, Y. Influence of flowability, casting time and formwork geometry on fiber orientation and mechanical properties of UHPFRC. *Cem. Concr. Res.*, 2017, **95**, 164–177.
22. Pajak, M. and Ponikiewski, T. Flexural behavior of self-compacting concrete reinforced with different types of steel fibers. *Constr. Build. Mater.*, 2013, **47**, 397–408.
23. Rizzuti, L. and Bencardino, F. Effects of fibre volume fraction on the compressive and flexural experimental behaviour of SFRC. *Contemp. Eng. Sci.*, 2014, **7**(8), 379–390.
24. Liu, R. and Liu, Y. Steel fiber reinforced concrete and its application performance. *Int. J. Multidiscip. Res. Dev.*, 2016, **3**(6), 341–343.

25. Alberti, M. G., Enfedaque, A., and Gálvez, J. On the mechanical properties and fracture behavior of polyolefin fiber reinforced self-compacting concrete. *Constr. Build. Mater.*, 2014, **55**, 274–288.
26. Stahli, P. and Van Mier, J. G. M. Manufacturing, fibre anisotropy and fracture of hybrid fibre concrete. *Eng. Fract. Mech.*, 2007, **74**(1–2), 223–242.
27. Kim, D. J., Park, S. H., Ryu, G. S., and Koh, K. T. Comparative flexural behavior of hybrid ultra high performance fiber reinforced concrete with different macro fibers. *Constr. Build. Mater.*, 2011, **25**(11), 4144–4155.
28. Vicente, M. A., Mínguez, J., and González, D. C. Computed tomography scanning of the internal microstructure, crack mechanisms, and structural behavior of fiber-reinforced concrete under static and cyclic bending tests. *Int. J. Fatigue*, 2019, **121**, 9–19.
29. Kang, S.-T. and Kim, J.-K. Numerical simulation of the variation of fiber orientation distribution during flow molding of ultra high performance cementitious composites (UHPCC). *Cem. Concr. Compos.*, 2012, **34**(2), 208–217.
30. Svec, O., Skocek, J., Stang, H., Olesen, J. F., and Poulsen, P. N. Flow simulation of fiber reinforced self compacting concrete using lattice Boltzmann method. In *Dissemination. 8th International Congress on the Chemistry of Cement, Madrid, Spain, July 3-8, 2011*.
31. The OpenFOAM Foundation Ltd, 2020. OpenFOAM. <https://openfoam.org/>
32. Herrmann, H., Goidyk, O., Naar, H., Tuisik, T., and Braunbrück, A. The influence of fibre orientation in self-compacting concrete on 4-point bending strength. *Proc. Estonian Acad. Sci.*, 2019, **68**(3).
33. Herrmann, H., Boris, R., Goidyk, O., and Braunbrück, A. Variation of bending strength of fiber reinforced concrete beams due to fiber distribution and orientation and analysis of microstructure. *IOP Conf. Ser.: Mater. Sci. Engineering*, 2019, **660**, 012059.
34. Boulekbache, B., Hamrat, M., Chemrouk, M., and Amziane, S. Flowability of fibre-reinforced concrete and its effect on the mechanical properties of the material. *Constr. Build. Mater.*, 2010, **24**(9), 1664–1671.
35. Herrmann, H., Goidyk, O., and Braunbrück, A. Influence of the flow of self-compacting steel fiber reinforced concrete on the fiber orientations, a report on work in progress. In *Short Fibre Reinforced Cementitious Composites and Ceramics* (Herrmann, H. and Schnell, J., eds). Springer, 2019, 97–110.
36. Severstal Metiz. Hendix prime 75/52 – hooked ends fiber. <http://www.severstalmetiz.ru>

Teraskiudbetoonplaadi tugevuse mittehomoogensuse sõltuvus teraskiudude ruumilisest orientatsioonist

Dmitri Kartofelev, Oksana Goidyk ja Heiko Herrmann

Käesolevas eksperimentaalses artiklis on uuritud isetihenduva kiudbetooni tugevuse sõltuvust teraskiudude ruumilisest orientatsioonist ja betooni valuprotseduurist. Tugevuskarakteristikute mõõtmiseks kasutati purustavat nelja punkti paindekatsset. Mõõtmistulemuste analüüs näitas, et teraskiudude *soositud* orientatsioon tõstab betoontala paindetugevust kuni 25%, keskmist purunemisejärgset vastuvõetud koormust kuni 65% ja plastse energia absorbeerimise võimet kuni 65%. Käesoleva artikli tulemused näitavad teraskiudude jaotustiheduse ja ruumilise orientatsioonilise jaotuse tähtsust lõpp-produkti üldisele tugevusele. Töös esitatud järeldused kehtivad ka teistele kiududega tugevdatud metamaterjalidele.

Appendix5

V

O. Goidyk, M. Heinštein, and H. Herrmann. CFD comparison of the influence of casting of samples on the fiber orientation distribution. *Fibers*, 11(1):6, 2023

CFD Comparison of the influence of casting of samples on the fiber orientation distribution

Oksana Goidyk ^{1,†} , Mark Heinštein ²  and Heiko Herrmann ^{3,†,*} 

¹ Tallinn University of Technology, School of Science, Department of Cybernetics; oksana.goidyk@taltech.ee

² Tallinn University of Technology, School of Science, Department of Cybernetics; markhe@taltech.ee

³ Tallinn University of Technology, School of Science, Department of Cybernetics; hh@cens.ioc.ee

* Correspondence: hh@cens.ioc.ee

† These authors contributed equally to this work.

Abstract: Nowadays, the development of the proper numerical simulations that aimed to visualize the casting process of the fresh concrete flow is the promising challenge in the construction industry. To be able to predict the orientation and spatial distribution of the short fibers by using numerical tools may strongly simplify the investigations of the fibered composite materials. The main goal of this research is to analyze the difference in the final fiber orientation distribution that was produced by various casting methods of the fresh concrete flow with the short fibers simulated by a special numerical tool with using an OpenFOAM software. This paper demonstrates the comparison of the different casting methods of the concrete mixture with various flowabilities. The testing specimen was produced by the different ways: the filling of the formwork according to EN 14651, from the center and from one edge of formwork by using Computational Fluid Dynamics. The influence of different casting methods in combination with four specific sets of the rheological parameters on the final fiber orientation distribution is discussed. The presented outcomes of the simulations demonstrate that even minor change in the casting procedure can significantly alter the final characteristics of the material. Based on the obtained results, one can conclude that the presented approach may be implemented for the visualisation of the realistic filling of the formwork with the fibered concrete mixture.

Keywords: fiber concrete; casting simulation; computational fluid dynamics; fiber orientations;

Citation: Goidyk, O.; Heinštein, M.; Herrmann, H. CFD Comparison of the influence of casting of samples on the fiber orientation distribution. *Fibers* **2022**, *1*, 0. <https://doi.org/>

Received:

Accepted:

Published:

Publisher's Note: MDPI stays neutral with regard to jurisdictional claims in published maps and institutional affiliations.

Copyright: © 2022 by the authors. Submitted to *Fibers* for possible open access publication under the terms and conditions of the Creative Commons Attribution (CC BY) license (<https://creativecommons.org/licenses/by/4.0/>).

1. Introduction

Research and development of advanced composite materials are one of the most important aspects in the building industry. This requirement originates from the environmental impact of the building industry in terms of CO₂ production and use of raw materials and also from the need to build higher buildings with lighter stronger structures. The use of fibers in concrete provides the improvement of load-bearing properties and ensures the increased serviceability of concrete products. The addition of fibers reduces crack propagation and even allows the transfer of stresses through the crack in the concrete. The fibers aligned in the stress direction can contribute to the force transmission. Depending on the place of filling and the direction of the concrete flow in the formwork, the orientation distribution of fibers in the concrete may vary.

Many research groups have contributed into the study and improvement of the rheological properties of the ordinary concrete, as well as of fiber reinforced concrete. Roussel has established the connection between the proper measurements of rheological properties (yield stress and thixotropy) and casting processes of the slabs and walls [1]. Hu et al. have studied the influence of coarse aggregate on the rheology of concrete and pointed out that a higher amount of coarse and fine aggregate, in general, results in higher rheological parameters (yield stress and viscosity) [2]. Kostrzanowska-Siedlarz and Gołaszewski have analyzed the rheological properties (plastic viscosity and yield

37 stress) and how it changes over time [3]. Jiao et al. has indicated that the rheological
38 properties, such as plasticity, viscosity and elasticity under shear stress have an impor-
39 tant impact on the constructing, forming or casting process [4]. Boulekbache et al. have
40 studied how the rheology of fibre-reinforced concrete impacts on the fiber orientation
41 and distribution and how the flexural strength may be strongly improved by the proper
42 fiber orientation in the direction of the tensile stresses in the fresh concrete with good
43 workability [5]. Ponikiewski and Gołaszewski have demonstrated that embedding of
44 fibers into concrete mixture has the negative impact on its workability and rheological
45 properties, however, optimal addition of superplasticizer improves its properties [6].
46 Khaloo et al. have demonstrated that increasing the steel fiber volume fraction has re-
47 duced the workability of self-compacting concrete and that the addition high percentages
48 of fibers led to decrease of other rheological parameters [7].

49 Recently, special attention is paid to the evaluation of the filling methods of fresh
50 concrete and its influence on the orientational and spatial fiber distribution inside of
51 fibre reinforced self-compacting concrete and ultra high performance fibre reinforced
52 concrete. Torrijos et al. have analyzed the influence of the casting/placing procedure
53 of fibre reinforced self-compacting concretes with different fiber length on post-peak
54 behavior [8,9]. Ponikiewski et al. have demonstrated a very strong dependence of the
55 location of concrete casting on fiber distribution and presented the possibility to estimate
56 the uniformity of fiber distribution throughout the scanned elements by using X-ray
57 Computed Tomography [10]. Sucharda et al. have presented an approach to identify the
58 specific material characteristics by applying inverse analysis. They found that the size of
59 the specific fracture energy is the most significant input parameter [11].

60 Vicente et al. have studied the influence of fiber orientation and fiber content on
61 residual tensile strength and fatigue under static and cyclic bending tests [12]. Voutetaki
62 et al. has discussed the impact of the embedded synthetic fibers on the compressive
63 strength and the damage-detection procedure [13]. The results of the investigations
64 presented by Barnett et al. have demonstrated that the panels poured from the center
65 have shown a higher strength due to the alignment of fibers that have a tendency to be
66 aligned perpendicular to the direction of flow and led to more fibers bridging the radial
67 cracks occurred during the mechanical testing [14].

68 Ferrara et al. have provided experimental evidence that the casting process can be
69 used to efficiently orient the fibers along the direction of the tensile stresses within the
70 structural element [15]. Zhou and Uchida have studied fiber orientation in ultra high
71 performance fiber reinforced concrete by using the transparent model with fibers and
72 compared with X-ray Computed Tomography analysis [16,17]. Yoo et al. have presented
73 a study that investigates the influence of fiber length and placement method on the
74 flexural behavior of ultra high performance self-compacting concrete [18].

75 In general, the composition of concretes is regulated by EN 206-1. The standard EN
76 206-1 refers to the standard EN 12390 for the testing of hardened concrete. Part EN 12390-
77 5 deals with the testing of the flexural strength. The test aims to record the maximum
78 force that can be absorbed during specimen bending. The load is applied perpendicular
79 to the direction in which the specimens are filled. In principle, the requirements of the EN
80 206-1 standard apply to fiber-reinforced concrete, thus also the technical requirements
81 for the composition. The standard 12390 was adopted for fiber concrete in the form of
82 the standard EN 14651 [19]. This standard describes the procedure for determining the
83 flexural strength of fiber-reinforced concrete specimens and specifies the procedure of
84 preparing and testing of the specimens. It describes the evaluation of the tensile behavior
85 of metallic fiber concrete in terms of determination of residual flexural tensile strength
86 values defined from load-deflection curve or the load-crack mouth opening displacement
87 curve obtained by applying a center-point load. Since the formulation of the standard EN
88 14651 a lot of research on the influence of fiber orientations on mechanical properties has
89 been conducted and published [1–10,14–18,20–24], additionally research on the influence
90 of the flow of concrete mass on the fiber orientations has been published [8–10,25–29].

91 However, there have been no studies published that investigate the fiber orientations
92 obtained by the sample preparation according to EN 14651.

93 Full-scale experiments according to EN 14651 with subsequent computed tomog-
94 raphy analysis of fiber distribution are highly time- and cost-consuming procedures,
95 therefore, numerical simulations can significantly simplify the planning and developing
96 stage of research and construction. Knowing exactly how the filling process affects the
97 fiber distribution could be used as a guide for the technological design of casting and
98 filling procedures with fiber-reinforced concrete.

99 The most widely used applications for numerical simulations in concrete materials
100 technology are the rheometry simulations [30,31], the simulation and optimization of the
101 mixing process [32,33], the casting and placement optimization [26,27,34], the simulation
102 of the tests in hardening state [35]. A detailed overview of existing applications of
103 numerical simulations is presented by several researchers [36,37]. It has been shown,
104 that numerical techniques provide flow prediction for a variety of viscosities with a high
105 reliability level [38,39].

106 Mechanical models for fiber concrete have been developed by several research
107 teams, several of these models take the fiber orientation distribution into account. Since
108 the fiber orientation distribution is often anisotropic [40–43], after homogenization, the
109 resulting macroscopic mechanical material model is also anisotropic [20–24].

110 The use of fiber-reinforced concretes is also widespread in the manufacture of pre-
111 cast concrete elements, among other things [44]. Due to the correct dosage of fibers,
112 cracking is considerably prevented. Concrete and reinforcing steel damage under in-
113 creased loads as a result of sulfate action, freeze-thaw cycles and alkali-silica reaction
114 is a durability problem in tunnel, canal and shaft structures. The optimally controlled
115 placement of the concrete in the formwork contributes to the achievement of the de-
116 sign approaches of the use of fibers. Controlled production in the precast plants has
117 scheduling advantages for the construction progress, which, however, should not be
118 achieved at the expense of the necessary curing. Slackly reinforced precast concrete
119 elements are usually already removed from the mold the day after concreting and stored
120 in the plant's yard. Early shrinkage of the concrete causes cracking, which is partly
121 counteracted by the use of fibers. Especially in the case of highly loaded bar-shaped
122 elements, shrinkage cracks with expansion potential are critical and should definitely
123 be prevented by suitable measures. One of the motivations of this study is to develop
124 practical guidelines for the optimal concreting process in precast plants in order to
125 achieve reliable and reproducible final states of the concrete matrix.

126 The main aim of the research presented here is to analyze the influence of the
127 casting method of test-specimen on the fiber distribution and pointing out which casting
128 conditions might lead to the preferable fiber orientation. Tests on fiber reinforced
129 specimen have already shown favourable fiber distribution for achieving higher flexural
130 strength on concrete slabs [25]. According to EN 14651 [19], the specimen should be
131 rotated by 90 degrees around the longitudinal axes for bending test while in-situ casting
132 would preserve the bottom layer. That fact raises the question if the fiber distribution is
133 invariant under this rotation, or if a different fiber distribution is in fact tested. Therefore,
134 the numerical simulations are aimed to investigate the variability of the fiber orientation
135 distribution in different boundary layers of the specimens.

136 This paper presents the results of numerical simulations of the casting process of
137 fresh self-compacting concrete with short fibers using different pouring methods: the
138 filling of the formwork according to EN 14651 and pouring from the middle and from
139 the end of the formwork. Additionally, the rheological parameters (yield stress and
140 plastic viscosity) have been varied to represent different flowabilities, like super-liquid,
141 self-leveling, high-viscous and slump.

142 2. Materials and Methods

143 2.1. Sample preparation and testing according to EN 14651

144 The specimens for the standard test according to EN 14651 are prisms with a square
 145 base with dimensions of 15 cm * 15 cm and a specimen length of 550 to 700 mm. The
 146 maximum length of the steel fibers is limited to 60 mm. The specimen formwork is filled
 147 in two steps. In the first step, 2/3 of the concrete volume is poured in the middle of the
 148 mold. The remaining 1/3 is divided in half and poured into the mold at its two ends. In
 149 the simulations described below, the simulated concrete is considered non-compacted,
 150 so the mold is filled up to the top edge. Since the filling side may show unevenness after
 151 curing of the concrete, the specimen is rotated once by 90 degrees during load application
 152 when measuring the tensile strength. The rotation results in two plane-parallel surfaces,
 153 which are required for the bending tensile measurement.

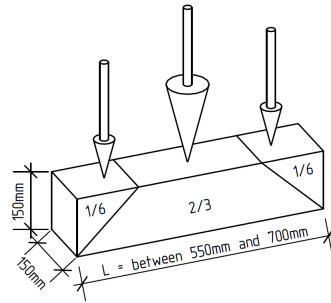


Figure 1. Casting of samples according to EN 14651, arrows denote filling areas.

154 2.2. Computational Fluid Dynamics Simulations

155 Fresh concrete behaves like a Bingham-plastic when it is cast, which means below
 156 the critical shear stress (yield stress τ_0) it behaves rigid, when the critical shear stress is
 157 surpassed, it shows a linear relation between shear stress and shear rate.
 158 The flow of the fresh concrete mass can be modeled with the incompressible Navier-
 159 Stokes equations

$$\nabla \cdot u = 0 \quad (1)$$

$$\frac{\partial u}{\partial t} + \nabla \cdot (uu) - \nabla \cdot (v \nabla u) = -\nabla p \quad , \quad (2)$$

160 with the kinematic viscosity $\nu = \frac{\mu}{\rho}$ and the dynamic viscosity μ . In the implementation,
 161 the Bingham-plastic behaviour is approximated by a Herschel-Bulkley viscosity model:

$$\mu_{\text{eff}} = \begin{cases} \mu_0 & , |\dot{\gamma}| \leq \dot{\gamma}_0 \\ k|\dot{\gamma}|^{n-1} + \tau_0|\dot{\gamma}|^{-1} & , |\dot{\gamma}| \geq \dot{\gamma}_0 \end{cases} \quad (3)$$

162 with $\mu_0 = k|\dot{\gamma}_0|^{n-1} + \tau_0|\dot{\gamma}_0|^{-1}$, a large μ_0 and $n = 1$ is used to approximate a Bingham-
 163 plastic behaviour, k dominates the viscosity when the material flows. In a Herschel-
 164 Bulkley model, the shear stress τ and shear rate $\dot{\gamma}$ are related as follows: $\tau = \tau_0 + k\dot{\gamma}^n$.
 165 To these equations an equation for the fiber orientations is needed. Here, the alignment
 166 or orientation tensors [45–47] come into play. The orientations of the fibers are described
 167 by an evolution equation for the second order orientation tensor a_{ij} [48,49]

$$\begin{aligned} \frac{D a_{ij}}{D t} &= -\frac{1}{2}(\omega_{ik} a_{kj} - a_{ik} \omega_{kj}) \\ &+ \frac{1}{2} \frac{(r^2 - 1)}{(r^2 + 1)} (\dot{\gamma}_{ik} a_{kj} + a_{ik} \dot{\gamma}_{kj} - 2 \dot{\gamma}_{kl} a_{ijkl}) \\ &+ 2 D_r (\delta_{ij} - 3 a_{ij}), \end{aligned} \quad (4)$$

168 where $\frac{D}{D t}$ is the material derivative (co-moving derivative), ω_{ij} is the vorticity tensor,
 169 $r = L/D$ is the aspect ratio of the fibers, L is the fiber length, D is the diameter. The
 170 terms $D_r = C_I \dot{\gamma}$ as suggested in [50] and $\dot{\gamma}$, which is the scalar magnitude of the rate of
 171 strain tensor, are given by:

$$\begin{aligned} D_r &= C_I \dot{\gamma} \\ &= \begin{cases} \dot{\gamma} 0.03(1 - e^{-0.224\Phi r}) & \text{if } \Phi r \leq 1.3 \\ \dot{\gamma} 0.0184e^{-0.7148\Phi r} & \text{if } \Phi r > 1.3 \end{cases}, \end{aligned} \quad (5)$$

$$\Phi = nL \frac{\pi D^2}{4} \quad (7)$$

$$\dot{\gamma} = |\dot{\gamma}_{ij}| = \sqrt{\frac{1}{2}(\dot{\gamma}_{ij}\dot{\gamma}_{ji})}, \quad (8)$$

172 where C_I is the fiber-fiber interaction coefficient which serves to randomize the orienta-
 173 tion state [49] and n is the fiber number density.

174 Since the equation of change for the second-order orientation tensor contains the
 175 fourth-order orientation tensor, a closure approximation that allows to calculate a_{ijkl}
 176 from a_{ij} is required. The IBOF-5 closure approximation suggested in [51] is used here:

$$\begin{aligned} a_{ijkl} &= \beta_1 S(\delta_{ij}\delta_{kl}) + \beta_2 S(\delta_{ij}a_{kl}) + \beta_3 S(a_{ij}a_{kl}) + \beta_4 S(\delta_{ij}a_{km}a_{ml}) \\ &+ \beta_5 S(a_{ij}a_{km}a_{ml}) + \beta_6 S(a_{im}a_{mj}a_{kn}a_{nl}), \end{aligned} \quad (9)$$

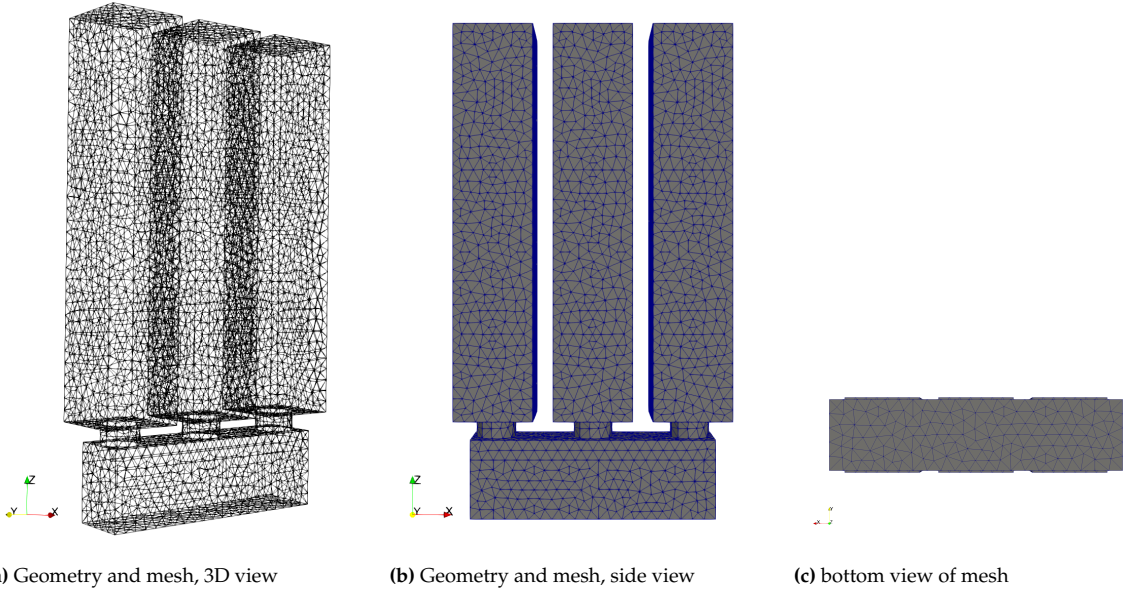
177 where $S(T_{ijkl}) = \frac{1}{24} \sum_{\text{perm}(ijkl)} T_{ijkl}$ is the symmetrization operator, with the sum carried
 178 out over all permutations of $ijkl$, and the coefficients β are functions of the second and
 179 third invariants of a_{ij} , see [51].

180 For the simulation interFiberFoam [27], a modified interFoam solver from the
 181 OpenFOAM 2.3.0 library, was used [52]. The implementation is adapted from the
 182 icoFiberFoam presented in [49]. The solver uses the so-called Weller-VOF (volume of
 183 fluid) method [53] to simulate multiphase free-surface flow. The solver was extended
 184 to include calculations of the equation of change for the second-order fiber orientation
 185 tensor field in the concrete phase [27]. At every time-step, Eq. (4) was solved to simulate
 186 the evolution of the fiber orientation tensors in the concrete phase. The simulation is
 187 one-way coupled — the flow-field affects the fiber orientation distribution whereas the
 188 fiber orientation has no effect on the flow-field. Verification of the solver had been done
 189 in [27] by comparison with results of simulations published by other researchers.

190 The geometry simulated is the beam geometry according to EN 14651, with three
 191 casting containers, see Figure 2. All simulations are performed on the same mesh, only
 192 the initial filling of the containers is changed. The geometry has been modeled and
 193 meshed in Gmsh [54]. Any number of containers can be active at the same time or one
 194 after the other. Post-processing has been done in ParaView [55].

195 For the atmosphere above the mold, fixed total pressure and a zero gradient bound-
 196 ary condition for the velocity were applied.

197 At the walls of the mold, a zero gradient condition was applied for the pressure
 198 field while a planar state of orientation in the plane of the walls was assumed for the
 199 fibers.



(a) Geometry and mesh, 3D view

(b) Geometry and mesh, side view

(c) bottom view of mesh

Figure 2. Geometry and mesh of the simulation, the mesh has 7023 nodes and 37020 cells. Geometry: $W \times L \times H$: $0.15 \text{ m} \times 0.62 \text{ m} \times 0.15 \text{ m}$, inlet $\varnothing 10 \text{ cm}$, located centered on the beam axis and 8 cm from the end-walls. Modeling and meshing in Gmsh [54].

200 The material parameters used in the simulation are given in Table 1 and results of
 201 simulated flowability tests are given in Table 2.

Table 1. Transport properties used in the OpenFOAM simulation, notation follows the naming in OpenFOAM, i.e. ρ is the density, τ_0 is the yield stress, k controls the viscosity of the flowing mass and ν_0 is the viscosity used if stress is below yield stress. The parameters are in the range published by [56,57]

	case	OpenFOAM value	physical value
ρ	super-liquid	2300	$2300 \frac{\text{kg}}{\text{m}^3}$
	self-leveling	2300	$2300 \frac{\text{kg}}{\text{m}^3}$
	high-viscous	2300	$2300 \frac{\text{kg}}{\text{m}^3}$
	slump	2300	$2300 \frac{\text{kg}}{\text{m}^3}$
τ_0	super-liquid	0.017391	40 Pa
	self-leveling	3.47e-02	79.810 Pa
	high-viscous	5.47e-02	125.81 Pa
	slump	9.47e-02	217.81 Pa
κ	super-liquid	0.010870	$25 \text{ Pa} \cdot \text{s}^n$
	self-leveling	2.17e-02	$49.910 \text{ Pa} \cdot \text{s}^n$
	high-viscous	4.17e-02	$95.910 \text{ Pa} \cdot \text{s}^n$
	slump	9.17e-02	$210.91 \text{ Pa} \cdot \text{s}^n$
ν_0	all cases	1000	$1000 \frac{\text{m}^2}{\text{s}}$
n	all cases	1	1

Table 2. Obtained rheological properties of the simulated SFRC mass using simulated funnel flow test and flow table test (with Abram's cone, dropping of plate was not simulated).

case	funnel outflow time	flow table diameter
super-liquid	1 s	–
self-leveling	2.5-3.2 s	108 cm
high-viscous	5-7 s	78 cm
slump	16 s	62 cm

202 3. Results

203 3.1. Dynamics of filling the form

204 An intermediate state of the filling of the formwork can be seen in Fig. 3, the
 205 screenshots are taken at different time-steps for different flowabilities to show differences
 206 in flow behaviour.

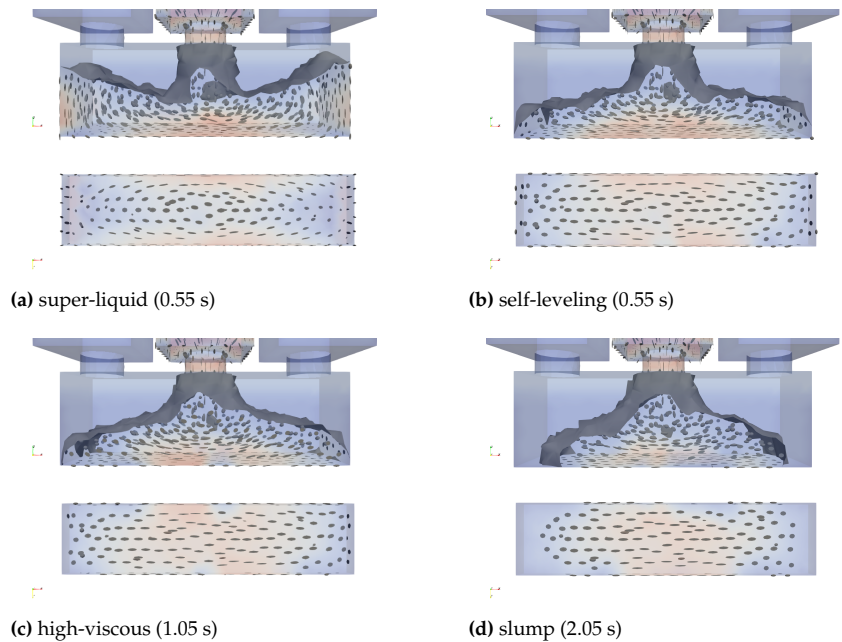


Figure 3. Comparison of the flow behaviour, shown are intermediate time-steps.

207 3.1.1. Super-liquid

208 The mold is filled very quickly. In the normative simulation set-up, the concrete
 209 is already pressed up against the sidewalls of the mold during filling from the central
 210 container. The subsequent filling from the side containers stimulates turbulent mixing
 211 of the mold contents at the mold edges. During the filling processes from only one
 212 container, there are also strong wave excursions at the surface, which quickly subside
 213 again and the concrete surface rapidly levels off horizontally. Figure 3a demonstrates the
 214 behavior of super-liquid mixture. As one can see from the image, the mixture is highly
 215 liquid and at the time-step 0.55 s the formwork is filled almost at the half. Additionally,
 216 the mixture splashes at the sidewalls of the formwork.

217 3.1.2. Self-leveling

218 The mold is filled more slowly and the concrete is not pressed upwards at the end
219 faces of the mold. The sloshing up is not visible, the concrete level in the mold center is
220 higher than at the mold edges. In the edge areas, the concrete already in the mold is more
221 clearly damped by the concrete flowing out of the edge containers. During edge filling,
222 there is a uniform flat increase in the level of the filling material. After completion of the
223 filling, air bubbles rising at the concrete surface can be assumed, which disappear after
224 the upward rise. In the case of one-sided filling, it can be seen that when the concrete
225 reaches the opposite side, the filling height is approximately the same at the filling point
226 and in the center of the mold. Figure 3b illustrates the behavior of self-leveling mixture.
227 At the time-step 0.55 s the mixture has a quite visible cone-shape that demonstrates the
228 proper viscosity of the self-leveling mixture.

229 3.1.3. High-viscous

230 A clear concrete cone can be seen in the normative filling. The filling from both
231 sides in the second step suggests the formation of three filling areas in the front mold
232 view. There is no pronounced mixing of the different fill quantities. When filling from
233 one side or in the middle, it can be seen that the concrete levels off much more slowly.
234 When filling from the edge, a uniform slope from the filling point along the entire mold
235 length can be seen when reaching the opposite formwork wall. Figure 3c shows the
236 behavior of high-viscous mixture. And we can see even more visible cone-shape of
237 the mixture. In addition, the mixture reaches the sidewalls later in time than in case
238 of self-leveling mixture (at time-step 1.05 s) which may verify that the mixture is more
239 viscous.

240 3.1.4. Slump

241 In the normative filling process, concrete cones with a clear valley between the cone
242 tips can be seen even during the second filling step. The concrete surface does not level
243 out completely. Complete displacement of the air bubbles cannot be seen. In the case of
244 one-sided filling, the slope on the concrete surface remains even after the container has
245 been completely emptied. Figure 3d demonstrates the behavior of slump mixture. As
246 we can notice the mixture is so high-viscous that even at the time-step 2.05 s the mixture
247 has a strong cone-shape and it flows so slow that still did not reach the sidewalls of the
248 formwork.

249 3.2. Obtained final fiber orientation distributions

250 The results of the numerical simulations of the fiber concrete flow with different
 251 rheological parameters and performed by several casting methods are demonstrated
 252 in Table 3. The fiber orientation distributions are represented by the ellipsoidal glyphs.
 253 A spherical shape of the glyphs represents isotropic distribution; the elongated (cigar)
 254 shape represents the zones where the fibers were well-aligned with each other; and the
 255 penny-shaped glyphs represents a fiber distribution with orientations mostly within a
 256 plane (planar isotropy).

257 The obtained results are presented by two views: a front view of the specimen and a
 258 bottom view. The front view contains the glyphs of the whole volume, while the bottom
 259 view only shows the bottom layer.

260 The results of the normative filling process according to EN 14651 are shown in the
 261 first column of Table 3 and in Fig. 5. The second column depicts the results of only center
 262 casting, which one may be tempted to do with sufficiently flowable concrete mass in
 263 practice. And the third column shows casting from one end (in this case left side). Each
 264 method is compared for four flowabilities ranging from (unrealistically) super-liquid,
 265 over realistic self-leveling and high-viscous to slump.

266 In the following, first general observations valid for all cases are mentioned, and
 267 then for each flowability the different casting methods are compared.

268 A general observation is, that under the (final) casting points the fibers tend to
 269 be aligned along the beam axis close to the bottom layer, and tend to become vertical
 270 aligned at large distance from the final casting point, which can be the center of the beam
 271 in the normative filling simulation.

272 Another observation is that the higher the viscosity and yield stress, the better the
 273 fibers are aligned with each other and correlation exists on a longer range.

274 Concerning different viscosities of a mixture, in general one can conclude that
 275 the super-liquid cases have produced more isotropic and random fiber orientation
 276 distribution. In addition, with the increasing of the viscosity the fibers have become
 277 better aligned in one direction. However, the most viscous case—the slump case—has
 278 demonstrated that a highly dense material can create the air bubbles in the formwork
 279 during casting.

280 Quantitative orientation measures in form of the scalar order parameter S , the
 281 biaxiality b and the director d , which is the eigenvector of the according to amount
 282 largest eigenvalue of the alignment tensor, are presented in Table 4. The scalar order
 283 parameter S is $S = \frac{3}{2}\lambda_1$ ($|\lambda_1| \geq |\lambda_2| \geq |\lambda_3|$), $b_S = \frac{1}{2}(\lambda_3 - \lambda_2)$, $b_S = \text{sign}(S)b$, with the
 284 biaxiality $b \in [0, \frac{1}{3}|S|]$ and $S \in [-\frac{1}{2}, 1]$, see [47,58]. $S = 1$ is perfectly aligned fibers,
 285 $S = 0$ isotropic and $S = -\frac{1}{2}$ is planar isotropic, see [58,59]. The two probes are located
 286 2.5 cm above the bottom and centered in the other directions for probe 1, and 2.5 cm
 287 from the side wall and centered in the other directions for probe 2, see Fig. 4. Thus they
 288 would be at the tip of a notch cut into the bottom or side, respectively.

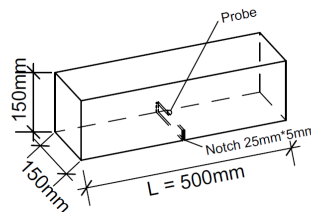


Figure 4. Sketch showing the location of the fiber orientation probe, probe 1 is located for use with the casting bottom as notched surface, and probe 2 is located for use with a side wall as notched surface.

289 3.2.1. Super-liquid

290 Looking at the numerical simulations of the super-liquid case one can note from
291 Table 4, that the director and the scalar order parameter vary quite a bit between the
292 casting methods. Normative casting leads to a low scalar order parameter of only
293 0.09 and director in y -direction with an inclination towards the x -direction for the
294 bottom probe, while the side probe shows a scalar order parameter of 0.44 with almost
295 z orientation. Even a short waiting time between the castings changes the values or
296 the scalar order parameter to 0.36 and 0.53, respectively, and the director of probe 1
297 towards z -direction. Both, center and side castings show planar orientations for probe 1,
298 indicated by the negative scalar order parameter, and moderate to good alignment in
299 z -direction for probe 2.

300 These tendencies can also be observed when looking at the glyphs presented in the
301 first row of Table 3.

302 The presented fiber orientation distributions are not beneficial for the transferring
303 the tensile stresses and will not prevent and bridge the cracks.

304 3.2.2. Self-leveling

305 Looking at the plots in Table 3 of the numerical simulations for the self-leveling
306 case, one can notice some pattern in the distribution of glyphs emerging. The alignment
307 glyphs in the side view start to follow a circle around the inflow point. For the center
308 casting, this means fibers are starting to have a tendency to be aligned along the beam
309 axis in the bottom layer, but the director turns upwards with increasing distance from
310 the center. The same tendency of the director turning upwards can be observed for the
311 side casting, though less pronounced here. In the case of the normative casting, there are
312 regions between the three casting points where the director is pointed upwards.

313 Numerically one can see from Table 4, that the probe 1 shows the director is aligned
314 along the x -axis for the center and side casting with a moderate fiber alignment of
315 $S = 0.38$, while the normative casting shows a tendency of flat-isotropic distribution in
316 the x - y -plane. For probe 2, the situation is reversed with moderately aligned fibers in z
317 direction for the normative casting, and plane-isotropy in the x - z -plane for the center
318 and side-castings.

319 3.2.3. High-viscous

320 The high-viscous case shows the highest degree of alignment in the center casting
321 at probe 1, but all casting positions show at least moderate alignment in x -direction, see
322 Table 4. The scalar order parameter is positive for all casting positions and on both probe
323 locations. In the normative casting the director at probe 2 is almost along z -axis, while in
324 the center and edge casting it is oriented in x -direction.

325 The visual trend observed in the self-leveling case is more pronounced here, the
326 glyphs presented in in Table 3 follow the same trend.

327 3.2.4. Slump

328 Visually, the same trends as in the high-viscous and self-leveling cases can be ob-
329 served in Table 3. Quantitatively one can see from Table 4, that the degree of orientation
330 is higher at probe 1 for the normative and center casting, but lower for the edge cast-
331 ing. At probe 2, in the normative casting there is a planar-isotropic orientation in the
332 x - z -plane, while in the center casting the orientation is in x -direction and for the edge
333 casting somewhat tilted from the x in negative z -direction.

334 4. Discussion

335 The standard EN 14651 has been prepared by the Technical Committee CEN/TS 229
336 Precast concrete products. In this context, it is worth mentioning that the development
337 of technologies for predictable fiber distribution has good chances especially in the field
338 of precast concrete products. In precast plants controllable manufacturing conditions

Table 4. Orientation parameters at two probe positions, the probes are located 2.5 cm above the bottom and centered in the other directions for probe 1, and 2.5 cm from the side wall and centered in the other directions for probe 2. The scalar order parameter S is $S = \frac{3}{2}\lambda_1$ ($|\lambda_1| \geq |\lambda_2| \geq |\lambda_3|$), $b_S = \frac{1}{2}(\lambda_3 - \lambda_2)$, $b_S = \text{sign}(S)b$, with the biaxiality $b \in [0, \frac{1}{3}|S|]$ and $S \in [-\frac{1}{2}, 1]$, see [58]. $S = 1$ is perfectly aligned fibers, $S = 0$ isotropic and $S = -\frac{1}{2}$ is planar isotropic, see [47,59].

cast position	flowability	position	S	b	$\text{EV}(\lambda_1)$
Norm	super-liquid	bottom 1	0.09	0.03	(-0.41, -0.91, -0.061)
Norm	super-liquid	side 2	0.44	0.02	(-0.015, 0.24, 0.97)
Norm rest	super-liquid	bottom 1	0.36	0.05	(-0.099, 0.099, -0.99)
Norm rest	super-liquid	side 2	0.53	0.03	(0.001, 0.17, 0.98)
Center	super-liquid	bottom 1	-0.12	0.03	(0.208, 0.007, 0.98)
Center	super-liquid	side 2	0.42	0.06	(0.044, 0.049, 0.99)
Side	super-liquid	bottom 1	-0.19	0.04	(-0.75, -0.075, 0.65)
Side	super-liquid	side 2	0.37	0.11	(0.21, 0.085, 0.97)
Norm	self-leveling	bottom 1	-0.25	0.08	(0.045, 0.042, -0.99)
Norm	self-leveling	side 2	0.38	0.09	(-0.26, -0.101, -0.96)
Center	self-leveling	bottom 1	0.37	0.10	(0.99, 0.15, 0.034)
Center	self-leveling	side 2	-0.33	0.10	(0.078, -0.99, 0.15)
Side	self-leveling	bottom 1	0.38	0.08	(0.98, 0.031, 0.18)
Side	self-leveling	side 2	-0.37	0.12	(0.19, 0.96, -0.22)
Norm	high-viscous	bottom 1	0.35	0.07	(0.99, -0.002, 0.007)
Norm	high-viscous	side 2	0.37	0.10	(-0.17, -0.14, -0.97)
Center	high-viscous	bottom 1	0.63	0.05	(0.99, 0.05, -0.008)
Center	high-viscous	side 2	0.42	0.10	(0.99, 0.05, 0.073)
Side	high-viscous	bottom 1	0.51	0.05	(0.99, 0.074, 0.11)
Side	high-viscous	side 2	0.41	0.09	(0.84, -0.045, 0.54)
Norm	slump	bottom 1	0.59	0.05	(0.99, 0.007, -0.009)
Norm	slump	side 2	-0.28	0.09	(0.024, -0.96, 0.27)
Center	slump	bottom 1	0.65	0.04	(1.0, 0.01, -0.01)
Center	slump	side 2	0.40	0.07	(0.99, -0.04, -0.12)
Side	slump	bottom 1	0.38	0.08	(0.98, 0.007, -0.19)
Side	slump	side 2	0.29	0.09	(0.83, 0.054, -0.56)

339 prevail, which allow high reproducibility of components and precast elements with lower
340 tolerance deviations. In addition, it is possible —especially in precast construction—
341 to arrange the filling side of the precast elements at correct angles to the subsequent
342 loading direction. This possibility is often not available for in situ casting.

343 As can be seen from the Tables 3 and 4, the most beneficial fiber orientation in the
344 bottom layer were present in the case of the high-viscous and slump flow that had been
345 cast by the normative filling method and from the center of the formwork.

346 However, as is required in standard EN14651, that the concrete sample needs to be
347 rotated about 90 degrees around the longitudinal axis, which means the fiber orientation
348 distribution in the side becomes the bottom in the bending test and has to cope with the
349 strongest tension. As can be seen from Fig. 6, the fiber orientations can be quite different.

350 Simulations of different casting scenarios show, that extreme care must be taken
351 when trying to reproduce reality in the simulation, it also shows that for simulations to be
352 used in predicting fiber distributions in structural elements, care must be taken to ensure
353 the building crew follows exactly the prescribed casting procedure. As Fig. 7 shows
354 even a short pause between casting from different positions can alter fiber orientation
355 distributions.

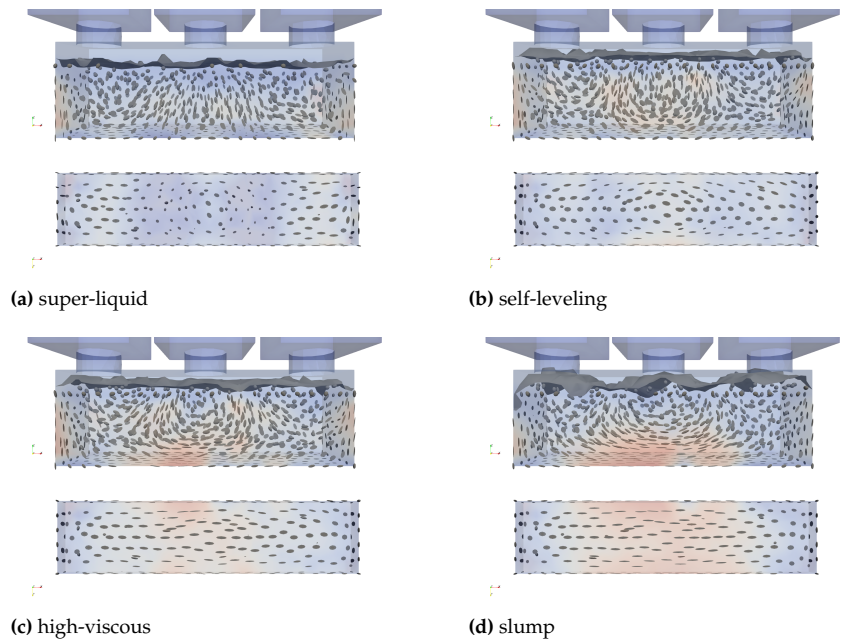


Figure 5. Comparison of the castings according to EN 14651 (first center, then edges)

356 5. Conclusions

357 This paper assesses an evaluation possibility of the final fiber orientation distribution
 358 that was obtained by the different casting methods using a numerical tool for
 359 the simulation of fresh concrete flow with short fibers. The simulations were done on a
 360 specimen according to EN 14651 standard. Four different concrete types with different
 361 rheological properties were simulated. The behaviour of the different concretes and the
 362 evaluation of the flow properties of the concretes was rechecked with the cone pouring
 363 method. For the simulations a modified interFoam solver from the OpenFOAM 2.3.0
 364 library was used. The visualisation was performed in ParaView. The results of the
 365 numerical simulation showed that higher the viscosity and yield stress, the better the
 366 fibers are aligned with each other and correlation exists on a longer range. In general,
 367 it was concluded, that the highly liquid cases have produced more isotropic and random
 368 fiber orientation distribution.

369 Finally, it can be concluded, that further simulation investigations on this topic
 370 are thoughtful for evaluation of mechanical properties of fiber reinforced specimen.
 371 The simulations have great potential to be used in precast plants for optimizing the
 372 production process.

373 **Author Contributions:** Conceptualization, H.H.; methodology, H.H.; software, H.H.; simulation,
 374 O.G., M.H. and H.H.; data curation, H.H.; writing—original draft preparation, H.H. (methods),
 375 O.G. and M.H. (Introduction, Discussion); writing—review and editing, H.H., O.G. and M.H.;
 376 visualization, O.G. and H.H.; supervision, H.H.; project administration, H.H.; funding acquisition,
 377 H.H. All authors have read and agreed to the published version of the manuscript.

378 **Funding:** This work was supported by the Estonian Research Council grant (PUT1146).

379 **Institutional Review Board Statement:** Not applicable

380 **Informed Consent Statement:** Not applicable

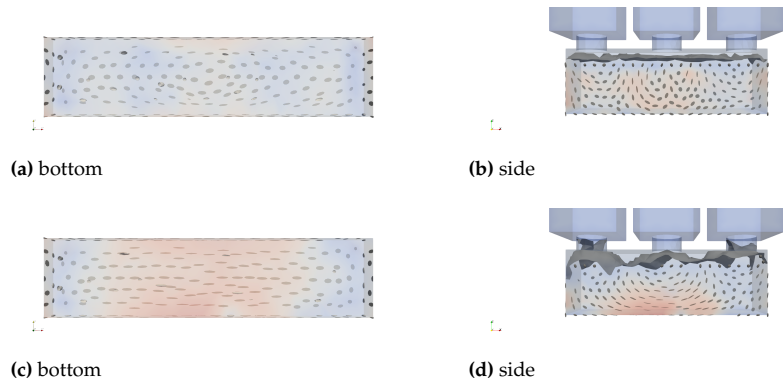


Figure 6. Side-by-side comparison of the fiber orientations in the bottom layer and in the side layer. One can see the difference in the bottom layer orientation distributions differs from the side distributions, since in a bending test, the part that is on the under or top side take the largest stress, turning a sample side-ways changes the tested distribution.

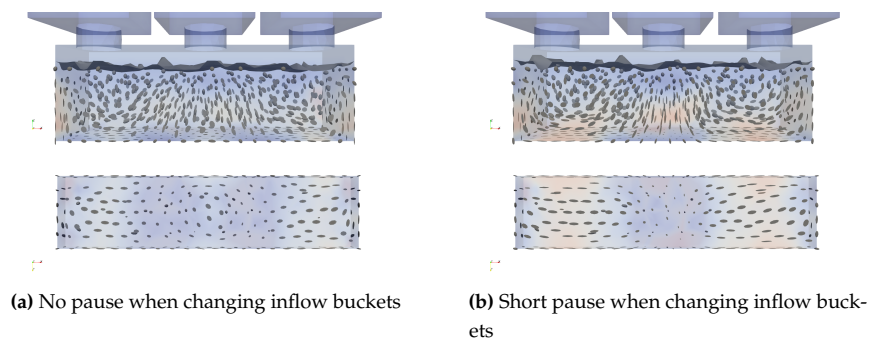


Figure 7. Comparison of a super-liquid casting having no pause between center and side castings with one having a few seconds pause between the center and the side castings to let the concrete mass settle a bit.

381 **Data Availability Statement:** The data presented in this study are openly available in TalTech
 382 Data Repository at DOI [10.48726/j4gda-mjn32](https://doi.org/10.48726/j4gda-mjn32).

383 **Acknowledgments:** The simulations were carried out in the High Performance Computing Centre
 384 of TalTech.

385 **Conflicts of Interest:** The authors declare no conflict of interest. The funders had no role in the
 386 design of the study; in the collection, analyses, or interpretation of data; in the writing of the
 387 manuscript, or in the decision to publish the results.

388 Abbreviations

389 The following abbreviations are used in this manuscript:

390	CFD	Computational fluid dynamics
	FVE	Finite volume elements
391	SFRC	Short fiber reinforced concrete
	VOF	Volume of fluid
	IBOF	invariant-based optimal fitting

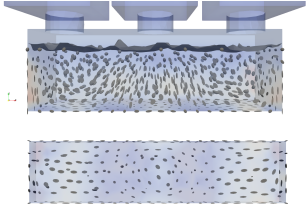
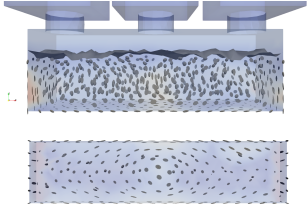
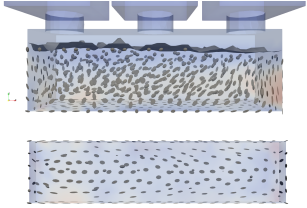
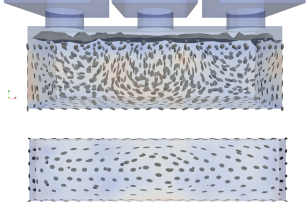
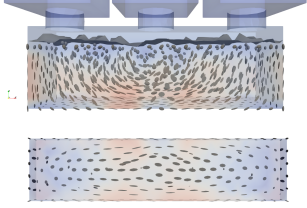
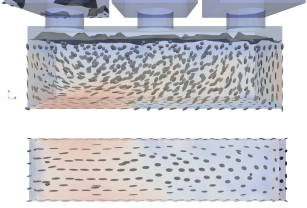
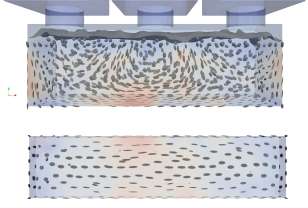
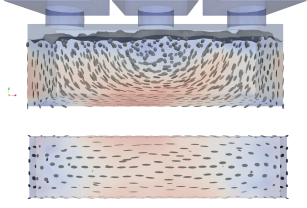
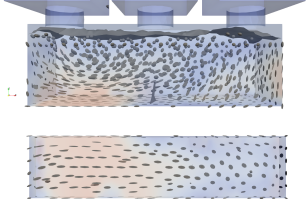
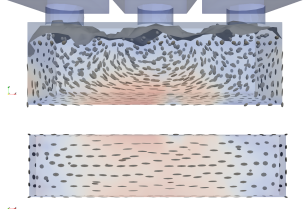
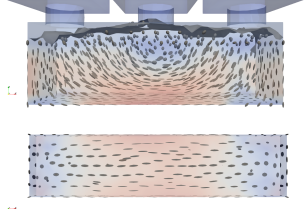
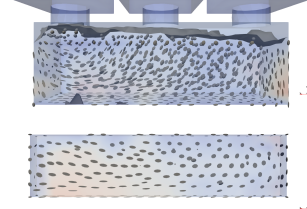
References

1. Roussel, N. Rheology of fresh concrete: from measurements to predictions of casting processes. *Materials and Structures* **2007**, *40*, 1001–1012.
2. Hu, J.; Wang, K. Effect of coarse aggregate characteristics on concrete rheology. *Construction and Building Materials* **2011**, *25*, 1196–1204.
3. Kostrzanowska-Siedlarz, A.; Gołaszewski, J. Rheological properties of high performance self-compacting concrete: effects of composition and time. *Construction and Building Materials* **2016**, *115*, 705–715.
4. Jiao, D.; Shi, C.; Yuan, Q.; An, X.; Liu, Y.; Li, H. Effect of constituents on rheological properties of fresh concrete-A review. *Cement and concrete composites* **2017**, *83*, 146–159.
5. Boulekbache, B.; Hamrat, M.; Chemrouk, M.; Amziane, S. Flowability of fibre-reinforced concrete and its effect on the mechanical properties of the material. *Construction and Building Materials* **2010**, *24*, 1664–1671.
6. Ponikiewski, T.; Gołaszewski, J. Properties of Steel Fibre Reinforced Self-compacting Concrete for Optimal Rheological and Mechanical Properties in Precast Beams. *Procedia Engineering* **2013**, *65*, 290–295. CONCRETE AND CONCRETE STRUCTURES 2013 - 6th International Conference, Slovakia, doi:10.1016/j.proeng.2013.09.045.
7. Khaloo, A.; Raisi, E.M.; Hosseini, P.; Tahsiri, H. Mechanical performance of self-compacting concrete reinforced with steel fibers. *Construction and building materials* **2014**, *51*, 179–186.
8. Torrijos, M.; Tobes, J.; Barragán, B.; Zerbino, R. Orientation and distribution of steel fibres in self-compacting concrete. Proceedings of the 7th RILEM symposium on fiber reinforced concrete: design and applications (BEFIB 2008), 2008, p. 729e38.
9. Torrijos, M.C.; Barragán, B.E.; Zerbino, R.L. Placing conditions, mesostructural characteristics and post-cracking response of fibre reinforced self-compacting concretes. *Construction and Building Materials* **2010**, *24*, 1078–1085.
10. Ponikiewski, T.; Katzer, J. X-ray computed tomography of fibre reinforced self-compacting concrete as a tool of assessing its flexural behaviour. *Materials and Structures* **2016**, *49*, 2131–2140.
11. Sucharda, O.; Lehner, P.; Konečný, P.; Ponikiewski, T. Investigation of fracture properties by inverse analysis on selected SCC concrete beams with different amount of fibres. *Procedia Structural Integrity* **2018**, *13*, 1533–1538.
12. Vicente, M.A.; Mínguez, J.; González, D.C. Computed tomography scanning of the internal microstructure, crack mechanisms, and structural behavior of fiber-reinforced concrete under static and cyclic bending tests. *International Journal of Fatigue* **2019**, *121*, 9–19.
13. Voutetaki, M.E.; Naoum, M.C.; Papadopoulos, N.A.; Chalioris, C.E. Cracking Diagnosis in Fiber-Reinforced Concrete with Synthetic Fibers Using Piezoelectric Transducers. *Fibers* **2022**, *10*, 5.
14. Barnett, S.J.; Lataste, J.F.; Parry, T.; Millard, S.G.; Soutsos, M.N. Assessment of fibre orientation in ultra high performance fibre reinforced concrete and its effect on flexural strength. *Materials and Structures* **2010**, *43*, 1009–1023.
15. Ferrara, L.; Ozyurt, N.; Di Prisco, M. High mechanical performance of fibre reinforced cementitious composites: the role of “casting-flow induced” fibre orientation. *Materials and Structures* **2011**, *44*, 109–128.
16. Van Mier, J.; Ruiz, G.; Andrade, C.; Yu, R.; others. Fiber orientation in ultra high performance fiber reinforced concrete and its visualization. Proceedings of the Eighth International Conference on Fracture Mechanics of Concrete and Concrete Structures, 2013.
17. Zhou, B.; Uchida, Y. Influence of flowability, casting time and formwork geometry on fiber orientation and mechanical properties of UHPFRC. *Cement and Concrete Research* **2017**, *95*, 164–177.
18. Yoo, D.Y.; Kang, S.T.; Yoon, Y.S. Effect of fiber length and placement method on flexural behavior, tension-softening curve, and fiber distribution characteristics of UHPFRC. *Construction and Building materials* **2014**, *64*, 67–81.
19. EN 14651: Test method for metallic fibered concrete—measuring the flexural tensile strength (limit of proportionality (LOP), residual). European Committee for Standardization, Brussels, 2005.
20. Herrmann, H.; Eik, M.; Berg, V.; Puttonen, J. Phenomenological and numerical modelling of short fibre reinforced cementitious composites. *Meccanica* **2014**, *49*, 1985–2000. doi:10.1007/s11012-014-0001-3.
21. Eik, M.; Puttonen, J.; Herrmann, H. An orthotropic material model for steel fibre reinforced concrete based on the orientation distribution of fibres. *Composite Structures* **2015**, *121*, 324–336. doi:10.1016/j.compstruct.2014.11.018.
22. Herrmann, H. Generalized Continua as Models for Classical and Advanced Materials; Springer International Publishing: Cham, 2016; chapter An Improved Constitutive Model for Short Fibre Reinforced Cementitious Composites (SFRC) Based on the Orientation Tensor, pp. 213–227. doi:10.1007/978-3-319-31721-2_10.
23. Mishurova, T.; Rachmatulin, N.; Fontana, P.; Oesch, T.; Bruno, G.; Radi, E.; Sevostianov, I. Evaluation of the probability density of inhomogeneous fiber orientations by computed tomography and its application to the calculation of the effective properties of a fiber-reinforced composite. *International Journal of Engineering Science* **2018**, *122*, 14–29. doi:10.1016/j.ijengsci.2017.10.002.
24. Herrmann, H. A constitutive model for linear hyperelastic materials with orthotropic inclusions by use of quaternions. *Continuum Mechanics and Thermodynamics* **2021**. doi:10.1007/s00161-021-00979-4.
25. Kartofelev, D.; Goidyk, O.; Herrmann, H. A case study on the spatial variability of strength in a SFRSCC slab and its correlation with fibre orientation. *Proceedings of the Estonian Academy of Sciences* **2020**, *69*, 298–310. doi:https://doi.org/10.3176/proc.2020.4.03.
26. Gram, A. Modelling Bingham Suspensional Flow. PhD thesis, Royal Institute of Technology (KTH), Stockholm, Sweden, 2015.

27. Herrmann, H.; Lees, A. On the Influence of the Rheological Boundary Conditions on the Fibre Orientations in the Production of Steel Fibre Reinforced Concrete Elements. *Proceedings of the Estonian Academy of Sciences* **2016**, *65*, 408–413. Open-Access CC-BY-NC 4.0, doi:10.3176/proc.2016.4.08.
28. Eiduks, M.; Krasnikovs, A.; Dunskis, E.; Kononova, O. Investigation of Fiber Orientation in Viscous Fluid. *Scientific Journal of Riga Technical University* **2010**, *33*, 98–102.
29. Kononova, O.; Krasnikovs, A.; Lapsa, V.; Kalinka, J.; Galushchak, A. Internal Structure Formation in High Strength Fiber Concrete during Casting. *International Journal of Mechanical, Aerospace, Industrial, Mechatronic and Manufacturing Engineering* **2011**, *5*, 2489–2492.
30. Roussel, N. Correlation between yield stress and slump: comparison between numerical simulations and concrete rheometers results. *Materials and structures* **2006**, *39*, 501–509.
31. Thrane, L.N.; Szabo, P.; Geiker, M.; Glavind, M.; Stang, H. Simulation of the test method “L-Box” for self-compacting concrete. *Annual Transactions of the NORDIC rheology society* **2004**, *12*, 47–54.
32. Krenzer, K.; Mechtcherine, V.; Palzer, U. Simulating mixing processes of fresh concrete using the discrete element method (DEM) under consideration of water addition and changes in moisture distribution. *Cement and Concrete Research* **2019**, *115*, 274–282.
33. Wallevik, J.E.; Wallevik, O.H. Concrete mixing truck as a rheometer. *Cement and Concrete Research* **2020**, *127*, 105930.
34. Vasilic, K.; Schmidt, W.; Kühne, H.C.; Haamkens, F.; Mechtcherine, V.; Roussel, N. Flow of fresh concrete through reinforced elements: experimental validation of the porous analogy numerical method. *Cement and Concrete Research* **2016**, *88*, 1–6.
35. Marcalikova, Z.; Bujdos, D.; Cajka, R. Approach to numerical modelling of fiber reinforced concrete. *Procedia Structural Integrity* **2020**, *25*, 27–32.
36. Vasilic, K.; Gram, A.; Wallevik, J.E. Numerical simulation of fresh concrete flow: insight and challenges. *RILEM Technical Letters* **2019**, *4*, 57–66.
37. Roussel, N.; Spangenberg, J.; Wallevik, J.; Wolfs, R. Numerical simulations of concrete processing: From standard formative casting to additive manufacturing. *Cement and Concrete Research* **2020**, *135*, 106075.
38. Roussel, N.; Gram, A.; Cremonesi, M.; Ferrara, L.; Krenzer, K.; Mechtcherine, V.; Shyshko, S.; Skocec, J.; Spangenberg, J.; Svec, O.; Thrane, L.N.; Vasilic, K. Numerical simulations of concrete flow: A benchmark comparison. *Cement and Concrete Research* **2016**, *79*, 265–271. doi:10.1016/j.cemconres.2015.09.022.
39. Kulasegaram, S.; Karihaloo, B.L.; Ghanbari, A. Modelling the flow of self-compacting concrete. *International Journal for Numerical and Analytical Methods in Geomechanics* **2011**, *35*, 713–723. doi:10.1002/nag.924.
40. Oesch, T.S. Investigation of Fiber and Cracking Behavior for Conventional and Ultra-High Performance Concretes Using X-Ray Computed Tomography. PhD thesis, University of Illinois at Urbana-Champaign, 2015.
41. di Prisco, M.; Ferrara, L.; Lamperti, M.G.L. Double edge wedge splitting (DEWS): an indirect tension test to identify post-cracking behaviour of fibre reinforced cementitious composites. *Materials and Structures* **2013**, *46*, 1893–1918. doi:10.1617/s11527-013-0028-2.
42. Pujadas, P.; Blanco, A.; Cavalaro, S.; de la Fuente, A.; Aguado, A. Fibre distribution in macro-plastic fibre reinforced concrete slab-panels. *Construction and Building Materials* **2014**, *64*, 496–503. doi:10.1016/j.conbuildmat.2014.04.067.
43. Herrmann, H.; Pastorelli, E.; Kallonen, A.; Suuronen, J.P. Methods for Fibre Orientation Analysis of X-ray Tomography Images of Steel Fibre Reinforced Concrete (SFRC). *Journal of Materials Science* **2016**, *51*, 3772–3783. doi:10.1007/s10853-015-9695-4.
44. Banthia, N.; Bindiganavile, V.; Jones, J.; Novak, J. Fiber-reinforced concrete in precast concrete applications: Research leads to innovative products. *PCI journal* **2012**, *57*.
45. Hess, S.; Köhler, W. *Formeln zur Tensor-Rechnung*; Palm & Enke: Erlangen, 1980.
46. Ehrentraut, H.; Muschik, W. On Symmetric irreducible tensors in d-dimensions. *ARI - An International Journal for Physical and Engineering Sciences* **1998**, *51*, 149–159. doi:10.1007/s007770050048.
47. Herrmann, H.; Beddig, M. Tensor series expansion of a spherical function for use in constitutive theory of materials containing orientable particles. *Proceedings of the Estonian Academy of Sciences* **2018**, *67*, 73–92. Open-Access CC-BY-NC 4.0, doi:10.3176/proc.2018.1.04.
48. Advani, S.G.; Tucker III, C.L. The Use of Tensors to Describe and Predict Fiber Orientation in Short Fiber Composites. *Journal of Rheology* **1987**, *31*, 751–784. doi:10.1122/1.549945.
49. Heinen, K. Mikrostrukturelle Orientierungszustände strömender Polymerlösungen und Fasersuspensionen. Phd thesis, Universität Dortmund, 2007.
50. Folgar, F.; Tucker, C.L. Orientation Behavior of Fibers in Concentrated Suspensions. *Journal of Reinforced Plastics and Composites* **1984**, *3*, 98–119, [<http://jrp.sagepub.com/content/3/2/98.full.pdf+html>]. doi:10.1177/073168448400300201.
51. Chung, D.H.; Kwon, T.H. Invariant-based optimal fitting closure approximation for the numerical prediction of flow-induced fiber orientation. *Journal of Rheology* **2002**, *46*, 169–194. doi:10.1122/1.1423312.
52. The OpenFOAM Foundation. OpenFOAM. <http://www.openfoam.org>, 2014. V. 2.3.0.
53. Damián, S.M. An Extended Mixture Model for the Simultaneous Treatment of Short and Long Scale Interfaces. Ph.d. thesis, Universidad Nacional del Litoral, Santa Fe, Argentina, 2013.
54. Geuzaine, C.; Remacle, J.F. Gmsh: A 3-D finite element mesh generator with built-in pre- and post-processing facilities. *International Journal for Numerical Methods in Engineering* **2009**, *79*, 1309–1331, [<https://onlinelibrary.wiley.com/doi/pdf/10.1002/nme.2579>]. doi:<https://doi.org/10.1002/nme.2579>.

55. Henderson, A.; Ahrens, J.; Law, C. *The ParaView Guide*; Kitware Inc.: Clifton Park, NY, 2004.
56. de Larrard, F.; Ferraris, C.F.; Sedran, T. Fresh concrete: A Herschel-Bulkley material. *Materials and Structures* **1998**, *31*, 494–498. doi:10.1007/BF02480474.
57. Lashkarbolouk, H.; Halabian, A.M.; Chamani, M.R. Simulation of concrete flow in V-funnel test and the proper range of viscosity and yield stress for SCC. *Materials and Structures* **2014**, *47*, 1729–1743. doi:10.1617/s11527-013-0147-9.
58. Herrmann, H.; Eik, M. Some comments on the theory of short fibre reinforced material. *Proceedings of the Estonian Academy of Sciences* **2011**, *60*, 179–183. doi:10.3176/proc.2011.3.06.
59. Jankun-Kelly, T.J.; Mehta, K. Superellipsoid-based, real symmetric traceless tensor glyphs motivated by nematic liquid crystal alignment visualization. *IEEE Transactions on Visualization and Computer Graphics (Proceedings Visualization/Information Visualization 2006)*, 2006, pp. 1197–1204. doi:10.1109/TVCG.2006.181.

Table 3. Comparison of fiber orientations for different flowabilities and casting points. The ellipsoidal glyphs represent the fiber orientation distribution, an isotropic distribution is represented by a spherical glyph, a distribution with well aligned fibers is shown by a cigar shaped glyph. An additional hint is given by the colors from blue to red.

	according to EN standard	only center casting	only edge casting
super-liquid			
self-leveling			
high-viscous			
slump			

Curriculum Vitae

1. Personal data

Name	Oksana Goidyk
Date and place of birth	29 May 1985 Samara, Russia
Nationality	Russian

2. Contact information

Address	Tallinn University of Technology, School of Science, Department of Cybernetics, Ehitajate tee 5, 19086 Tallinn, Estonia
Phone	+372 569 27 721
E-mail	oksana.goidyk@taltech.ee

3. Education

2016–...	Tallinn University of Technology, School of Science, EAED02 - Building and Civil Engineering and Architecture, PhD studies
2002–2008	Samara State Aerospace University, Faculty of Aircrafts, Spacecrafts and booster blocks, MSc

4. Language competence

Russian	native
Estonian	beginning
English	fluent

5. Professional employment

2022–2023	Keskkonnaprojekt, Researcher
2021–2022	Tallinn University of Technology, School of Science, Department of Cybernetics, Engineer
2016–2021	Tallinn University of Technology, School of Science, Department of Cybernetics, Early Stage Researcher
2010–2015	Design Bureau "Arsenal" (Russia), Engineer/constructor

7. Computer skills

- Operating systems: Linux, Windows
- Document preparation: LaTeX, MS Word
- Programming languages: Python, C, Matlab
- Scientific packages: R-Statistics, OpenFOAM

9. Defended theses

- 2008, Manufactory of aircraft assembling components, MSc, supervisor Ass. Prof. Oleg Lomovscoi, Samara State Aerospace University

10. Field of research

- Natural Sciences and Engineering, Material Science, Civil engineering, hydraulic engineering, offshore technology, soil mechanics

11. Scientific work

Papers

1. H. Herrmann, A. Braunbrück, T. Tuisk, O. Goidyk, and H. Naar. An initial report on the effect of the fiber orientation on the fracture behavior of steel fiber reinforced self-compacting concrete. In H. Herrmann and J. Schnell, editors, *Short fibre reinforced cementitious composites and ceramics*, pages 33–50. Springer, 2019
2. H. Herrmann, O. Goidyk, and A. Braunbrück. Influence of the flow of self-compacting steel fiber reinforced concrete on the fiber orientations, a report on work in progress. In H. Herrmann and J. Schnell, editors, *Short Fibre Reinforced Cementitious Composites and Ceramics*, pages 97–110. Springer, 2019
3. H. Herrmann, O. Goidyk, H. Naar, T. Tuisk, and A. Braunbrück. The influence of fibre orientation in self-compacting concrete on 4-point bending strength. *Proceedings of the Estonian Academy of Sciences*, 68(3):337–346, 2019
4. D. Kartofelev, O. Goidyk, and H. Herrmann. A case study on the spatial variability of strength in a SFRSCC slab and its correlation with fibre orientation. *Proceedings of the Estonian Academy of Sciences*, 69(4):298–310, 2020
5. O. Goidyk, M. Heinštein, and H. Herrmann. CFD comparison of the influence of casting of samples on the fiber orientation distribution. *Fibers*, 11(1):6, 2023

Conference presentations

1. Goidyk, O.; Braunbrück, A.; Marjapuu, R.-R.; Tuisk, T.; Herrmann, H. (2017). Towards benchmark cases for computational fluid dynamics for casting of fiber concrete. M2D2017 : Proceedings of the 7th International Conference on Mechanics and Materials in Design (Albufeira/Portugal, 11-15 June 2017). Ed. Silva Gomes, J.F.; Mequid, Shaker A. Porto: FEUP-INEGI, 2017, 229-230.
2. Goidyk, O.; Heinštein, M.; Herrmann, H.; (2022) Preparation of SFRC testing specimens simulated by CFD. CEBACOM 2022 - The First International Cement Based Composites Congress - 29-30 June 2022.

Elulookirjeldus

1. Isikuandmed

Nimi Oksana Goidyk
Sünniaeg ja -koht 29.05.1985, Samara, Venemaa
Kodakondsus Vene

2. Kontaktandmed

Aadress Tallinna Tehnikaülikool, Kübernetika Instituut,
Ehitajate tee 5, 19086 Tallinn, Estonia
Telefon +372 5690270721
E-post oksana.goidyk@taltech.ee

3. Haridus

2016–... Tallinna Tehnikaülikool, Inseneriteaduskond,
EAED02/16 - Ehitus ja arhitektuur, doktoriõpe
2002–2008 Tallinna Samara osariigi lennundusülikool, Lennukiteaduskond,
Kosmoselaevad ja ülemised etapid, MSc *cum laude*
1992–2002 Keskharidus

4. Keelteoskus

vene keel emakeel
eesti keel algtase
inglise keel kõrgtase

5. Teenistuskäik

2022–2023 OÜ Keskkonnaprojekt, teadur
2021–2022 Tallinna Tehnikaülikool, Loodusteaduskond, Küberneetika instituut, insener
2016–2021 Tallinna Tehnikaülikool, Loodusteaduskond, Küberneetika instituut,
doktorant-nooremteadur
2010–2015 Disaini osakond "Arsenal" (Peterburi, Venemaa), disaini insener

6. Arvutioskused

- Operatsioonisüsteemid: Linux, Windows
- Kontoritarkvara: Office, LibreOffice, LaTeX
- Programmeerimiskeeled: Python, C, MatLab (algtase)
- Teadustarkvara paketid: R-statistics, OpenFOAM

7. Kaitstud lõputööd

- 2008, Lõputöö Lennukite montaažitöökoja kujundus, MSc, juhendaja dotsent Oleg Lomovskoi, Samara osariigi lennundusülikool

8. Teadustöö põhisuunad

- Loodusteadused ja tehnika, materjaliteadus, tsiviilehitus, hüdrotehnika, avamere-tehnoloogia, pinnasemehaanika

9. Teadustegevus

Teadusartiklite, konverentsiteeside ja konverentsiettekannete loetelu on toodud ingliskeelse elulookirjelduse juures.

ISSN 2585-6901 (PDF)
ISBN 978-9916-80-270-0 (PDF)